8-2023

Roles of soil pores in determining water retention and microbial dynamics

Huihui Sun
hsun16@vols.utk.edu

To the Graduate Council:

I am submitting herewith a dissertation written by Huihui Sun entitled "Roles of soil pores in determining water retention and microbial dynamics." I have examined the final electronic copy of this dissertation for form and content and recommend that it be accepted in partial fulfillment of the requirements for the degree of Doctor of Philosophy, with a major in Environmental and Soil Sciences.

Jie Zhuang, Major Professor

We have read this dissertation and recommend its acceptance:

Mark Radosevich, Shuo Qian, Qiang He, Jaehoon Lee

Accepted for the Council:

Dixie L. Thompson

Vice Provost and Dean of the Graduate School

(Original signatures are on file with official student records.)

ROLES OF SOIL PORES IN DETERMINING WATER RETENTION AND MICROBIAL DYNAMICS

A Dissertation Presented for the

Doctor of Philosophy

Degree

The University of Tennessee, Knoxville

Huihui Sun

August 2023

ACKNOWLEDGEMENTS

First and foremost, my most profound appreciation goes to my advisor, Dr. Jie Zhuang, for offering me the opportunity to enjoy science. His dedicated support and guidance throughout the research project make the work in this dissertation to be possible. He has always provided me with valuable suggestions for both academic study and life and encouraged me during my tough time like a friend. I am deeply grateful for his assistance at every stage of my doctoral research.

I would particularly like to express my gratitude to Dr. Mark Radosevich. He provides me with professional feedback and guidance greatly improving my research. Many thanks to Dr. Shuo Qian at the Oak Ridge National Laboratory. Our collaborative work in using advanced small-angle neutron scattering techniques supplies an opportunity to solve challenging research questions. I would also like to extend thanks to Dr. Jaehoon Lee and Dr. Qiang He. Thanks for serving on my Ph.D. committee and giving thoughtful questions and suggestion for my research.

I am also indebted to the members of Dr. Zhuang's and Dr. Radosevich' lab. Thank you, Dr. Xiaolong Liang, Dr. Regan McDearis, Zhibo Cheng, and Ninghui Xie for your kind help in my lab work in the past four years. Thanks to the Department of Biosystems Engineering and Soil Science in the University of Tennessee and the Graduate Advancement, Training and Education program for funding support.

Lastly, thanks to my parents, grandparents, and parents-in-law for their love and unconditional support to let me pursue my dream. Thanks to my sister for taking care of our family when I was away from home. My biggest thanks to my beloved husband, Yanchen Sun, for your companionship and engagement over the past ten years. You make me feel how

amazing it is to be married to a person in the same research area. Special thanks to our brainstorming about science in daily life.

ABSTRACT

Soil pore provides an essential habitat for microbial communities to participate in various biogeochemical processes. The complex pore spaces, which are defined by the arrangement of particles of varying sizes, govern the distribution of water for microbial dispersal and movement and microbial interaction with one another, such as bacterial cell-to-cell and bacterium-virus interactions. This research focused on exploring how soil pores influence a soil water retention and bacterial interactions and quantify the spatial distribution of bacteria and viruses in fine scale of soil pores. Using a mathematical model, this study simulated soil water retention curve based on the relationship between soil pores and water retention characteristics. A fractional bulk density (FBD) concept was proposed in the model to estimate pore water content under varying matric potential. Comparing the estimated results of the water retention curve with the measured data, the model behaved overall well. The proposed model provides an easy way to evaluate the impacts of soil pores on water conservation in soils. Based on the concept in the FBD model, sand media with different pore sizes coupled with different surface properties were used to evaluate conjugation-based bacterial cell-to-cell interactions. The presence of sand increased conjugation frequency compared to sand-free controls. The frequencies were a function of pore size and bacterial adhesion on sand surfaces with smaller pores and more adhesion lowering bacterial conjugation frequency. Collision of bacteria in pore spaces promoted their interactions, while limited motility of bacteria trapped in smaller pores or adhered to sand surfaces reduced the interactions. To further investigate microbial activity in fine scale pores, the spatial distribution of bacteria and viruses in soil was characterized by using advanced small angle X-ray/neutron scattering techniques. Bacteria and viruses have their optimal strategies for survival in soil pores in response to soil harsh environments. Bacteria preferred to colonize in the pores

greatly close to their sizes and viruses aggregated to prevent penetrating into nanopores. These observations highlighted soil pore-associated water and microbial dynamics and advance the understanding of the functions of soil pores in soil ecosystems.

TABLE OF CONTENTS

LIST OF TABLES

LIST OF FIGURES

Chapter 1. Introduction

Soil bacterial and viral communities sustain key functions in soils such as carbon and nutrient cycling, plant health, and agricultural sustainability (Kuzyakov and Mason-Jones, 2018; Williamson et al., 2017; Wilpiszeski et al., 2019). Soil microbes influence soil biogeochemical cycling by decomposing organic matter into inorganic forms of carbon, nitrogen, phosphorus, and other nutrients (Ciric et al., 2012). Viruses that infect bacteria are a major cause of bacterial mortality and thereby also dramatically alter biogeochemical processes (Jover et al., 2014).

As habitats of prokaryotes and viruses, soils can be viewed as a complex 3D structure consisting of pore spaces and packed aggregates (Bailey et al., 2013). The pores and aggregates are important in shaping interactions between bacterial cells since bacteria occupy specialized niches that exist within and between aggregates (Tecon et al., 2018). The spatial interactions of bacteria in soil pores have a crucial influence on the spread of viruses between bacterial cells through induced lysis and horizontal gene transfer. As a result, bacterial distribution in pores affect the function and evolution of bacterial communities and hence influence biogeochemical cycles (Weitz and Wilhelm, 2012). Moreover, soil aggregates can influence bacterial/viral distribution and functions (e.g., based on control of physicochemical stresses) through spatial confinement. Across aggregate structures, interaggregate pore spaces range from 10 to 30 μm while intra-aggregate pore spaces range from 1 to 2 μm (Bailey et al., 2013). The pore sizes, volumes, and connectivity are coupled to control the diffusion of solutes or water and the mobility of bacteria and viruses. For example, bacteria and viruses can become spatially separated from dissolved nutrients under low moisture conditions (Or et al., 2007). Therefore, more complete understanding virus-bacterium-pore relationships may lead to improved management and soil ecosystem health. However, previous studies paid little attention to the constraints imposed by pore structure on soil inhabitants (i.e., bacteria and viruses).

To better understand biotic and abiotic interactions governed by pore structure, porous matrix-based experiments were used to investigate bacterial cell-to-cell interactions and bacterial/viral distribution in response to pore hydrology and solution chemistry in this study. Characterizing the pore-bacterium-virus relationships at pore-scales will allow for a refined understanding of soil biogeochemical processes.

1.1 Microbes in soil environment

Soil microbes (e.g., bacteria, viruses) are the drivers of key biogeochemical cycles of carbon, nitrogen, and phosphorous (Tecon and Or, 2017). The roles of soil bacteria in directing nutrients through the soil-food-web are termed the "Microbial Loop" (Clarholm, 1985; Zwart et al., 1994). Briefly, roots of plants release carbon into soil to stimulate organic nitrogen mineralization from exudates. Bacteria use the root-released carbon and soil organic matter (SOM)-released nitrogen for growth. Predatory soil animals feed on bacteria, further releasing inorganic nitrogen. Plants then take up the mineral nitrogen and create a feedback effect that enhances the release of organic carbon into soil (Crowther et al., 2019; Kuzyakov and Mason-Jones, 2018).

Soil microbes share their habitat with a vast diversity of neighbors, resulting in microbial interactions including competition and cooperation mediated by diffusible metabolites and signals (Little et al., 2008; Van Elsas et al., 2006; Velicer and Vos, 2009), and horizontal gene transfer (HGT) mediated by conjugative pili (Soucy et al., 2015). The conjugation as one of the most important mechanisms of HGT occurs through direct donor-recipient physical cell contact and single-stranded DNA is transferred from the donor cell to the recipient cell (Macé et al., 2022; Soucy et al., 2015; Waksman, 2019). Before the transfer can occur, transfer (*tra*) genes

(Dtr and T4S genes) must be expressed and a T4SS (type IV secretion system) assembled. Single-stranded DNA (ssDNA) molecules transferred from donor to recipient bacterial cells are ubiquitous in the microbial world (Koraimann and Wagner, 2014). Donor cells secret ssDNA facilitated by proteins that can initiate a rolling circle type replication by cleaving one strand of the double-stranded DNA (dsDNA) at a site termed *oriT* (origin of transfer) (Guglielmini et al., 2013; Waksman, 2019). The nucleoprotein complex consists of the nicked plasmid DNA and the proteins required for DNA transfer and replication (termed Dtr) (Bhatty et al., 2013). The Dtr complex is docked to the T4S (type IV secretion) complex via protein-protein interactions after the T4S complex has been pre-assembled in the cell envelope (Bhatty et al., 2013; Zechner et al., 2012). ssDNA is then translocated through the conjugation channel (the T4S apparatus) directly into the cytoplasm of the recipient (Zechner et al., 2012). The DNA in the cytoplasm of recipient cells is recircularized to regenerate a circular ssDNA which can be reconstituted to the double stranded plasmid DNA (Wilkins, 2002). Strategies to secure successful gene transfer in natural environments require sensing mechanisms that ensure that *tra* genes are turned on at the right time and the right place (Koraimann and Wagner, 2014). The conjugation process enables the transfer of genetic material not only within but also across genera (Yu et al., 2021). The multitude of microorganisms shares a pseudo-common genetic pool, which could blur the boundaries between distinct phylogenetic clades (Rodríguez-Beltrán et al., 2021). The plasmids have an important role in bacterial evolution by transferring beneficial traits to recipients and positively contributing to recipient fitness (Rodríguez-Beltrán et al., 2021). For example, plasmids are often associated with toxin resistance genes, metabolic genes, virulence factors and a wide range of secreted factors (Soucy et al., 2015). When these elements are accepted by recipients, the recipients can expand their ecological niches (Rodríguez-Beltrán et al., 2021).

Viruses are ubiquitous in the environment and can greatly influence microbial community structure and functions (Kuzyakov and Mason-Jones, 2018). To infect bacterial hosts, viruses must come in direct physical contact with their hosts. For example, when a tailed virus encounters a suitable host, its tail will first bind to the surface of the bacterium at specific receptors (Kuzyakov and Mason-Jones, 2018). Many studies have shown that viruses are the most abundant biological entities in the sea, typically 10^8 to 10^9 per liter in surface water (5-25 times the bacterial abundance) (Børsheim, 1993; Fuhrman, 1999; Paul et al., 1993; Steward et al., 1996; Wommack et al., 1992). In soil, viral abundance is up to 10^{10} per gram, and this value might be underestimated due to extraction and detection methods (Williamson et al., 2017). Viruses with huge numbers are known to affect microbial dynamics, metabolism, and biogeochemistry (Brum and Sullivan, 2015; Emerson et al., 2018; Guidi et al., 2016; Suttle, 2007). Viral infection with very high rates is now recognized as a top-down (predation) control of bacterial mortality and biomass turnover in soil and aquatic environments (Kuzyakov and Mason-Jones, 2018; Zimmerman et al., 2020). Previous studies indicated that up to 46% of the bacterial population in aquatic environment are affected by viral lytic infection (Bi et al., 2021; Jover et al., 2014; Weinbauer, 2004). By lysing about 20%-50% of bacteria per day in the ocean, viruses involve carbon and other nutrients back into the dissolved pool (Bi et al., 2021; Brum and Sullivan, 2015; Suttle, 2007; Weitz and Wilhelm, 2012). This process of virus-mediated recycling of nutrient is known as the "Viral Shunt" (Jover et al., 2014). The viral shunt has strong implications for soil and aquatic nutrient cycling, and the high rates of viral infection in soil drive the viral shunt. Viruses infect and lyse bacterial cells, releasing nitrogen into the rhizosphere. The nitrogen is directly available for plants and increases root growth and development and meanwhile facilitates carbon release into the rhizosphere (Kuzyakov and

Mason-Jones, 2018). Viruses also contribute to horizontal gene transfer through transduction (Mann et al., 2003; Suttle, 2007). Viruses reprogram the metabolism of their hosts via the expression of virus-encoded auxiliary metabolic genes (AMGs) (Roux et al., 2016). The metabolic functions of AMGs include carbon, nitrogen, and sulphur metabolism, photosynthesis, and phosphate scavenging (Hsieh and Wanner, 2010; Roux et al., 2016; Sullivan et al., 2006).

Soil pore heterogeneity coupled with different microbial sizes controls the accessibility of pore space for microbes, influencing their interactions such as viral infection of bacteria, hence, impacting biogeochemical cycles. Studies showed that the size of most viruses ranges from 30 nm to 80 nm whereas bacteria ranges from 0.2 μm to 5 μm. Consequently, viruses are on average 20-50 times smaller than bacterial cells, and viral volume is 8,000-125,000 times smaller than the volume of bacterial cells (Kuzyakov and Mason-Jones, 2018). Due to this large difference in size, viruses, in theory, can occupy all pores available to bacteria, but bacteria cannot access the soil pores smaller than 200 nm that may contain a considerable portion of the viral biomass. Thus, if the small pores and larger pores become hydrologically disconnected viruses may become physically separated from their bacterial hosts when soil moisture becomes limiting. This spatial context controls the probability for a virus to encounter bacterial host, infect it and possible mediate transfer of DNA. Ultimately, by constraining the distribution and potential interaction of viruses and their host organisms, soil pore structure and impact soil biogeochemistry. Unfortunately, detailed evidence in this regard is completely lacking. Developing a better understanding of how soil pore network affects contacts among bacteria and viruses is very important for revealing basic principles that govern soil microbial community diversity, dynamics, and functioning.

1.2 Soil as microbial habitat

Soil structure is the 3D arrangement of the aggregates and pore space across different scales (Schlüter et al., 2020). The individual soil particles with sizes ranging from 50 to 2,000 μm, from 2 to 50 μm, and less than 2 μm are classified as sand, silt, and clay, respectively (Hillel, 2003; Ochsner, 2022). Soil structure describes the shape, size, and spatial arrangement of sand, silt, and clay. The different sized particles are often organized into 3D assemblages called aggregates (Ochsner, 2022). Different aggregation of soil particles results in heterogeneous arrangement of soil pores between particles. The heterogeneous soil pores, where hydration conditions and nutrients diffusive fluxes fluctuate, are key factors promoting microbial diversity in soil (Dion, 2008; Kraemer et al., 2016).

1.2.1 Soil aggregates

Soil aggregates are the basic components of solid phase of soil structure, and aggregation results from particle rearrangement, flocculation, and cementation (Bronick and Lal, 2005; Duiker et al., 2003; Han et al., 2021; Six et al., 2000). Soil aggregates are classified as two groups, i.e., microaggregates (53-250 μm) and macroaggregates (250-2,000 μm) (Six and Paustian, 2014). Microaggregates (Cl-P-OM) are formed from organic molecules (OM) attached to clay (Cl) and polyvalent cations (P). As hierarchical structure, microaggregates are bound horizontally (x) and vertically (y) together into macroaggregates ($[(\text{Cl-P-OM})_x]_y$). In turn, macroaggregates are formed around particulate organic matter (POM) and can release microaggregates during breakdown (Six et al., 1999; Tisdall and Oades, 1982). The bonds within microaggregates are more persistent than the bonds between macroaggregates (Edwards and Bremner, 1967; Rabot et al., 2018; Schlüter et al., 2020).

The distribution and relative abundance of macro- and microaggregates influence biogeochemical cycles (e.g., C, N, P, S), gas diffusion, water content, and flow channel shape (Wilpiszeski et al., 2019). In general, microaggregates physically protect organic matter, and macroaggregates regulate water flow and gas diffusion (Carminati et al., 2007; Sexstone et al., 1985; Tisdall and Oades, 1982). Nearly 90% of soil organic carbon in surface soils was found within aggregates and intra-microaggregate organic carbon accounted for 20-40% of the 90% organic carbon (Carter and Stewart, 1995; Jastrow, 1996). The decomposition and metabolization of soil organic matter (SOM) decreased with decreasing aggregate size, which was manifested by plant residue abundance from macro- to microaggregates (John et al., 2005). Consequently, microaggregate SOM may be stored for a longer time than macroaggregate SOM. The age of organic carbon in macro- and microaggregates was about 15-50 and 100-300 years, respectively (Lobe et al., 2011). Besides carbon, the cycling of N, P, and S is also affected by aggregate structure. The accumulation of organic N, P, and S in microaggregates was intensive compared to that in the bulk soil (Angers and Giroux, 1996). The C:N and C:P ratios decreased from macroaggregates to microaggregates (Angers and Giroux, 1996). Moreover, the emissions of the greenhouse gases N_2O, CO_2, and CH_4 were also associated with soil aggregates size (Sey et al., 2008). Microaggregates produced more CO_2 than macroaggregates and bulk soil. The emissions of N_2O were related to soil water saturation and oxygen diffusion. For example, at 80% water saturation, oxygen diffusion diffuse into microaggregates was retarded while macroaggregates remained oxic (Sey et al., 2008). Denitrification was dominant in microaggregates while nitrification was more prevalent in macroaggregates and bulk soil at 80% water saturation. Under these conditions, denitrification contributed up to 95% of N_2O

production from microaggregates, while nitrification was responsible for 97-99% of the N_2O production from macroaggregates and bulk soil (Sey et al., 2008).

1.2.2 Soil pore system

The soil pore system regulates water retention and infiltration, gaseous exchanges, and SOM and nutrient dynamics (Rabot et al., 2018). Soil pore structure contributes to the diversity of microbes and regulates their activities (Rabot et al., 2018). These microbes can in turn shape the soil pore structure as feedback, modifying the distribution of water and air (Rabot et al., 2018; Tecon and Or, 2017). Understanding the links between soil pores and microbial diversity and activity is key to the assessment of biological processes.

Soil pore space is formed between the solid components of soil (i.e., mineral and organic matter) (Paul, 2014). Like the aggregate hierarchy, pores are classified as macro-, meso-, and micropores depending on their sizes. Although there is no consensus on the size thresholds between these categories, soil pores can generally form a tripartite group, including transmission pores, storage pores, and residual pores (Greenland, 1977; Van Elsas et al., 2019). Transmission pores (approximately 60-300 μm) are the main conduits for gaseous, water and nutrient flow, and these pores form the majority of pore space in the soil microbial habitat. Storage pores (approximately 0.2-60 μm) can store water for plants and microorganisms (i.e., they do not drain under the force of gravity). Pores with neck diameters of approximately less than 0.2 μm are residual pores which remain water-filled and also can protect SOM from decomposition by limiting bacterial access.

In addition to pore size, the shape of soil pores determines soil habitability for microbes (Paul, 2014). The shape factor divides pores into different geometrical groups: regular (more or

less rounded), irregular, and elongated pores (Pagliai and Vignozzi, 2002). The regular can be distinguished by two types: spherical pores and channels or chambers. The former is formed by entrapped air during soil drying, which have very smooth walls, while the channels or chambers are formed by biological activity (e.g., root growth, movement of soil fauna), which possess rough walls with deposits of faunal excrement or root exudates. The irregular pores are the common soil pores with irregular walls and can be isolated or interconnected. The elongated pores can be distinguished in two types: cracks and thin fissures (planes). The cracks are typical of clay soils with a depleted soil organic matter content, while the thin fissures are the typical transmission pores. For the characterization of elongated pores, not only shape and width of the pores but also the length should be determined. Among these three parameters, the length may reflect the continuity of pores which can determine the flow of water through soil. For water movement through soil, the irregularity and orientation of elongated pores are also important. For example, the very regular elongated pores tend to seal when the soil is wet and prevent water movement since their pores are flat and smooth. The pores are tightly packed and do not allow water to flow easily through them. In contrast, the moderately regular elongated pores allow water movement under wet conditions. These pores have walls and small gaps or spaces between the walls of adjacent pores prevent them from fully accommodating with each other. These pores provide a pathway for water to flow in a specific direction. The orientation of pores in soil is determined by the ratio vertical/horizontal dimension. The process of soil water movement depends on whether a vertical or horizontal pore orientation is dominant.

The soil pore system is affected by hydraulic stress, soil organic matter, clay, biota, and ionic bridging. Wetting and drying cycles (hydraulic stress) can change soil pore systems. The volume of nonrigid soil increases during water uptake while the volume shrinks after water

removal (Peng and Horn, 2007). During drying, there are two shrinkage components, including vertical and horizontal directions, in the non-rigid soils. The horizontal shrinkage can produce soil cracks that changes soil pore shape (Liu et al., 2003). In addition, wetting and drying cycles can bring soil minerals and organic matter into contact to create an aggregated state which might make pore size smaller or block pore throats influencing pore connectivity (McCarthy et al., 2008). Soil organic matter alters soil porosity and pore size distribution by mineral encapsulation of colloidal soil organic matter (McCarthy et al., 2008). Clay acts as an aggregant and binds particles together to influence pore size and pore connectivity (Bronick and Lal, 2005). Biological activity is one of the main drivers of aggregate formation. For example, bacteria and fungi can secrete polymeric substances as a glue to aggregate inorganic particles and organic materials. This process can also occur in the earthworm's gut. Fungal hyphae and plant roots can hold aggregates together (Totsche et al., 2010). Moreover, surface-adhered microbial colonies facilitate mineral weathering to affect soil formation and pore size and shape (Goudie and Viles, 2012; Tecon and Or, 2017). Metal ions (e.g., Ca^{2+}, Mg^{2+}, Al^{3+}, and Fe^{3+}) in soil change soil structure through cationic bridging with clay particles and soil organic matter. The cation Na^{+} is a highly dispersive agent, due to its large hydrated radius, resulting directly in the breakup (i.e., dispersion) of aggregates which directly influence soil pore systems (Bronick and Lal, 2005). Many agricultural management practices affect soil pore systems: tillage, mulching and residue management, manuring, crop cultivation, and mechanical compaction. Tillage can disrupt soil aggregates, compact soil, disturb plant and animal communities that contribute to aggregation, inhibit microbial and faunal activities that contribute to aggregation (Bronick and Lal, 2005). Increased tillage can result in the reduction of macropores and biochannels that influence water movement (e.g., preferential flow) and nutrient availability. Mulch and crop residue management

can increase aggregate and soil pore stability by decreasing erosion. Manuring results in increased porosity by increasing biological activity. Crop cultivation can change soil aggregate by crop rotations and cover cropping. Mechanical compaction due to tracked heavy machines and cattle trampling affects soil deformation. It can reduce total porosity and the proportion of larger pores and increase bulk density (Gabriels et al., 2020; Gürsoy, 2021).

The soil pore system (i.e., pore shape, pore size distribution, pore arrangement) could affect many important processes that are related to plant growth, such as storage and movement of water and gases, solute movements, ease of root growth (Ochsner, 2022). There are two specific requirements. Firstly, soil must have enough large pores. Large pores allow rapid infiltration of surface water followed by early drainage and oxygen does not become limiting. Large pores also favor the initiation of root growth. Secondly, since large pores have poor water holding capacity, the soil should have enough small pores to resist gravitational drainage (Cary and Hayden, 1973). Although the pores larger than 500 μm have some useful effects on root penetration and water movement, when the soil with a high percentage of this pore class (>70-80% of the total porosity), the stability of soil aggregates is poor due to surface cracks developed after irrigation or rainfall, which does not favor plant growth (Pagliai et al., 1983).

1.2.3 Soil surface

Soil has high specific surface area with values ranging between 10^{-1} to 10^{2} m^2 g^{-1} from sandy to clayey soils (Tecon and Or, 2017). Despite high bacterial abundance in soil, only 0.1% of the surface area is estimated to be covered by bacterial cells (Chenu and Stotzky, 2001; Schmidt and Eickhorst, 2014; Young et al., 2008). Raynaud and Nunan (2014) estimated that if a soil with moderate specific surface area of 10^{1} m^2 g^{-1}, bacterial density of 10^{10} cells g^{-1} and 1000

cells per colony that are uniformly distributed over the surface would yield average spacing between adjacent colonies of 500 μm in radius. Therefore, the separation distances of bacteria on soil surfaces likely impacts bacterial mobility, dispersion, and cell-cell interactions between colonies.

Bacterial adhesion on soil surfaces is influenced by many factors, including material and cell surface properties (e.g., surface charge, surface wettability, roughness, topography, stiffness, and combination of properties). The impact of surface charge on bacterial adhesion can be described using the classical theory of Derjaguin, Landau, Verwey, and Overbeek (DLVO) (Derjaguin, 1934; Derjaguin and Landau, 1941; Verwey et al., 1948) (Azeredo et al., 1999; Michen and Graule, 2010; Zhang et al., 2019). According to DLVO theory, van der Waals and electrostatic interactions are major forces that determine cellular interactions with soil surfaces (Renner and Weibel, 2011). If the net charge of soil particles is equal to zero at a particular pH, this electrically neutral state is termed an isoelectric point (IEP) (Michen and Graule, 2010). The same term also applies to bacteria (Michen and Graule, 2010). The IEP of a bacterium is determined by the balance between charging of anionic and cationic acid/base groups in the cell surface, as well as specific adsorption of some ions at the cell surface (Rijnaarts et al., 1995). Bacterial cell wall surfaces contain carboxyl, amino, and phosphate groups, which can gain or lose a proton giving the cell surface a net electrical charge under different pH of the surrounding environment (Rijnaarts et al., 1999). At typical soil pH, bacteria usually possess a net negative charge, and thereby exhibit more adhesion on positively charged surfaces (Chen et al., 2019; Kovačević et al., 2016; Oh et al., 2018). For example, previous studies demonstrated that bacteria, such as *Pseudomonas aeruginosa*, *Escherichia coli*, and *Staphylococcus aureus*, had greater adhesion on positively charged poly acrylic acid (PAA), poly allylamine hydrochloride

(PAHC), and poly diallyldimethylammonium chloride (PDADMAC) surfaces (Kovačević et al., 2016; Zhu et al., 2015), while reduced bacterial adhesion was observed on the negatively-charged poly styrenesulfonate (PSS) and polyeletrolyte multilayers (PEM) surfaces (Guo et al., 2018; Kovačević et al., 2016). However, despite negatively charged surfaces that inhibit bacterial adhesion, some bacteria can overcome the electrostatic repulsion and even bind to the surfaces due to their surface appendages (e.g., fimbriae) (Ueshima et al., 2002). Ionic strength of the background electrolyte is also a critical factor influencing bacterial adhesion in porous media. The electric double layer energy of interaction is dependent on the ionic strength of the medium. The ionic strength is directly correlated with the thickness of the double layer (Azeredo et al., 1999). In the DLVO theory, an increase in bacterial adhesion can occur when the electric double layer is compressed due to the increased concentration of electrolytes in the range of 0 to 0.1-0.2 M (Mills et al., 1994).

Hydrophobicity is an important factor that governs bacterial adhesion. Previous studies observed that bacteria with hydrophobic cell surfaces prefer hydrophobic material surfaces while those with hydrophilic cell surfaces prefer hydrophilic material surfaces (An and Friedman, 1998; Krasowska and Sigler, 2014). The influence of surface roughness on bacterial adhesion has also been investigated. In general, surface roughness positively correlates with the degree of bacterial adhesion (Cheng et al., 2019). Higher surface roughness provides a concave area for bacterial adhesion due to the increases of surface area and protects bacteria against shear forces (Bollen et al., 1996; Shen et al., 2020; Yoda et al., 2014). Surface topography affects bacterial adhesion by changing physicochemical properties of the surface. The main mechanisms of the effects of surface topography on bacterial adhesion include physicochemical forces, cell membrane deformation, chemical gradients at the solid-liquid interface, hydrodynamics, surface

wettability and air entrapment, and topography-induced cell ordering and segregation (Cheng et al., 2019). Stiffness is another important factor. Bacterial adhesion increases with increasing stiffness of poly(ethylene glycol) dimethacrylate (PEGDMA) and agar hydrogels surfaces (Guégan et al., 2014; Kolewe et al., 2015). However, a negative correlation between polydimethysiloxane (PDMS) surface stiffness and adhesion was observed (Song et al., 2018; Straub et al., 2019).

1.2.4 Soil aqueous phase

Soil water types include gravitational water, capillary water, and hygroscopic water. Gravitational water is that in soil large pores and is readily lost by gravitational force. Capillary water resides in soil micropores and is retained against the force of gravity due to capillary or matric forces. Hygroscopic water describes water held at very high energy very near the soil surfaces. This water is held so tightly it cannot be removed even by evaporative forces or root suction.

Soil water content is considered saturated when all the pore space is filled with water. Soil is in this state only during intense rainfall or flooding events. Most of the time, soil is unsaturated. The water remaining in the soil is retained by capillary forces in corners and crevices between soil grains or adsorbed as thin liquid films on soil surfaces (Or et al., 2007; Tecon and Or, 2017). Soil water potential is used to define the energy state of soil water. Total soil water potential is the sum of matric, osmotic, gravitational, and pressure potentials. In unsaturated soils, matric potential resulting from capillarity and adsorption is the primary component as most of the water in macropores has drained away due to gravity. Pore size and pore shape as well as surface properties determine soil water matric potential (Hillel, 2003).

Soil pore architecture can cause water hysteresis during wetting (sorption) and drying (desorption). Essentially, water hysteresis is a phenomenon at the same water matric potential the equilibrium water content is higher during drying than in wetting. There are two possible causes: the "ink bottle" effect and air entrapment (Ochsner, 2022). The ink bottle is an analogy of soil pores with a non-uniform radius. Capillary rise is an important phenomenon that can cause the ink bottle effect. Capillary rise is the process that a liquid can rise in a narrow space against the force of gravity due to the attractive forces between the liquid and surrounding solid surfaces. The capillary meniscus forms in this phenomenon. The height of the meniscus can be obtained from the equation below:

$$h = \frac{2\sigma \cos \alpha}{\rho g r}$$

where σ is the surface tension of the fluid (N m^{-1}), α is the contact angle of the liquid-gas interface on the wall of the tube, ρ is the fluid density (kg m^{-3}), g is the acceleration due to gravity (m s^{-2}), and r is the radius of the capillary (m). From the equation, the smaller the radius of the capillary (r), the greater the height of the capillary meniscus. If there are two types of capillary tubes inserted into water, one is a uniformly narrow tube, and another is non-uniform with narrow open and end but relatively large cavity in the middle. During wetting, capillary rise could only rise water to the bottom of the middle cavity. During drying, water can be retained in the cavity. Thus, the non-uniformity of soil pores can cause hysteresis during wetting and drying cycles. The second potential cause of water hysteresis is air entrapment. Air can be trapped in the interior soil pores when a drained soil is rewetted. This air cannot be removed easily. During rewetting, the maximum value of soil water content is lower than the true saturated water content. However, the impact of air-entrapment can be changed over time through soil chemical, physical, and biological processes. Such hysteresis results in heterogeneity of resource

distribution, which is connected to changes in soil resource availability for bacteria, particularly to changes in dissolved organic carbon and nitrogen species (Banerjee et al., 2016; Lal, 2006).

1.3 Influence of soil pores on microbial motility, dispersion, and interaction in soil

The soil pore system influences the soil microbial community through spatial isolation, water availability, nutrient availability, gas diffusion, chemical signal diffusion, changes in salinity, and protection from predators. The complexity of the soil pore network can cause periods of bacterial spatial isolation from neighboring cells and/or nutrients and resources. The spatial isolation limits bacterial dispersion and interaction with others. When two bacterial colonies are separated in unconnected pores or the physical pathways are too small for the passage of cells, these two colonies cannot contact and physically interact even though the distance separating them is very small. If the pores housing the separated colonies of cells are hydrologically connected, small soluble molecules can be exchanged offering indirect interactions. Once hydrologic connectivity is broken during drying only gaseous substances can be exchanged. A previous study estimated that 15%-50% of the soil porosity is physically inaccessible to bacterial cells due to the entrapment of cells in closed pores or pore throats smaller than 0.2 μm (Chenu and Stotzky, 2001).

Bacteria in soils mainly rely on the liquid phase for motility. When soil is nearly saturated or very wet, the advection of water can transport bacteria for a long distance at rates that exceed 1 m day^{-1} (Wang et al., 2013). However, in unsaturated soils advective transport is not possible. Dry conditions strongly limit bacterial movement (Gargiulo et al., 2008; Or et al., 2007). During drying, the remaining liquid in soils is typically adsorbed as thin water films on soil surfaces or retained by capillary forces in corners and crevices (Or et al., 2007). If the value

of soil matric potential is known, the thickness of aqueous films adsorbed by van der Waals surface forces on soil surface can be predicted. The thickness of the water film on the soil surface is predicted based on the equation below:

$$l(\mu) = \sqrt[3]{\frac{A_{svl}}{6\pi\rho\mu}}$$

where l is water film thickness, the unit is m, A_{svl} is the Hamaker constant (~ -6×10^{-20} J for water on silicate surfaces), ρ is water density (1,000 kg m^{-3}), and μ is the matric water potential (Pa). The equation is assumed on most smooth mineral surfaces. The calculated thickness of water films ranges from 10 to 20 nm at relatively wet conditions near field capacity (matric potential of -5 to -30 kPa). However, for the natural soil, the water films are at least one order of magnitude thicker than the predicted values. It is reasonable to consider capillary condensation within the surface roughness elements and additional surface forces such as electrostatic interaction effects (Tuller and Or, 2005; Wang and Or, 2010). Even so, the water films are still too thin to support immersion of bacterial cells (~0.2 to 5 μm) or cell motion at low matric potential conditions. The following equation gives the maximum size of a spherical or cylindrical bacterial cell that would be fully immersed in liquid behind a curved liquid-gas meniscus:

$$R = r(\mu)\frac{1-\sin\alpha}{1+\sin\alpha}$$

$$r(\mu) = \frac{\sigma}{|\mu|}$$

where R is the maximum radius, α is the angle between two surfaces forming a crevice or channels, σ is the liquid-gas surface tension (0.073 J m^{-2}), and $r(\mu)$ is the radius of curvature of the liquid-gas meniscus which is determined via the Young-Laplace equation. For example, for α=30º and μ=-30 kPa (field capacity), the value of R is equal to 0.81 μm which is smaller than

average bacterial cell sizes. Therefore, unsaturated conditions restrict bacterial motion but promote bacterial attachment on soil surface. Soil pore water velocity also influences bacteria movement. For example, increased pore water velocity due to high rainfall intensity can increase bacterial release rates from soil and favor bacteria transport (Blaustein et al., 2016).

Nutrients, gas diffusive fluxes, bacterial chemical signal, and salinity in highly heterogeneous soil pores constantly fluctuate under natural conditions. These patchy resource distributions in unsaturated soils play important roles in bacteria distribution, diversity and function (Young and Crawford, 2004). Soil bacteria could be divided into two groups based on their growth strategies (i.e., copiotrophs and oligotrophs) (Fierer et al., 2007). The nutrient gradients in soils might shape the distribution and activity of these two groups. In addition, large pores with high oxygen concentration are dominated by aerobic bacteria while small pores contain aerobic and anaerobic bacteria (Gupta and Germida, 2015). In soil pores, gas diffusion and supply of nutrients are strongly influenced by soil water content. As the fraction of water-filled pores increases with wetting, an increase in diffusion of soluble nutrients and a reduction in gas diffusion occurs. Consequently, these two opposing processes determine aerobic bacterial activity (Moyano et al., 2013). Moreover, soil water content is related to the substrate availability for bacteria as the energy driving them to mine nutrients concentrated in the mineral-associated organic matter pool (Jilling et al., 2018; Keiluweit et al., 2015; Nottingham et al., 2015). Under wetter conditions, the persistence of mineral-associated organic matter is linked to it concentration, while the relationship is weaker or absent under drier conditions (Heckman et al., 2023). Further, soil pore geometry and air-water interfaces can influence the diffusion, exchange and activity of bacterial chemical signals, such as small peptides and acyl-homoserine lactones (Papenfort and Bassler, 2016; Tecon and Or, 2017). Salinity varies spatially and temporally in

soils, and it affects bacteria via changes in the osmotic potential. Wetting and drying induce osmotic stress in bacteria. Hypoosmotic stress may lead to cell lysis and hyperosmotic stress also has influences on bacterial growth and activity. In addition to osmotic effects, high salt results in cation-specific inhibition of metabolic processes, the suppression of microbial attachment to surface via increased ionic strength, or inhibition of bacterial mobility (Or et al., 2007). Overall, high salinity in soils leads to cell death, lower metabolism, and lower cell mobility, thereby affecting the interactions between cells or between cell and viruses.

Soil bacteria can be preyed upon by other bacteria, fungi, and protozoa. They can also be infected by bacteriophages (i.e., viruses that infect bacteria). The soil pore system has direct impact on bacterial social interactions. Species that coexistence within soil pore spaces could increase the potential for physical interactions while separation in different pores would minimize interactions. For example, the pore volume available for viruses, bacteria, and protozoa is different due to their different sizes. The pore volume available for protozoa (assumed size >10 μm) is just one third of the volume available for bacteria. For viruses, they can access all the pores available for bacteria (Kuzyakov and Mason-Jones, 2018). The soil pores provide a shelter for bacteria from the predation of protozoa although bacteria cannot escape viral infection from physical separation and must rely on other defense mechanisms.

1.4 Tools to study microbial activity in soil

There are several modern characterization techniques that allow for investigation of 2D and 3D microstructures of soil pores and for correlating the structure to microbial activity. The characterization techniques include ultra-small angle or small angle neutron and x-ray scattering (e.g., U/SANS and U/SAXS) focused ion beam tomography (FIB-T), electron tomography (ET),

atom probe tomography (APT), backscattered scanning electron microscopy (BSEM), X-ray computed tomography (XCT), mercury intrusion porosimetry (MIP), and physical gas adsorption (Cnudde and Boone, 2013; Giesche, 2006; Groen et al., 2003; Keller et al., 2011; Radlinski, 2006; Zachara et al., 2016). The characteristics of pores from nanoscale to microscale, including pore volume, pore size distribution, pore connectivity, and pore geometry, could be obtained by these techniques. Further, combining isotope labeling with imaging techniques is a powerful tool for distinguishing microbes from the porous matrix with nanometer or micrometer resolution (Wilpiszeski et al., 2019). In addition to directly characterizing the microbes in soil pores using nanoscale techniques, artificial soil pore systems might also be used for the studies of microbes at relevant pore scales. Artificial soil pore systems can simulate measured pore properties of real soil. Using 3D printing technology and microfluidic approaches create defined pore systems to study microbial communities at different length scales (e.g., nano, micro) (Borer et al., 2018). Moreover, the mathematical modeling directly replicate soil structure and microbial activity (Wu et al., 2012).

Compared with other techniques, U/SANS and U/SAXS are the only non-intrusive techniques allowing exploration of pore structure (Melnichenko, 2016). In addition, U/SANS and U/SAXS enjoy the advantage of measuring total porosity and pore morphology with detecting both closed and open pores over a wide range from 10Å to 25 μm (Anovitz and Cole, 2015). U/SANS and U/SAXS can also provide the textural properties (e.g., surface roughness or aggregation) by giving fractal information of the pore network (Liu et al., 2021). These two techniques are based on the same principle, which refers to the deflection of a beam of radiation (X-ray or neutron) from its original direction by interaction with the electrons (X-ray scattering) or nuclei (neutron scattering) (Glatter et al., 1982; Melnichenko, 2016). Neutrons and X-rays

have been widely used for the microscale and nanoscale structural characterization. Materials such as porous solids, bones, cements, rocks, and clays, have heterogeneous structure with length scales from nanometers to microns. The application of complementary neutron and X-ray scattering methods allow characterization of such multi-hierarchical structures all levels. The parameters include averaged particle sizes, shapes, distribution, and surface-to-volume ratio. Both neutrons and X-rays are sensitive to the detailed 3D structure, but these two probes also interact differently with materials. X-ray photons interact primarily with the electron cloud surrounding the atomic nucleus. X-rays are less sensitive to light atoms. They are suitable for high-resolution imaging which is useful for structural studies of single particles. Neutrons interact with the nuclei of the specimen. They are particularly sensitive to light atoms and have high penetration. Neutrons are suitable for studying the dynamics and structure of interacting assemblies of particles (e.g., Fe or Co nanoparticles) (Thomson et al., 2005). Therefore, the sum of the information obtained from these two advanced techniques would be greater than that obtained from either technique separately.

The intensity, *I*, of the scattered neutrons or X-rays is measured as a function of the scattering vector, *Q*, which is related to the wavelength, λ, and scattering angle, θ, by $Q = (4\pi/\lambda)\sin\theta$. The function of the intensity, *I*(*Q*), and the scattering vector, *Q*, is determined by the geometry of the pore-matrix interface at various length scales (Figure 1.2). The scattering pattern can be related to pore size distribution if the shape of the pores is known or assumed. The relationship can be described as shown in the equation below:

$$I(Q) = N(\Delta\rho^*)^2 \int V^2(r) f(r) P(Q,r) dr + Bkg$$

where *N* is the number density of scatterers (e.g., pores), $(\Delta\rho^*)^2$is the scattering contrast between the pore and solid matrix which equals the difference of scattering length density (SLD) between

the pore and solid matrix, $V(r)$ is the pore volume, $f(r)$ is the pore size distribution, and Bkg is the scattering background. $P(Q, r)$ is the scattering form factor that describes scattering from a single pores and is dependent on both its shape and size. (Figure 1.3). Example shows in Figure 1.3.

1.5 Rationale, approach, hypotheses, and research objectives

As a porous "skin" of the Earth, soil has a complex architecture yielding a heterogeneous pore system. This porous system regulates water dynamics and drives microbial activities (e.g., dispersion, retention, mobility, and cell-to-cell interactions). However, agricultural management practices modify the soil porous system and then affect soil water dynamics and microbial activities. Therefore, the relationships among soil pore networks, water, and microbes are significant for optimizing agricultural management practices. Based on the literature review, no direct evidence showed how soil pore characteristics (e.g., size, shape, connectivity) control cell-to-cell interactions and the distribution of bacteria and viruses. In addition, previous studies paid little attention to the soil pores, which couple hydrology and solution chemistry, in influencing the spatial distribution of bacteria and viruses. The use of small-angle scattering techniques could be a powerful approach to examining the distribution of microbes in the porous system under variable conditions.

The overall goal of this project was to explore how soil pores influence soil water retention and bacterial interactions and quantify how spatial distribution of bacteria and viruses in fine scale soil aggregates. To achieve the goal, this research developed a mathematical model (Task 1), employing microcosm experiments (Task 2), and used small angle scattering techniques (Task 3) to implement three research tasks. Specifically, we proposed a fractional bulk density (FBD) concept, which was used to develop a mathematical model to estimate pore

water content under varying matric potential. Next, the FBD concept was used to explore bacterial cell-to-cell physical encounters and interactions in laboratory-scale sand microcosms with different pore size distributions. Additionally, the influence of soil surface properties on bacterial cell-to-cell interactions was evaluated using model cell bioreporters previously developed to estimate cell-cell interactions via conjugation; a horizontal gene transfer mechanism in bacteria that requires physical cell-cell contact. In these microcosm experiments, bacterial cells *Psudomonas putida* (*P. putida*) KT2440 as the recipient strain and *P. putida* KT2440::*lacl*^{q}*-pLpp-mCherry-Km*^{R} as donor strain were used to observe the exchange of a conjugative plasmid as a proxy for physical cell-cell interactions (Klümper et al., 2015). The number of bacterial cells was enumerated by cultivation on solid selective media. Soil aggregates were used as porous matrices to evaluate water-microbe interactions in pores. Bacteriophage, MS2, and its host, *E. coli* C3000, were chosen as model bacteria and virus the experiments in Task 3. The bacteria/viruses were equilibrated in porous matrices (soil macroaggregates) under saturated conditions. After equilibrium, the samples were analyzed by SAS techniques. The USAXS, SANS, and USANS data were corrected and analyzed using a software package "IRENA" for analysis to obtain pore size distribution.

The current research is based on the following hypotheses:

Hypothesis 1: Soil water retention characteristic can be estimated by a modeling approach based on the impacts of soil pores on water conservation.

Hypothesis 2: Soil pore systems have a directly influence on physical contact-based bacterial interactions, such as conjugation. The frequency of bacterial interactions is a function of pore

size distribution and bacterial adhesion on sand surfaces with larger pores and more adhesion lowering the frequency.

Hypothesis 3: Bacteria prefer to stay in the pores closest to their sizes on micro-scale of soil pores. Viruses are ubiquitous on micro- and nano-scales but have highly abundant in locations of bacteria.

The research objectives, based on the hypotheses, are as follows:

Objective 1: To identify and estimate soil water retention characteristics for all soil textures and a wide range of soil bulk density using a modeling approach.

Objective 2: To investigate if and how different sized pores and bacterial adhesion influence cell-to-cell interactions.

Objective 3: To characterize the distribution of bacteria and viruses in differently sized pores of soil aggregates.

References

An YH, Friedman RJ. Concise review of mechanisms of bacterial adhesion to biomaterial surfaces. Journal of biomedical materials research 1998; 43: 338-348.

Angers D, Giroux M. Recently deposited organic matter in soil water‐stable aggregates. Soil Science Society of America Journal 1996; 60: 1547-1551.

Anovitz LM, Cole DR. Characterization and analysis of porosity and pore structures. Reviews in Mineralogy and geochemistry 2015; 80: 61-164.

Azeredo J, Visser J, Oliveira R. Exopolymers in bacterial adhesion: interpretation in terms of DLVO and XDLVO theories. Colloids and Surfaces B: Biointerfaces 1999; 14: 141-148.

Bahadur J, Radlinski AP, Melnichenko YB, Mastalerz M, Schimmelmann A. Small-angle and ultrasmall-angle neutron scattering (SANS/USANS) study of New Albany shale: A treatise on microporosity. Energy & Fuels 2015; 29: 567-576.

Bailey VL, McCue LA, Fansler SJ, Boyanov MI, DeCarlo F, Kemner KM, et al. Micrometer-scale physical structure and microbial composition of soil macroaggregates. Soil Biology and Biochemistry 2013; 65: 60-68.

Banerjee S, Helgason B, Wang L, Winsley T, Ferrari BC, Siciliano SD. Legacy effects of soil moisture on microbial community structure and N2O emissions. Soil Biology and Biochemistry 2016; 95: 40-50.

Bhatty M, Gomez JAL, Christie PJ. The expanding bacterial type IV secretion lexicon. Research in microbiology 2013; 164: 620-639.

Bi L, Yu DT, Du S, Zhang LM, Zhang LY, Wu CF, et al. Diversity and potential biogeochemical impacts of viruses in bulk and rhizosphere soils. Environmental microbiology 2021; 23: 588-599.

Blaustein RA, Hill RL, Micallef SA, Shelton DR, Pachepsky YA. Rainfall intensity effects on removal of fecal indicator bacteria from solid dairy manure applied over grass-covered soil. Science of the Total Environment 2016; 539: 583-591.

Bollen CM, Papaioanno W, Van Eldere J, Schepers E, Quirynen M, Van Steenberghe D. The influence of abutment surface roughness on plaque accumulation and peri‐implant mucositis. Clinical oral implants research 1996; 7: 201-211.

Borer B, Tecon R, Or D. Spatial organization of bacterial populations in response to oxygen and carbon counter-gradients in pore networks. Nature communications 2018; 9: 769.

Børsheim KY. Native marine bacteriophages. FEMS Microbiology Ecology 1993; 11: 141-159.

Bronick CJ, Lal R. Soil structure and management: a review. Geoderma 2005; 124: 3-22.

Brum JR, Sullivan MB. Rising to the challenge: accelerated pace of discovery transforms marine virology. Nature Reviews Microbiology 2015; 13: 147-159.

Carminati A, Kaestner A, Ippisch O, Koliji A, Lehmann P, Hassanein R, et al. Water flow between soil aggregates. Transport in Porous Media 2007; 68: 219-236.

Carter MR, Stewart BA. Structure and organic matter storage in agricultural soils. Vol 8: CRC press, 1995.

Cary J, Hayden C. An index for soil pore size distribution. Geoderma 1973; 9: 249-256.

Chen C, Petterson Tr, Illergård J, Ek M, Wågberg L. Influence of cellulose charge on bacteria adhesion and viability to PVAm/CNF/PVAm-modified cellulose model surfaces. Biomacromolecules 2019; 20: 2075-2083.

Cheng Y, Feng G, Moraru CI. Micro-and nanotopography sensitive bacterial attachment mechanisms: a review. Frontiers in microbiology 2019; 10: 191.

Chenu C, Stotzky G. Interactions between microorganisms and soil particles: an overview.

Interactions between soil particles and microorganisms: Impact on the terrestrial ecosystem 2001: 3-40.

Ciric V, Manojlovic M, Nesic L, Belic M. Soil dry aggregate size distribution: effects of soil type and land use. Journal of soil science and plant nutrition 2012; 12: 689-703.

Clarholm M. Interactions of bacteria, protozoa and plants leading to mineralization of soil nitrogen. Soil Biology and Biochemistry 1985; 17: 181-187.

Cnudde V, Boone MN. High-resolution X-ray computed tomography in geosciences: A review of the current technology and applications. Earth-Science Reviews 2013; 123: 1-17.

Crowther TW, Van den Hoogen J, Wan J, Mayes MA, Keiser A, Mo L, et al. The global soil community and its influence on biogeochemistry. Science 2019; 365.

Derjaguin B. Friction and adhesion. IV. The theory of adhesion of small particles. Kolloid Zeits 1934; 69: 155-164.

Derjaguin B, Landau L. The theory of stability of highly charged lyophobic sols and coalescence of highly charged particles in electrolyte solutions. Acta Physicochim. URSS 1941; 14: 58.

Dion P. Extreme views on prokaryote evolution. Microbiology of extreme soils 2008: 45-70.

Duiker SW, Rhoton FE, Torrent J, Smeck NE, Lal R. Iron (hydr) oxide crystallinity effects on soil aggregation. Soil Science Society of America Journal 2003; 67: 606-611.

Edwards AP, Bremner J. Microaggregates in soils 1. Journal of Soil Science 1967; 18: 64-73.

Emerson JB, Roux S, Brum JR, Bolduc B, Woodcroft BJ, Jang HB, et al. Host-linked soil viral ecology along a permafrost thaw gradient. Nature microbiology 2018; 3: 870-880.

Fierer N, Bradford MA, Jackson RB. Toward an ecological classification of soil bacteria. Ecology 2007; 88: 1354-1364.

Fuhrman JA. Marine viruses and their biogeochemical and ecological effects. Nature 1999; 399:

541-548.

Gabriels D, Horn R, Villagra M, Hartmann R. Assessment, prevention, and rehabilitation of soil structure caused by soil surface sealing, crusting, and compaction. Methods for assessment of soil degradation. CRC Press, 2020, pp. 129-165.

Gargiulo G, Bradford S, Simunek J, Ustohal P, Vereecken H, Klumpp E. Bacteria transport and deposition under unsaturated flow conditions: The role of water content and bacteria surface hydrophobicity. Vadose Zone Journal 2008; 7: 406-419.

Giesche H. Mercury porosimetry: a general (practical) overview. Particle & particle systems characterization 2006; 23: 9-19.

Glatter O, Kratky O, Kratky H. Small angle X-ray scattering: Academic press, 1982.

Goudie AS, Viles HA. Weathering and the global carbon cycle: Geomorphological perspectives. Earth-Science Reviews 2012; 113: 59-71.

Greenland D. Soil damage by intensive arable cultivation: temporary or permanent? Philosophical Transactions of the Royal Society of London. B, Biological Sciences 1977; 281: 193-208.

Groen JC, Peffer LA, Pérez-Ramírez J. Pore size determination in modified micro-and mesoporous materials. Pitfalls and limitations in gas adsorption data analysis. Microporous and mesoporous materials 2003; 60: 1-17.

Guégan C, Garderes J, Le Pennec G, Gaillard F, Fay F, Linossier I, et al. Alteration of bacterial adhesion induced by the substrate stiffness. Colloids and Surfaces B: Biointerfaces 2014; 114: 193-200.

Guglielmini J, de la Cruz F, Rocha EP. Evolution of conjugation and type IV secretion systems. Molecular biology and evolution 2013; 30: 315-331.

Guidi L, Chaffron S, Bittner L, Eveillard D, Larhlimi A, Roux S, et al. Plankton networks driving

carbon export in the oligotrophic ocean. Nature 2016; 532: 465-470.

Guo S, Kwek MY, Toh ZQ, Pranantyo D, Kang E-T, Loh XJ, et al. Tailoring polyelectrolyte architecture to promote cell growth and inhibit bacterial adhesion. ACS applied materials & interfaces 2018; 10: 7882-7891.

Gupta VV, Germida JJ. Soil aggregation: Influence on microbial biomass and implications for biological processes. Soil Biology and Biochemistry 2015; 80: A3-A9.

Gürsoy S. Soil compaction due to increased machinery intensity in agricultural production: its main causes, effects and management. Technology in Agriculture 2021: 1-18.

Han S, Delgado-Baquerizo M, Luo X, Liu Y, Van Nostrand JD, Chen W, et al. Soil aggregate size-dependent relationships between microbial functional diversity and multifunctionality. Soil Biology and Biochemistry 2021; 154: 108143.

Heckman KA, Possinger AR, Badgley BD, Bowman MM, Gallo AC, Hatten JA, et al. Moisture-driven divergence in mineral-associated soil carbon persistence. Proceedings of the National Academy of Sciences 2023; 120: e2210044120.

Hillel D. Introduction to environmental soil physics: Elsevier, 2003.

Hsieh Y-J, Wanner BL. Global regulation by the seven-component Pi signaling system. Current opinion in microbiology 2010; 13: 198-203.

Jastrow J. Soil aggregate formation and the accrual of particulate and mineral-associated organic matter. Soil Biology and Biochemistry 1996; 28: 665-676.

Jilling A, Keiluweit M, Contosta AR, Frey S, Schimel J, Schnecker J, et al. Minerals in the rhizosphere: overlooked mediators of soil nitrogen availability to plants and microbes. Biogeochemistry 2018; 139: 103-122.

John B, Yamashita T, Ludwig B, Flessa H. Storage of organic carbon in aggregate and density

fractions of silty soils under different types of land use. Geoderma 2005; 128: 63-79.

Jover LF, Effler TC, Buchan A, Wilhelm SW, Weitz JS. The elemental composition of virus particles: implications for marine biogeochemical cycles. Nature Reviews Microbiology 2014; 12: 519-528.

Keiluweit M, Bougoure JJ, Nico PS, Pett-Ridge J, Weber PK, Kleber M. Mineral protection of soil carbon counteracted by root exudates. Nature Climate Change 2015; 5: 588-595.

Keller LM, Holzer L, Wepf R, Gasser P, Münch B, Marschall P. On the application of focused ion beam nanotomography in characterizing the 3D pore space geometry of Opalinus clay. Physics and Chemistry of the Earth, Parts A/B/C 2011; 36: 1539-1544.

Klümper U, Riber L, Dechesne A, Sannazzarro A, Hansen LH, Sørensen SJ, et al. Broad host range plasmids can invade an unexpectedly diverse fraction of a soil bacterial community. The ISME journal 2015; 9: 934-945.

Kolewe KW, Peyton SR, Schiffman JD. Fewer bacteria adhere to softer hydrogels. ACS applied materials & interfaces 2015; 7: 19562-19569.

Koraimann G, Wagner MA. Social behavior and decision making in bacterial conjugation. Frontiers in cellular and infection microbiology 2014; 4: 54.

Kovačević D, Pratnekar R, Godič Torkar K, Salopek J, Dražić G, Abram A, et al. Influence of polyelectrolyte multilayer properties on bacterial adhesion capacity. Polymers 2016; 8: 345.

Kraemer SA, Wielgoss S, Fiegna F, Velicer GJ. The biogeography of kin discrimination across microbial neighbourhoods. Molecular ecology 2016; 25: 4875-4888.

Krasowska A, Sigler K. How microorganisms use hydrophobicity and what does this mean for human needs? Frontiers in cellular and infection microbiology 2014; 4: 112.

Kuzyakov Y, Mason-Jones K. Viruses in soil: nano-scale undead drivers of microbial life,

biogeochemical turnover and ecosystem functions. Soil Biology and Biochemistry 2018; 127: 305-317.

Lal R. Encyclopedia of soil science: CRC Press, 2006.

Little AE, Robinson CJ, Peterson SB, Raffa KF, Handelsman J. Rules of engagement: interspecies interactions that regulate microbial communities. Annu. Rev. Microbiol. 2008; 62: 375-401.

Liu C-W, Cheng S-W, Yu W-S, Chen S-K. Water infiltration rate in cracked paddy soil. Geoderma 2003; 117: 169-181.

Liu Y, Paskevicius M, Sofianos MV, Parkinson G, Li C-Z. In situ SAXS studies of the pore development in biochar during gasification. Carbon 2021; 172: 454-462.

Lobe I, Sandhage-Hofmann A, Brodowski S, Du Preez CC, Amelung W. Aggregate dynamics and associated soil organic matter contents as influenced by prolonged arable cropping in the South African Highveld. Geoderma 2011; 162: 251-259.

Macé K, Vadakkepat AK, Redzej A, Lukoyanova N, Oomen C, Braun N, et al. Cryo-EM structure of a type IV secretion system. Nature 2022; 607: 191-196.

Mann NH, Cook A, Millard A, Bailey S, Clokie M. Bacterial photosynthesis genes in a virus. Nature 2003; 424: 741-741.

McCarthy JF, Ilavsky J, Jastrow JD, Mayer LM, Perfect E, Zhuang J. Protection of organic carbon in soil microaggregates via restructuring of aggregate porosity and filling of pores with accumulating organic matter. Geochimica et Cosmochimica Acta 2008; 72: 4725-4744.

Melnichenko YB. Small-Angle Scattering from Con ned and Interfacial Fluids. 2016.

Michen B, Graule T. Isoelectric points of viruses. Journal of applied microbiology 2010; 109: 388-397.

Mills AL, Herman JS, Hornberger GM, DeJesús TH. Effect of solution ionic strength and iron coatings on mineral grains on the sorption of bacterial cells to quartz sand. Applied and Environmental Microbiology 1994; 60: 3300-3306.

Moyano FE, Manzoni S, Chenu C. Responses of soil heterotrophic respiration to moisture availability: An exploration of processes and models. Soil Biology and Biochemistry 2013; 59: 72-85.

Nottingham AT, Turner BL, Stott AW, Tanner EV. Nitrogen and phosphorus constrain labile and stable carbon turnover in lowland tropical forest soils. Soil Biology and Biochemistry 2015; 80: 26-33.

Ochsner TE. Rain or shine: An introduction to soil physical properties and processes. 2022. Published by Oklahoma State University Libraries under the Creative Commons Attribution 2022; 4: 94-99.

Oh JK, Yegin Y, Yang F, Zhang M, Li J, Huang S, et al. The influence of surface chemistry on the kinetics and thermodynamics of bacterial adhesion. Scientific reports 2018; 8: 17247.

Or D, Smets BF, Wraith J, Dechesne A, Friedman S. Physical constraints affecting bacterial habitats and activity in unsaturated porous media–a review. Advances in Water Resources 2007; 30: 1505-1527.

Pagliai M, Lamarca M, Lucamante G. Micromorphometric and micromorphological investigations of a clay loam soil in viticulture under zero and conventional tillage. Journal of Soil Science 1983; 34: 391-403.

Pagliai M, Vignozzi N. The soil pore system as an indicator of soil quality. Advances in GeoEcology 2002; 35: 69-80.

Papenfort K, Bassler BL. Quorum sensing signal–response systems in Gram-negative bacteria.

Nature Reviews Microbiology 2016; 14: 576-588.

Paul E. Soil microbiology, ecology and biochemistry: Academic press, 2014.

Paul J, Rose J, Jiang S, Kellogg C, Dickson L. Distribution of viral abundance in the reef environment of Key Largo, Florida. Applied and environmental microbiology 1993; 59: 718-724.

Peng X, Horn R. Anisotropic shrinkage and swelling of some organic and inorganic soils. European Journal of Soil Science 2007; 58: 98-107.

Rabot E, Wiesmeier M, Schlüter S, Vogel H-J. Soil structure as an indicator of soil functions: a review. Geoderma 2018; 314: 122-137.

Radlinski AP. Small-angle neutron scattering and the microstructure of rocks. Reviews in Mineralogy and Geochemistry 2006; 63: 363-397.

Raynaud X, Nunan N. Spatial ecology of bacteria at the microscale in soil. PloS one 2014; 9: e87217.

Renner LD, Weibel DB. Physicochemical regulation of biofilm formation. MRS bulletin 2011; 36: 347-355.

Rijnaarts HH, Norde W, Lyklema J, Zehnder AJ. The isoelectric point of bacteria as an indicator for the presence of cell surface polymers that inhibit adhesion. Colloids and Surfaces B: Biointerfaces 1995; 4: 191-197.

Rijnaarts HH, Norde W, Lyklema J, Zehnder AJ. DLVO and steric contributions to bacterial deposition in media of different ionic strengths. Colloids and Surfaces B: Biointerfaces 1999; 14: 179-195.

Rodríguez-Beltrán J, DelaFuente J, Leon-Sampedro R, MacLean RC, San Millan A. Beyond horizontal gene transfer: the role of plasmids in bacterial evolution. Nature Reviews

Microbiology 2021; 19: 347-359.

Roux S, Brum JR, Dutilh BE, Sunagawa S, Duhaime MB, Loy A, et al. Ecogenomics and potential biogeochemical impacts of globally abundant ocean viruses. Nature 2016; 537: 689-693.

Schlüter S, Sammartino S, Koestel J. Exploring the relationship between soil structure and soil functions via pore-scale imaging. Elsevier, 2020.

Schmidt H, Eickhorst T. Detection and quantification of native microbial populations on soil-grown rice roots by catalyzed reporter deposition-fluorescence in situ hybridization. FEMS microbiology ecology 2014; 87: 390-402.

Sexstone AJ, Revsbech NP, Parkin TB, Tiedje JM. Direct measurement of oxygen profiles and denitrification rates in soil aggregates. Soil science society of America journal 1985; 49: 645-651.

Sey BK, Manceur AM, Whalen JK, Gregorich EG, Rochette P. Small-scale heterogeneity in carbon dioxide, nitrous oxide and methane production from aggregates of a cultivated sandy-loam soil. Soil Biology and Biochemistry 2008; 40: 2468-2473.

Shen C, Jin Y, Zhuang J, Li T, Xing B. Role and importance of surface heterogeneities in transport of particles in saturated porous media. Critical Reviews in Environmental Science and Technology 2020; 50: 244-329.

Six J, Elliott E, Paustian K. Aggregate and soil organic matter dynamics under conventional and no‐tillage systems. Soil Science Society of America Journal 1999; 63: 1350-1358.

Six J, Elliott E, Paustian K. Soil structure and soil organic matter II. A normalized stability index and the effect of mineralogy. Soil Science Society of America Journal 2000; 64: 1042-1049.

Six J, Paustian K. Aggregate-associated soil organic matter as an ecosystem property and a measurement tool. Soil Biology and Biochemistry 2014; 68: A4-A9.

Song F, Wang H, Sauer K, Ren D. Cyclic-di-GMP and oprF are involved in the response of Pseudomonas aeruginosa to substrate material stiffness during attachment on polydimethylsiloxane (PDMS). Frontiers in microbiology 2018; 9: 110.

Soucy SM, Huang J, Gogarten JP. Horizontal gene transfer: building the web of life. Nature Reviews Genetics 2015; 16: 472-482.

Steward GF, Smith DC, Azam F. Abundance and production of bacteria and viruses in the Bering and Chukchi Seas. Marine Ecology Progress Series 1996; 131: 287-300.

Straub H, Bigger CM, Valentin J, Abt D, Qin XH, Eberl L, et al. Bacterial adhesion on soft materials: passive physicochemical interactions or active bacterial mechanosensing? Advanced healthcare materials 2019; 8: 1801323.

Sullivan MB, Lindell D, Lee JA, Thompson LR, Bielawski JP, Chisholm SW. Prevalence and evolution of core photosystem II genes in marine cyanobacterial viruses and their hosts. PLoS Biol 2006; 4: e234.

Suttle CA. Marine viruses—major players in the global ecosystem. Nature reviews microbiology 2007; 5: 801-812.

Tecon R, Ebrahimi A, Kleyer H, Levi SE, Or D. Cell-to-cell bacterial interactions promoted by drier conditions on soil surfaces. Proceedings of the National Academy of Sciences 2018; 115: 9791-9796.

Tecon R, Or D. Biophysical processes supporting the diversity of microbial life in soil. FEMS microbiology reviews 2017; 41: 599-623.

Thomson T, Lee S, Toney M, Dewhurst C, Ogrin F, Oates C, et al. Agglomeration and sintering in annealed FePt nanoparticle assemblies studied by small angle neutron scattering and x-ray diffraction. Physical Review B 2005; 72: 064441.

Tisdall JM, Oades JM. Organic matter and water‐stable aggregates in soils. Journal of soil science 1982; 33: 141-163.

Totsche KU, Rennert T, Gerzabek MH, Kögel‐Knabner I, Smalla K, Spiteller M, et al. Biogeochemical interfaces in soil: the interdisciplinary challenge for soil science. Journal of Plant Nutrition and Soil Science 2010; 173: 88-99.

Trefalt G, Borkovec M. Overview of DLVO theory. Laboratory of Colloid and Surface Chemistry, University of Geneva, Switzerland 2014; 304.

Tuller M, Or D. Water films and scaling of soil characteristic curves at low water contents. Water Resources Research 2005; 41.

Ueshima M, Tanaka S, Nakamura S, Yamashita K. Manipulation of bacterial adhesion and proliferation by surface charges of electrically polarized hydroxyapatite. Journal of Biomedical Materials Research: An Official Journal of The Society for Biomaterials, The Japanese Society for Biomaterials, and The Australian Society for Biomaterials and the Korean Society for Biomaterials 2002; 60: 578-584.

Van Elsas JD, Trevors JT, Jansson JK, Nannipieri P. Modern soil microbiology: CRC press, 2006.

Van Elsas JD, Trevors JT, Rosado AS, Nannipieri P. Modern soil microbiology: CRC press, 2019.

Velicer GJ, Vos M. Sociobiology of the myxobacteria. Annual review of microbiology 2009; 63: 599-623.

Verwey EJW, Overbeek JTG, Van Nes K. Theory of the stability of lyophobic colloids: the interaction of sol particles having an electric double layer: Elsevier Publishing Company, 1948.

Waksman G. From conjugation to T4S systems in Gram‐negative bacteria: a mechanistic biology perspective. EMBO reports 2019; 20: e47012.

Wang G, Or D. Aqueous films limit bacterial cell motility and colony expansion on partially saturated rough surfaces. Environmental Microbiology 2010; 12: 1363-1373.

Wang Y, Bradford SA, Šimůnek J. Transport and fate of microorganisms in soils with preferential flow under different solution chemistry conditions. Water resources research 2013; 49: 2424-2436.

Weinbauer MG. Ecology of prokaryotic viruses. FEMS microbiology reviews 2004; 28: 127-181.

Weitz JS, Wilhelm SW. Ocean viruses and their effects on microbial communities and biogeochemical cycles. F1000 biology reports 2012; 4.

Wilkins BM. Plasmid promiscuity: meeting the challenge of DNA immigration control. Environmental Microbiology 2002; 4: 495-500.

Williamson KE, Fuhrmann JJ, Wommack KE, Radosevich M. Viruses in soil ecosystems: an unknown quantity within an unexplored territory. Annual Review of Virology 2017; 4: 201-219.

Wilpiszeski RL, Aufrecht JA, Retterer ST, Sullivan MB, Graham DE, Pierce EM, et al. Soil aggregate microbial communities: towards understanding microbiome interactions at biologically relevant scales. Applied and environmental microbiology 2019; 85: e00324-19.

Wommack K, Hill R, Kessel M, Russek-Cohen E, Colwell R. Distribution of viruses in the Chesapeake Bay. Applied and Environmental Microbiology 1992; 58: 2965-2970.

Wu M, Xiao F, Johnson-Paben RM, Retterer ST, Yin X, Neeves KB. Single-and two-phase flow in microfluidic porous media analogs based on Voronoi tessellation. Lab on a Chip 2012; 12: 253-261.

Yoda I, Koseki H, Tomita M, Shida T, Horiuchi H, Sakoda H, et al. Effect of surface roughness of

biomaterials on Staphylococcus epidermidis adhesion. BMC microbiology 2014; 14: 1-7.

Young IM, Crawford JW. Interactions and self-organization in the soil-microbe complex. Science 2004; 304: 1634-1637.

Young IM, Crawford JW, Nunan N, Otten W, Spiers A. Microbial distribution in soils: physics and scaling. Advances in agronomy 2008; 100: 81-121.

Zachara J, Brantley S, Chorover J, Ewing R, Kerisit S, Liu C, et al. Internal domains of natural porous media revealed: critical locations for transport, storage, and chemical reaction. Environmental Science & Technology 2016; 50: 2811-2829.

Zechner EL, Lang S, Schildbach JF. Assembly and mechanisms of bacterial type IV secretion machines. Philosophical Transactions of the Royal Society B: Biological Sciences 2012; 367: 1073-1087.

Zhang X, Zhou X, Xi H, Sun J, Liang X, Wei J, et al. Interpretation of adhesion behaviors between bacteria and modified basalt fiber by surface thermodynamics and extended DLVO theory. Colloids and Surfaces B: Biointerfaces 2019; 177: 454-461.

Zhu X, Jańczewski D, Guo S, Lee SSC, Parra Velandia FJ, Teo SL-M, et al. Polyion multilayers with precise surface charge control for antifouling. ACS applied materials & interfaces 2015; 7: 852-861.

Zimmerman AE, Howard-Varona C, Needham DM, John SG, Worden AZ, Sullivan MB, et al. Metabolic and biogeochemical consequences of viral infection in aquatic ecosystems. Nature Reviews Microbiology 2020; 18: 21-34.

Zwart K, Kuikman P, Van Veen J. Rhizosphere protozoa: their significance in nutrient dynamics. 1994.

Appendix

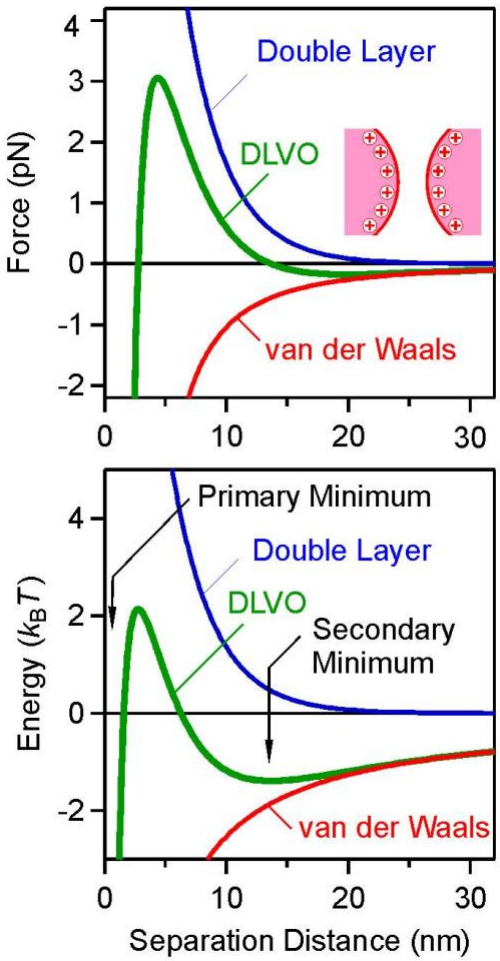

Figure 1.1 Conceptual diagram of DLVO theory (Trefalt and Borkovec, 2014).

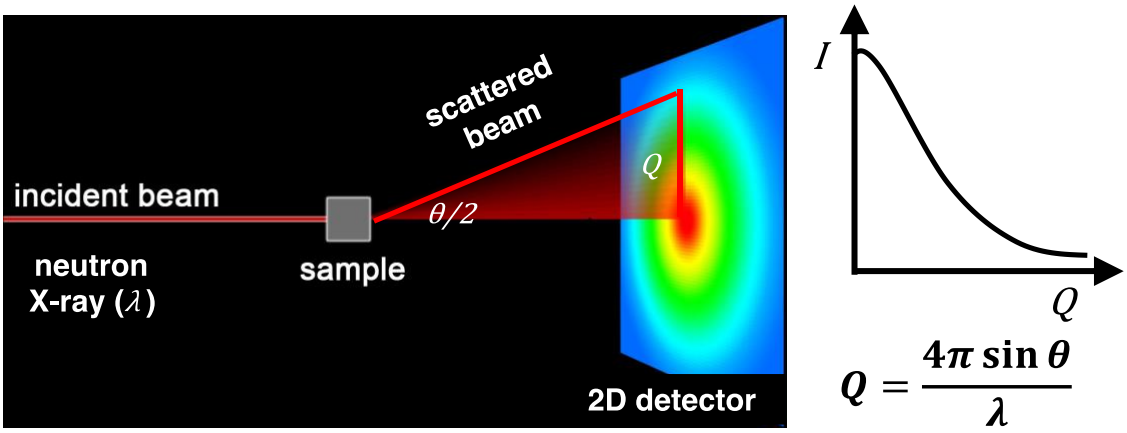

Figure 1.2 Schematic of small angle scattering technique.

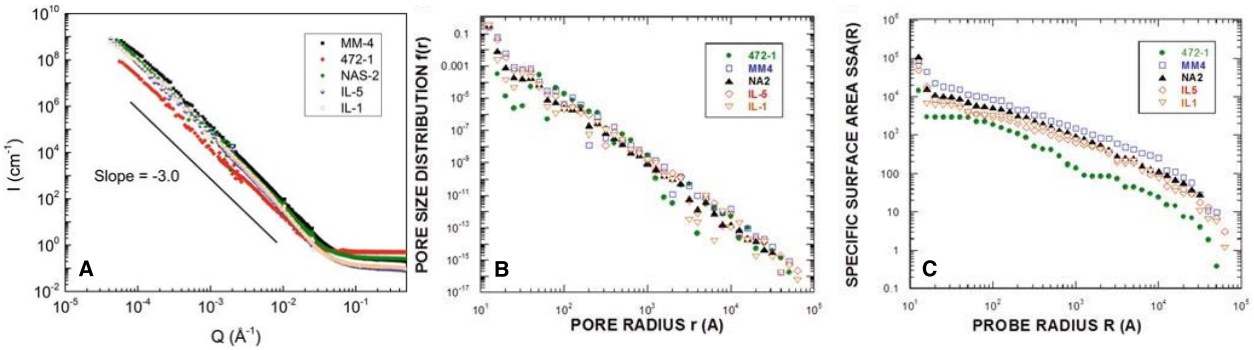

Figure 1.3 USANS and SANS profiles acquired from five samples of New Albany shales and data modeling (Bahadur et al., 2015). Panel (A) shows the *I* vs. *Q* and the straight line has a slope of -3 for comparison. Panel (B) shows pore size distribution calculated after model fitting. Panel (C) is specific surface area.

Chapter 2. Estimating Soil Water Retention for Wide Ranges of Pressure Head and Bulk Density Based on a Fractional Bulk Density Concept

Publication Note

The following chapter was published in the journal Scientific Report.

My contribution to this work was model development, data collection, statistical analysis, and manuscript preparation and revision.

2.1 Abstract

Soil water retention determines plant water availability and contaminant transport processes in the subsurface environment. However, it is usually difficult to measure soil water retention characteristics. In this study, an analytical model based on a fractional bulk density (FBD) concept was presented for estimating soil water retention curves. The concept allows partitioning of soil pore space according to the relative contribution of certain size fractions of particles to the change in total pore space. The input parameters of the model are particle size distribution (PSD), bulk density, and residual water content at water pressure head of 15,000 cm. The model was tested on 30 sets of water retention data obtained from various types of soils that cover wide ranges of soil texture from clay to sand and soil bulk density from 0.33 g/cm^3 to 1.65 g/cm^3. Results showed that the FBD model was effective for all soil textures and bulk densities. The estimation was more sensitive to the changes in soil bulk density and residual water content than PSD parameters. The proposed model provides an easy way to evaluate the impacts of soil bulk density on water conservation in soils that are manipulated by mechanical operation.

2.2 Introduction

Modeling of water flow and chemical movement in unsaturated soils has been emphasized by soil scientists and hydrologists for different purposes, such as estimating water root uptake, groundwater pollution risk, and soil erosion. However, high variability and complexity of soil texture in natural field make direct measurements of soil hydraulic properties costly and time-consuming. It is useful to utilize readily available information, such as soil texture and bulk density, to estimate soil hydraulic properties (Hwang and Powers, 2003; Jarvis et al., 2013; Wendroth et al., 2006). This approach can be highly beneficial to develop computationally efficient methods for evaluating soil hydraulic heterogeneity in large watersheds or agricultural fields while ensuring the economic feasibility of field investigation efforts within acceptable accuracy. Models with these benefits have been generally used to relate soil texture (expressed as particle size distribution), soil structural properties, bulk density, and/or organic matter content with soil water retention (Mamedov et al., 2016; Minasny and McBratney, 2018; Thiam et al., 2019; Tian et al., 2018). To date, many efforts have been made to estimate soil water retention using particle size distribution and other soil properties using multiple regression, neural network analyses and other methods (Babaeian et al., 2015; Garg et al., 2014; Haghverdi et al., 2012; McBratney et al., 2006; Nemes and Rawls, 2006; Patil and Singh, 2016; Zhuang et al., 2001). However, the applicability and accuracy of the models are more or less unsatisfactory. Although there are several prediction models derived on global soil hydraulic datasets, such as applying the Miller-Miller scaling approach to the soil dataset of SoilGrids1km to provide a global consistent soil hydraulic parameterization (Montzka et al., 2017), most of them possess a high correlation to particular soil types and thereby very likely fail to apply for other soils (Bullied et al., 2011; Lakzian et al., 2010; Terleev et al., 2010).

An important advancement in using soil particle size distribution to derive a soil water retention characteristic was the development of the physical empirical model (Arya et al., 1999; Arya and Paris, 1981). Later, Haverkamp and Parlange (1986) proposed a similar model by combining physical hypotheses with empirical representations and tested the model on sandy soil. Tyler and Wheatcraft (1989) interpreted the empirical scaling parameter α in the Arya and Paris model as being equivalent to the fractal dimension of a tortuous fractal pore. However, Arya et al. (1999) argued that the fractal scaling was limited in estimating the water retention in the complex soil matrix. In the optimized model of Arya et al. (1999), three methods for calculating the scaling parameter α were proposed, but the calculation still contained empirical component to some extent, making the model relatively difficult for broad application. The physical basis of the model of Arya and Paris (1981) or Arya et al. (1999) is weakened by the assumption that the void ratio of the bulk sample is equivalent to the void ratio of individual particle size class.

To improve the physical description of particle-pore relation, we assume that different fractions of soil particles may make different contributions to the total porosity or volumetric water content in the bulk soils and that soil pore volume and associated bulk density are specific for particle size fractions. This line of thinking might help derive a better physical model for mathematically estimating soil water characteristics. Therefore, the objective of this work was to apply a fractional bulk density (FBD) concept to the development of a soil water retention model that is effective for all soil textures and all soil bulk densities.

2.3 Materials and methods

2.3.1 Fractional bulk density concept

The first assumption is that soil particles with different sizes contribute to different porosities and water holding capacities in bulk soil. Based on a non-similar media concept (NSMC) defined by Miyazaki (1996), soil bulk density, ρ_b, as

$$\rho_b = \frac{M}{V} = \tau \rho_s \left(\frac{S}{S+d} \right)^3 \quad (1)$$

where M is mass of a given soil, and V is the volume of bulk soil, ρ_s is soil particle density, and S and d are characteristic lengths for solid phase and pore space, respectively. The parameter τ is a shape factor of the solid phase, defined as the ratio of the substantial volume of solid phase to the volume S^3. The value of τ is 1.0 for a cube and $\pi/6$ for a sphere. As pointed out by Miyazaki (1996), these characteristic lengths are not directly measurable but are representative lengths in the sense of the characteristic length in a similar media concept (SMC).

Following the approach of NSMC represented by Eq. (1), we conceptually defined the following equation

$$V = \frac{\sum_{i=1}^{n} m_i}{\rho_b} = \frac{m_1}{\rho_{b1}} + \frac{m_2}{\rho_{b2}} + \cdots \frac{m_n}{\rho_{bn}} \quad (2)$$

where m_i and ρ_{bi} are solid mass and equivalent bulk density of the i^{th} particle size fraction of soil sample, respectively. In this study, diameters of the first particle fraction and the last one are assumed to be 1 μm and 1,000 μm, respectively (Zhuang et al., 2001). This equation suggests that different particle size fractions are associated with different equivalent bulk densities due to their different contributions to soil pore space. As a result, the particles with the same size fraction could have different equivalent bulk densities in soils with different textures or after the soil particles are rearranged (e.g., compaction). A diagrammatic representation of the FBD concept for variation of soil pore space with soil particle assemblage is shown in Figure 2.1.

2.3.2 Calculation of soil volumetric water content

For a specific soil, Eq. (2) means

$$V_{pi}(\leq D_i)=f(D_{gi},\ M_i) \tag{3}$$

where $V_{pi}(\leq D_i)$ denotes the volume of the pores with diameter $\leq D_i$ generated by particles with diameters $\leq D_{gi}$ in unit volume soil. M_i is the accumulative mass percentage of the $\leq D_{gi}$ particles. Since the pore volume has the maximum value for given bulk soil and the accumulative distribution of pore volume could be generally hypothesized as a sigmoid curve for most of the natural soils (Buchan, 1989; Kosugi, 1994), we formulate Eq. (3) using a lognormal Logistic equation,

$$V_{pi}(\leq D_{gi})=\frac{V_{pmax}}{1+\kappa(D_{gi})^{b_i}} \tag{4}$$

where V_{pmax} is the maximum accumulative volume of pores pertinent to the particles smaller than or equal to the maximum diameter (D_{gmax}) in unit volume soil. In fact, here V_{pmax} is equal to the total porosity (φ_T) of the soil. V_{pi} ($\leq D_{gi}$) is the volume of the pores produced by $\leq D_{gi}$ particles in unit volume soil. The parameter b_i is a varying characteristic for the relative increment rate of the accumulative volume of pores with an increment of D_{gi}. By assuming the degree of saturation of pore space to be 100%, Eq. (4) changes into

$$\theta_i(\leq D_{gi})=\frac{\theta_s}{1+\kappa(D_{gi})^{b_i}} \tag{5}$$

where θ_s is saturated volumetric water content calculated with

$$\theta_s=\begin{cases}0.9\varphi_T,\ \rho_b<1\\ \varphi_T,\ \rho_b\geq 1\end{cases} \tag{6}$$

$$\varphi_T=\frac{\rho_s-\rho_b}{\rho_s} \tag{7}$$

In the above equations, ρ_b is measured bulk density and ρ_s is particle density (2.65 g/cm^3). The empirical parameter κ in Eqs. (4) and (5) is defined as

$$\kappa = \frac{\theta_s - \theta_r}{\theta_r} \tag{8}$$

where θ_r is measured residual water content. In this study, it is assumed to be volumetric water content at a pressure head of 15,000 cm water. The empirical parameter b_i is defined as

$$b_i = \frac{\varepsilon}{3} \log\left(\frac{\theta_s - \omega_i \theta_s}{\kappa \omega_i \theta_s}\right) \tag{9}$$

with ε, a particle size distribution index, calculated by

$$\varepsilon = \frac{(D_{40})^2}{D_{10} D_{60}} \tag{10}$$

where D_{10}, D_{40}, and D_{60} represent the particle diameters just below which the cumulative mass fractions of the particles are 10%, 40%, and 60%, respectively.

The parameter ω_i is coefficient for particles of the i^{th} size fraction, with a value varying between θ_r/θ_s and 1.0. Incorporating information of soil physical properties, the equation for estimating ω_i is given as

$$\omega_i = \frac{g}{1 + \kappa\left(\ln D_{gi}\right)^{\lambda}} \tag{11}$$

where g is defined as regulation coefficient varying in the range of 1.0-1.2, but in the present study it is consistently assumed as 1.2. λ is the ratio coefficient of particle size distribution fitted by the lognormal Logistic model as

$$M_i = \frac{M_T}{1 + \eta D_{gi}^{\lambda}} \tag{12}$$

where M_T represents the total mass percentage of all particles with different sizes and η is fitting parameter. We set M_T = 101 in the equation for the best fitting of the particle-size distribution. The continuous function of particle size distribution was generated from the discrete data of D_{gi} and M_i at cutting particle diameters of 1000, 750, 500, 400, 350, 300, 250, 200, 150, 100, 50, 30,

15, 7.5, 5, 3, 2, and 1 μm. Considering the difference in the upper limits of particle sizes associated with existing datasets of D_{gi} and M_i, the particle size distribution with the upper limit of 2,000 μm for the soils from Japan was normalized to the case with the upper limit of 1,000 μm (Eq. 24).

2.3.3 Calculation of pressure head of soil water

For the capillary tube diameter, D_i (μm), composed of particles with the size of D_{gi} (μm), Arya and Paris (1981) developed an expression

$$D_i = D_{gi}\left[\frac{2}{3} e n_i^{(1-\alpha)}\right]^{0.5} \tag{13}$$

where α is the empirical scaling parameter varying between 1.35 and 1.40 in their(1981) original model, but was thought to vary with soil particle size in the optimized model of Arya et al. (1999). In Tyler and Wheatcraft's (1989) model α is the fractal dimension of the pore. The parameter e is the void rate of the entire soil, assumed being unchanged with particle size. However, according to Eqs. (2) and (3), e in the Eq. (13) should vary with particle size and should be replaced by specific particle size e_i. n_i is the number of particles in the i^{th} particle class with a particle diameter, D_{gi} (μm), assuming that the particles are spherical and that the entire pore volume formed by assemblage of the particles in this class is represented by a single cylindrical pore. The equation for calculating n_i is given as (Arya and Paris, 1981)

$$n_i = \frac{6m_i}{\rho_s \pi D_{gi}^3} \times 10^{12} \tag{14}$$

where m_i is the mass of particles in the ith fraction with the particle diameter, D_{gi}. Here, we set $D_i = D_{min}$ and $D_{gi} = D_{gmin}$. Assuming that soil water has a zero contact angle and a surface tension of 0.075 N/m at 25°C, the minimum diameter of soil pore (D_{min}) is taken to be 0.2 μm, which is

equivalent to the pressure head of 15,000 cm water according to Young-Laplace equation. We set this minimum pore size to correspond the minimum particle size (D_{gmin}=1.0 μm). The model might thus not apply well to porous media with pores smaller than 0.2 μm. As a result, Eq. (13) is simplified into the following equation.

$$D_i=0.2D_{gi} \tag{15}$$

The equivalent capillary pressure (ψ_i) for the i^{th} particle size fraction can be calculated using

$$\psi_i=\frac{3000}{D_i}=\frac{15000}{D_{gi}} \tag{16}$$

where D_i is the pore diameter in μm, ψ_i is the water pressure in cm water, and D_{gi} is particle diameter in μm. In Eq. (16), the maximum pressure head (ψ_r=15,000 cm) corresponds to θ_r and D_{gmin} (1 μm). The minimum pressure head (ψ_0=15 cm) corresponds to θ_s and D_{gmax} (1,000 μm). These assumptions are arbitrary, or may be inappropriate for some soils, but we used them because they approximate the practical range of measurements well.

2.3.4 The resulting model of soil water retention

Eqs. (5) and (16) formulate a FBD-based model for estimation of soil water retention curve. To simplify the computation, the two equations are incorporated into an analytical form,

$$\theta=\frac{\theta_s}{1+(\frac{\theta_s-\theta_r}{\theta_r})(\frac{15,000}{\psi})^b} \tag{17}$$

where the parameter b can be obtained using

$$b=\frac{\varepsilon}{3}\log\{\frac{(\theta_s-\theta_r)[\ln(\frac{15,000.1}{\psi})]^{\lambda}-(g-1)\theta_r}{g(\theta_s-\theta_r)}\} \tag{18}$$

In Eq. (18), a value of 15,000.1 cm water was employed to consecutively predict the soil water content until pressure head of 15,000 cm water.

2.3.5 Soil dataset

Evaluation of the applicability of the proposed modeling procedure requires datasets that include soil bulk density, residual water content, and soil particle size distribution covering three particle diameters (D_{10}, D_{40}, and D_{60}) below which the cumulative mass fractions of particles are 10%, 40%, and 60%, respectively. In addition, measured water content and pressure head are required for the actual retention curve in order to compare with the result of the FBD-based model. In this study, the soil water retention data measured for 30 different soils, published by Yu et al. (1994), Chen and Wang (1979), Zhang and Miao (1985), Liu and Amemiya (1999), Hayano et al. (1997), and Yabashi et al. (1994) were collected for model verification (Table 2.1). The soils include soils in China (such as black soil, chernozem soil, cinnamon soil, brown earth, fluvo-aquic soil, albic soil, red earth, humid-thermo ferralitic, purplish soil, meadow soil, and yellow earth) and soils in Japan (such as volcanic ash soil and acolian sandy soil). The USDA soil taxonomy of these soils is provided in Table 2.1. The 30 soils range in texture from clay to sand and in bulk density from 0.33 g/cm^3 to 1.65 g/cm^3, which covers a much wider range of soil bulk density than any existing models or pedotransfer functions (da Silva et al., 2017; Fredlund et al., 2002; Saxton and Rawls, 2006; Vereecken et al., 1989). Particle size fractions (D_{gi}) were chosen as the upper limit of the diameters between successive sieve sizes. For the data set in which particle density was not determined, 2.65 g/cm^3 was used.

2.3.6 Statistical parameters for model verification

Four statistical properties, R^2, *RMSE*, mean residual error (*ME*), and *t* value were calculated to determine the accuracy of the FBD model. The R^2 values were computed at the same value of ψ, with the values of θ measured and estimated by the FBD model (Eq. 17). *RMSE* and *ME* were obtained, respectively, by

$$RMSE=[\frac{1}{n}\sum(\theta_{est}-\theta_{mea})^2]^{0.5} \quad (19)$$

$$ME=\frac{1}{n}\sum_{i=1}^{n}(\theta_{est}-\theta_{mea}) \quad (20)$$

where θ_{mea} is measured soil water content, θ_{est} is soil water content estimated with the FBD model, and *n* is the number of measured pairs of water content and pressure head. With the assumption of normal distribution and independence of differences between the water contents measured and estimated by the FBD model, *t* was calculated with

$$t=ME(\frac{RMSE^2-ME^2}{n-1})^{-0.5} \quad (21)$$

When calculated $|t|$ is larger than $t_{0.05}$ (the critical value of the Student's *t* distribution for $P = 0.05$ and n-1 degrees of freedom), the differences between the measured and estimated water contents are statistically significant. If $t < 0$, soil water contents are underestimated and vice versa. Thus, *t* is a measure for the systematic bias in the estimation. Values of *t* close to zero indicate that the measured and estimated soil water content do not differ systematically from each other or, equivalently, that there is no consistent bias. Values of *t* that differ greatly from zero indicate the presence of systematic bias. *RMSE* is a measure for the scatter of the data points around the 1:1 line. Low *RMSE* values indicate less scatter. Low *RMSE* values also imply low *ME*. Regarding the result that *t* is low while *RMSE* is high, it can be explained that negative and positive deviations distribute more evenly on two sides of the 1:1 line.

2.4 Results

2.4.1 Estimation accuracy

Model estimation of water retention characteristics for some soils is presented in Figure 2.2. The results indicate that the new procedure was in good agreement with the measured data for most of the soil textures except for sand in the range of pressure head from 15 cm water up to 15,000 cm water, which covers the entire range of available water content. Table 2.2 shows the coefficient of determination (R^2), root mean square error (*RMSE*), and *t* value of Student's *t* distribution of the FBD model along with those of curve fitting using the Campbell (1974) equation, which was extended from the similar media concept (Miller and Miller, 1956). The equation is expressed as

$$\theta=(\frac{\psi_e}{\psi})^{\frac{1}{q}}\theta_s \tag{22}$$

where ψ_e is air entry water potential and θ_s is saturated volumetric water content. Parameter q can be obtained according to

$$q=[\sum M_i(\ln D_{gi})^2-(\sum M_i \ln D_{gi})^2]^{0.5} \tag{23}$$

where D_{gi} is the diameter of the i^{th} particle-size fractions and M_i is the accumulative mass percentage of the $\leq D_{gi}$ particles.

RMSE values were computed from soil water contents measured and estimated as described in the section of methods. The results in Table 2.2 show that the mean value of *RMSE* of the FBD model is 0.0315 cm^3/cm^3 while that of the Campbell model is 0.0235 cm^3/cm^3. This result is acceptable because the Campbell model used the measured data directly to obtain ψ_e. The higher values of R^2 also support the applicability of the FBD model. Compared to the value of *t* for the results of Campbell fitting, there was no systemic bias for the FBD model, and that the FBD model only a little but insignificantly overestimated the soil water contents. In addition,

Figure 2.3 shows a comparison between the water contents measured and estimated by the FBD model for the 30 soils. The values coalesce to the 1:1 line with the *RMSE* being 0.0408 cm^3/cm^3. This *RMSE* value is larger than the average in Table 2.2. The discrepancy was due that different methods were used for averaging the *RMSE* values for individual soils and all soils. Mayr and Jarvis (1999) presented pedotransfer functions to estimate soil water retention parameters of the Brooks-Corey model. The resulting mean *RMSE* value in the dependent dataset was 0.0430 cm^3/cm^3 for the dependent dataset and 0.0480 cm^3/cm^3 for the independent dataset. Tomasella et al. (2000) derived a pedotransfer function to predict the water retention parameters of the van Genuchten equation. The mean *RMSE* values ranged from 0.0378 cm^3/cm^3 to 0.0584 cm^3/cm^3. Our model compares favorably with these pedotransfer functions in terms of mean *RMSE* value. It could thus be concluded that the FBD model behaved overall well, except for Acolian sandy soil (soil sample #01). For sandy soil, the relatively poor capture of the rapid change of water content is attributed to the limitation of applicability of capillary law (i.e., Young-Laplace equation) to sandy media and existence of macropores that reduce the pore continuity (Zhuang et al., 2001). The continuity of soil pores is the dominant factor that affects the performance of our proposed model.

The FBD model had relatively larger estimation errors for soils originated from ash parent materials (e.g., soil samples #05, 14, 16, and 22) than for other soils (Table 2.2). This is due likely to the oversimplification that accumulative soil particle size distribution is sigmoid whereas in fact the particle arrangement of soils developed from ash parent materials is very complex (i.e., non-sigmoid). The less accurate prediction for sandy soils relative to the other soil textures suggests that the assumption for cumulative particle size distribution to be single sigmoid is arbitrary, despite many soils demonstrate a typical sigmoid for their particle systems.

We infer that the sigmoid-type distribution is more applicable to the soils with a broader range of particle sizes that show a lognormal distribution of individual particle fractions (Hwang and Choi, 2006; Nimmo, 1997). Soil aggregates with hierarchical pore structure have dual-porosity system. Dual-porosity assumes that the porous medium consists of two interacting regions, one associated with the macropore or fracture system and one comprising micropores inside soil material. Bimodal pore-size distributions are frequently observed in dual-porosity soil (Li and Zhang, 2009). The water retention curve estimated for a wide range of water potentials (-15 to -15,000 cm water) is the sum of the effects of macropores and micropores (Šimůnek et al., 2003). The sigmoid-type distribution is more suitable for hierarchical soil aggregates than for less structured soils whose pore system is simply dominated by primary particles. Therefore, the proposed model does not perform well against the soils if their particle sizes have a narrow range (e.g., sandy soils).

2.4.2 Sensitivity analysis of model parameters

We performed a sensitivity analysis on the model parameters to identify those that most strongly affect the model behavior and to determine the required precision of the parameters. The parameters included in the sensitivity test were saturated water content (θ_s), residual water content (θ_r), rate coefficient (λ) of Logistic-type model for particle size distribution, and particle size distribution index (ε). The value of each parameter is assumed to increase or decrease by 20% of its actual value since its measurement error could be up to 20% according to our experience on field soil survey. By taking soil sample #22 as an example, the test was implemented to monitor the change in the estimated soil water content caused by changing the value of one parameter at a time while others remained constant. The sensitivity analysis not

only showed the influencing patterns of the parameters on the model behavior but also ranked the parameters in terms of the magnitude of influences. As shown in Figure 2.4, two parameters displaying high sensitivity are the θ_s and θ_r. They generally had the same ability to influence the model prediction. For λ and ε, although both were found not dominant in defining the model performance, accurate estimation for their values are still very important for the modeling results. The sensitivity analyses provided insights into the behavior of the FBD model expressed as Eq. (17). The analysis presented here underlies the notion that parameter values may have physical meanings no matter in whatever ways the related parameters are structured into a model.

2.5 Discussion

Particle size distribution forms a common descriptor of natural soils. It has been used routinely as one of the inputs to estimate some soil physical properties, for example, water retention characteristic (Jensen et al., 2015; Leung et al., 2015; Yang et al., 2014), bulk density (Keller and Håkansson, 2010), and hydraulic conductivity(Bardhan et al., 2016; Kroener et al., 2018; Salarashayeri and Siosemarde, 2012). In this study, two parameters, rate coefficient (λ in Eq. 12) of the Logistic-type model for particle size distribution and particle size distribution index (ε in Eq. 10), were employed to translate particle size distribution to soil water retention characteristic. However, some issues should be noted for the simulation. One is the estimation of λ in the case that the upper size limit of the particle size distribution is 1,000 μm for some soils while it is 2,000 μm for other soils. In order to perform a consistent comparison among all soils, the particle size distribution with the upper limit of 2,000 μm was normalized to that with the upper limit of 1,000 μm using a normalization formula,

$$M'_i = \frac{100 M_i}{M_{1,000}} \quad (24)$$

where M_i and M_i' are measured and normalized percentage content of particles with sizes smaller than or equal to the i^{th} particle size, respectively. $M_{1,000}$ denotes the percentage content of particles with a size smaller than or equal to 1,000 μm.

In addition, the calculation of ε involves three particle sizes (D_{10}, D_{40}, and D_{60}) below which the percentage contents of particles are 10%, 40%, and 60%, respectively. It is easy to identify D_{60} but relatively difficult to find D_{10} and D_{40}. Many soils whose content of particles with sizes smaller than or equal to the measured lower limit size (e.g., 1 μm or 2 μm) is larger than 10%. In this case, an exponential equation, which was obtained by fitting the relation between the cumulative percentage content and the corresponding particle sizes, was used to extrapolate and identify D_{10}. To minimize the deviations arising from the extrapolation, we used 50 μm as the upper size limit.

The proposed model is generally based on the assumption that the size of the particles and the density of their packing are the primary determinants of the pore size and pore volume. This, however, may not be the case under some conditions. There is no doubt that particle assembling and resulting pore characteristics play important roles in regulating physical, chemical, and biological functions of soils at various scales. Aggregation of primary particles into secondary and tertiary particles, root channels, and microcracks would account for a fraction of the pore volume with pore sizes not determined by the size distribution of primary particles. The abundance of such pores considerably determines the extent of deviation of prediction. Therefore, it is important to incorporate information of soil structure into soil hydraulic modeling if possible (Schwartz, 2016). There is no doubt that soil structure is a non-negligible factor for accurate estimation of soil hydraulic properties using pedotransfer functions (Pachepsky et al.,

2006; Pachepsky and Rawls, 2003). But this work seems difficult to initiate because soil structure information (e.g., soil aggregate size distribution) is mostly unavailable compared to soil basic properties (e.g., particle size distribution, organic matter content, and bulk density). Insufficiency of identification of soil structure indices still precludes the inclusion of soil structure characteristics into soil water retention modeling. Relevant efforts have been made in some large-scale models that consider soil structure. For instance, Fatichi et al. (2020) proposed to assess the impact of soil structure on global climate using an Ocean-Land-Atmosphere Model (OLAM). Although the model in this study does not explicitly include a structural component, we alternatively assume that soil bulk density could indirectly bring the influence of soil structure into the FBD model because soil bulk density is determined by actual soil structure.

The FBD model estimates soil water retention characteristics from particle size distribution, bulk density, and measured residual water content. The starting point is the similarity between the shapes of cumulative particle size distribution and soil water retention characteristics. Similarly, Arya and Paris (1981) and Haverkamp and Parlange (1986) used a simple equation to derive a set of soil water content according to the mass fraction of soil particles, and then a series of expressions were employed to regulate pressure head of soil water to pair with the water content equal to the measured. In our model, an opposite approach was used. A set of pressure head from 15 cm to 15,000 cm water were derived using a simple expression as Eq. (16), and then soil water contents were estimated with FBD-based equations to match the derived pressure head. Eventually, an analytical model, Eq. (17), was obtained. In the FBD-based model, the water retention function includes a residual water content in relation to the maximum pressure head (15,000 cm water) and the parameter (b) of soil pore size distribution. Similarly, the residual water content is considered in the models developed by van

Genuchten (1980) or Brooks and Corey (1964). However, Campbell (1974) described soil water retention curve by assuming there is no residual water content. An advantage of the Campbell equation is its excellent fitting capability, and thus we compared the FBD-based model to the Campbell model for evaluation on the estimation accuracy of the FBD model.

The selection of a Logistic-type equation for the model formulation is mainly due to the consideration that particle size distribution and pore size distribution in most soils are approximately lognormal (Bayat et al., 2015; Buchan, 1989; Hwang and Choi, 2006; Kosugi, 1994). The logistic growth equation generates a curve that tends towards an exponential form at low values and power form at high values with a power index smaller than 1. This characteristic implicitly includes the consideration that the drainage of water in small pores at large suction is usually expected to be more impaired than the release of water from large pores at small suctions (Ghanbarian-Alavijeh et al., 2011; Perfect, 2005).

2.6 Conclusions

An analytical model, which is based on a fractional bulk density concept, was presented for estimating soil water retention for the entire range of pressure heads that determine water availability. The proposed model was tested using 30 sets of soil water retention data measured for various textures of soils that cover a wide range of soil bulk density from 0.33 g/cm^3 to 1.65 g/cm^3. Results show that the proposed model can convert readily available soil physical properties into soil retention curves in very good agreement with the measurements, and the model is applicable to soils with limited data on soil particle size distribution at small loss of estimation accuracy in the middle portion of the soil water retention curve. Sensitivity analyses revealed that saturated and residual water contents were two parameters with high-sensitivity for

the accurate estimation of retention curves. The agreement with measurements supported the new model's underlying concepts. The model used a conceptual partitioning of pore space according to the relative contribution of certain sizes of particles to the change in pore space. This thinking underlies the assumption that the value of the key parameter (b_i) varies with particle size fraction for a given soil. In addition, the model assumed a sigmoid curve of water retention characteristic for most soils. However, these assumptions are worth further consideration on their relations to the physical reality of soils as well as possible improvements and extensions. Compared to subsurface soils, larger deviations should be expected mainly for surface soil materials where aggregation, cracking, and root effects may be pronounced. Further tests of the model and evaluation on the effects of hysteresis, aggregation, and expansibility should reveal the weaknesses of the model and identify additional variables needed for model improvement.

References

Arya, L.M., Leij, F.J., van Genuchten, M.T., Shouse, P.J., 1999. Scaling parameter to predict the soil water characteristic from particle-size distribution data. Soil Sci. Soc. Am. J. 63, 510-519.

Arya, L.M., Paris, J.F., 1981. A physicoempirical model to predict the soil moisture characteristic from particle-size distribution and bulk density data1. Soil Sci. Soc. Am. J. 45, 1023-1030.

Babaeian, E., Homaee, M., Vereecken, H., Montzka, C., Norouzi, A.A., van Genuchten, M.T., 2015. A comparative study of multiple approaches for predicting the soil-water retention curve: hyperspectral information vs. basic soil properties. Soil Sci. Soc. Am. J. 79, 1043-1058.

Bardhan, G., Russo, D., Goldstein, D., Levy, G.J., 2016. Changes in the hydraulic properties of a clay soil under long-term irrigation with treated wastewater. Geoderma 264, 1-9.

Bayat, H., Rastgo, M., Zadeh, M.M., Vereecken, H., 2015. Particle size distribution models, their characteristics and fitting capability. J. Hydrol. 529, 872-889.

Brooks, R.H., Corey, A.T., 1964. Hydraulic properties of porous media. Colorado State University.

Buchan, G.D., 1989. Applicability of the simple lognormal model to particle-size distribution in soils. Soil Sci. 147, 155-161.

Bullied, W.J., Bullock, P.R., Van Acker, R.C., 2011. Modeling the Soil-Water Retention Characteristic With Pedotransfer Functions for Shallow Seedling Recruitment. Soil Sci. 176, 57-72.

Campbell, G.S., 1974. A simple method for determining unsaturated conductivity from moisture retention data. Soil Sci. 117, 311-314.

Chen, Z.X., Wang, R.Z., 1979. The moisture retention of several important soils in China. Acta Pedol. Sin. 16, 277-281.

da Silva, A.C., Armindo, R.A., dos Santos Brito, A., Schaap, M.G., 2017. SPLINTEX: A physically-based pedotransfer function for modeling soil hydraulic functions. Soil Till. Res. 174, 261-272.

Fatichi, S., Or, D., Walko, R., Vereecken, H., Young, M.H., Ghezzehei, T.A., Hengl, T., Kollet, S., Agam, N., Avissar, R., 2020. Soil structure is an important omission in Earth System Models. Nat. Commun. 11, 1-11.

Fredlund, M.D., Wilson, G.W., Fredlund, D.G., 2002. Use of the grain-size distribution for estimation of the soil-water characteristic curve. Can. Geotech. J. 39, 1103-1117.

Garg, A., Garg, A., Tai, K., Barontini, S., Stokes, A., 2014. A computational intelligence-based genetic programming approach for the simulation of soil water retention curves. Transport Porous Med. 103, 497-513.

Ghanbarian-Alavijeh, B., Millán, H., Huang, G., 2011. A review of fractal, prefractal and pore-solid-fractal models for parameterizing the soil water retention curve. Can. J. Soil Sci. 91, 1-14.

Haghverdi, A., Cornelis, W.M., Ghahraman, B., 2012. A pseudo-continuous neural network approach for developing water retention pedotransfer functions with limited data. J. Hydrol. 442, 46-54.

Haverkamp, R.T., Parlange, J.Y., 1986. Predicting the water-retention curve from particle-size distribution: 1. Sandy soils without organic matter1. Soil Sci. 142, 325-339.

Hayano, M., Yabashi, S., Amemiya, Y., 1997. Case study on the estimation of soil water characteristics with soil bulk density distribution. J. Jpn. Soc. Hydrol. Water Resour. 10, 299-307.

Hwang, S.I., Choi, S.I., 2006. Use of a lognormal distribution model for estimating soil water

retention curves from particle-size distribution data. J. Hydrol. 323, 325-334.

Hwang, S.I., Powers, S.E., 2003. Using particle-size distribution models to estimate soil hydraulic properties. Soil Sci. Soc. Am. J. 67, 1103-1112.

Jarvis, N., Koestel, J., Messing, I., Moeys, J., Lindahl, A., 2013. Influence of soil, land use and climatic factors on the hydraulic conductivity of soil. Hydrol. Earth Syst. Sc. 17, 5185-5195.

Jensen, D.K., Tuller, M., de Jonge, L.W., Arthur, E., Moldrup, P., 2015. A New Two-Stage Approach to predicting the soil water characteristic from saturation to oven-dryness. J. Hydrol. 521, 498-507.

Keller, T., Håkansson, I., 2010. Estimation of reference bulk density from soil particle size distribution and soil organic matter content. Geoderma 154, 398-406.

Kosugi, K.i., 1994. Three-parameter lognormal distribution model for soil water retention. Water Resour. Res. 30, 891-901.

Kroener, E., Holz, M., Zarebanadkouki, M., Ahmed, M., Carminati, A., 2018. Effects of mucilage on rhizosphere hydraulic functions depend on soil particle size. Vadose Zone J. 17.

Lakzian, A., Aval, M.B., Gorbanzadeh, N., 2010. Comparison of pattern recognition, artificial neural network and pedotransfer functions for estimation of soil water parameters. Not. Sci. Biol. 2, 114-120.

Leung, A.K., Garg, A., Ng, C.W.W., 2015. Effects of plant roots on soil-water retention and induced suction in vegetated soil. Eng. Geol. 193, 183-197.

Li, X., Zhang, L.M., 2009. Characterization of dual-structure pore-size distribution of soil. Can. Geotech. J. 46, 129-141.

Liu, J., Amemiya, Y., 1999. The estimation of soil water retentivity for soil and aggregate-like soil

"Akadama" mixture. Environ. Control Biol. 37, 21-30.

Mamedov, A., Ekberli, I., Gülser, C., Gümüş, I., Çetin, U., Levy, G.J.G., 2016. Relationship between soil water retention model parameters and structure stability. Eurasian J. Soil Sci. 5.

Mayr, T., Jarvis, N.J., 1999. Pedotransfer functions to estimate soil water retention parameters for a modified Brooks–Corey type model. Geoderma 91, 1-9.

McBratney, A.B., Minasny, B., Viscarra Rossel, R., 2006. Spectral soil analysis and inference systems: A powerful combination for solving the soil data crisis. Geoderma 136, 272-278.

Miller, E.E., Miller, R.D., 1956. Physical theory for capillary flow phenomena. J. Appl. Phys. 27, 324-332.

Minasny, B., McBratney, A.B., 2018. Limited effect of organic matter on soil available water capacity. Eur. J. Soil Sci. 69, 39-47.

Miyazaki, T., 1996. Bulk density dependence of air entry suctions and saturated hydraulic conductivities of soils. Soil Sci. 161, 484-490.

Montzka, C., Herbst, M., Weihermüller, L., Verhoef, A., Vereecken, H., 2017. A global data set of soil hydraulic properties and sub-grid variability of soil water retention and hydraulic conductivity curves. Earth Syst. Sci. Data 9, 529-543.

Nemes, A., Rawls, W.J., 2006. Evaluation of different representations of the particle-size distribution to predict soil water retention. Geoderma 132, 47-58.

Nimmo, J.R., 1997. Modeling structural influences on soil water retention. Soil Sci. Soc. Am. 61, 712-719.

Pachepsky, Y.A., Rawls, W., Lin, H., 2006. Hydropedology and pedotransfer functions. Geoderma 131, 308-316.

Pachepsky, Y.A., Rawls, W.J., 2003. Soil structure and pedotransfer functions. Eur. J. Soil Sci. 54, 443-452.

Patil, N.G., Singh, S.K., 2016. Pedotransfer functions for estimating soil hydraulic properties: A review. Pedosphere 26, 417-430.

Perfect, E., 2005. Modeling the primary drainage curve of prefractal porous media. Vadose Zone J. 4, 959-966.

Salarashayeri, A., Siosemarde, M., 2012. Prediction of soil hydraulic conductivity from particle-size distribution. World Acad. Sci. Eng. Technol. 61, 454-458.

Saxton, K.E., Rawls, W.J., 2006. Soil water characteristic estimates by texture and organic matter for hydrologic solutions. Soil Sci. Soc. Am. 70, 1569-1578.

Schwartz, U., 2016. Factors affecting channel infiltration of floodwaters in Nahal Zin basin, Negev desert, Israel. Hydrol. Process. 30, 3704-3716.

Šimůnek, J., Jarvis, N.J., Van Genuchten, M.T., Gärdenäs, A., 2003. Review and comparison of models for describing non-equilibrium and preferential flow and transport in the vadose zone. J. Hydrol. 272, 14-35.

Terleev, V., Mirschel, W., Schindler, U., Wenkel, K., 2010. Estimation of soil water retention curve using some agrophysical characteristics and Voronin's empirical dependence. Int. Agrophys. 24, 381-387.

Thiam, M., Thuyet, D.Q., Saito, H., Kohgo, Y., 2019. Performance of the tangential model of soil water retention curves for various soil texture classes. Geoderma 337, 514-523.

Tian, Z.C., Gao, W.D., Kool, D., Ren, T.S., Horton, R., Heitman, J.L., 2018. Approaches for estimating soil water retention curves at various bulk densities with the extended van Genuchten Model. Water Resour. Res. 54, 5584-5601.

Tomasella, J., Hodnett, M.G., Rossato, L., 2000. Pedotransfer functions for the estimation of soil water retention in Brazilian soils. Soil Sci. Soc. Am. J. 64, 327-338.

Tyler, S.W., Wheatcraft, S.W., 1989. Application of fractal mathematics to soil water retention estimation. Soil Sci. Soc. Am. J. 53, 987-996.

Van Genuchten, M.T., 1980. A closed-form equation for predicting the hydraulic conductivity of unsaturated soils. Soil Sci. Soc. Am. 44, 892-898.

Vereecken, H., Maes, J., Feyen, J., Darius, P., 1989. Estimating the soil moisture retention characteristic from texture, bulk density, and carbon content. Soil Sci. 148, 389-403.

Wendroth, O., Koszinski, S., Pena-Yewtukhiv, E., 2006. Spatial association among soil hydraulic properties, soil texture, and geoelectrical resistivity. Vadose Zone J. 5, 341-355.

Yabashi, S., Amemiya, Y., Koh, S., Mizuniwa, C., Takahashi, S., 1994. Studies on the physical properties of horticultural soils, 2: Characteristics of the soil structure and soil water retentivity of Kanuma-tsuchi Tech. Bull. Fac. Hortic. Chiba Univ. 48, 135-140.

Yang, F., Zhang, G.L., Yang, J.L., Li, D.C., Zhao, Y.G., Liu, F., Yang, R.M., Yang, F., 2014. Organic matter controls of soil water retention in an alpine grassland and its significance for hydrological processes. J. Hydrol. 519, 3086-3093.

Yu, G.R., Nakayama, K., Yi, Y.L., 1994. Studies on the moisture characteristic curve and the water absorption character of soil. J. Agric. Meteorol. 50, 213-220.

Zhang, J., Miao, F.S., 1985. Water retention characteristics of different textural soils in Huanfan Plains. Acta Pedol. Sin. 22, 350-355.

Zhuang, J., Jin, Y., Miyazaki, T., 2001. Estimating water retention characteristic from soil particle-size distribution using a non-similar media concept. Soil Sci. 166, 308-321.

Appendix

Table 2.1 Physical properties of soils used in the study. ρ_b is bulk density (g/cm^3); θr is residual water content (cm^3/cm^3) at 15,000 cm water pressure head; ε is particle size distribution index. Soil water retention data of fluvo-aquic soil, red earth, humid-thermo ferralitic, purplish soil, meadow soil and yellow earth were measured with pressure membrane apparatus (Chen and Wang, 1979; Zhang and Miao, 1985). The soil water retention data of black soil, chernozem soil, cinnamon soil, brown earth, and albic soil were obtained using the suction and pressure plate method (Yu et al., 1994). The soil water retention data of volcanic ash soil and Acolian sandy soil were measured using the suction and pressure plate method (Hayano et al., 1997; Liu and Amemiya, 1999; Yabashi et al., 1994).

No.	Soil	USDA soil taxonomy	Texture	Particle percentage		ρ_b	θr	ε	Source
				<2 μm	<20 μm				
01	Acolian sandy soil	Entisols	Sand	0.11	0.53	1.65	0.024	1.37	(Liu and Amemiya, 1999)
02	Meadow soil	Inceptisols	Sandy loam	6.04	35.20	1.38	0.039	1.38	(Chen and Wang, 1979)
03	Fluvo-aquic soil	Inceptisols	Sandy loam	9.51	38.01	1.33	0.055	1.82	(Zhang and Miao, 1985)
04	Fluvo-aquic soil	Inceptisols	Sandy loam	10.20	33.20	1.27	0.051	1.87	(Zhang and Miao, 1985)
05	Volcanic ash soil	Andisols	Sandy loam	10.22	35.00	0.33	0.199	3.09	(Yabashi et al., 1994)
06	Fluvo-aquic soil	Inceptisols	Sandy loam	13.55	45.60	1.27	0.062	1.75	(Zhang and Miao, 1985)
07	Fluvo-aquic soil	Inceptisols	Loam	10.76	42.40	1.32	0.088	1.65	(Zhang and Miao, 1985)
08	Meadow soil	Inceptisols	Loam	13.27	44.37	1.28	0.054	1.74	(Chen and Wang, 1979)
09	Fluvo-aquic soil	Inceptisols	Loam	13.40	47.88	1.32	0.059	2.48	(Zhang and Miao, 1985)
10	Purplish soil	Inceptisols	Loam	16.32	48.04	1.30	0.092	1.58	(Chen and Wang, 1979)
11	Yellow earth	Inceptisols	Silt clay loam	27.35	73.87	1.29	0.108	1.61	(Chen and Wang, 1979)
12	Meadow soil	Inceptisols	Clay loam	22.09	47.32	1.29	0.082	1.95	(Chen and Wang, 1979)
13	Fluvo-aquic soil	Inceptisols	Clay loam	28.86	58.39	1.28	0.159	2.21	(Zhang and Miao, 1985)
14	Volcanic ash soil	Andisols	Clay loam	28.01	65.00	0.80	0.370	1.73	(Liu and Amemiya, 1999)
15	Chernozem soil	Mollisols	Sandy clay	30.14	48.56	1.24	0.148	4.57	(Yu et al., 1994)
16	Volcanis ash soil	Andisols	Sandy clay	34.56	45.60	0.70	0.263	1.57	(Hayano et al., 1997)
17	Fluvo-aquic soil	Inceptisols	Sandy clay	36.22	76.05	1.29	0.185	2.15	(Zhang and Miao, 1985)
18	Brown earth	Alfisols	Sandy clay	36.77	54.36	1.29	0.142	3.85	(Yu et al., 1994)
19	Fluvo-aquic soil	Inceptisols	Sandy clay	40.02	73.30	1.28	0.195	2.31	(Zhang and Miao, 1985)
20	Cinnamon soil	Alfisols	Sandy clay	40.12	59.37	1.19	0.138	3.74	(Yu et al., 1994)
21	Black soil	Mollisols	Sandy clay	42.18	59.34	1.15	0.186	3.44	(Yu et al., 1994)
22	Volcanis ash soil	Andisols	Sandy clay	45.37	63.28	0.82	0.385	3.14	(Liu and Amemiya, 1999)
23	Fluvo-aquic soil	Inceptisols	Silty clay	34.20	73.98	1.31	0.148	2.10	(Zhang and Miao, 1985)
24	Fluvo-aquic soil	Inceptisols	Silty clay	33.31	78.73	1.30	0.161	2.12	(Zhang and Miao, 1985)
25	Fluvo-aquic soil	Inceptisols	Silty clay	33.56	79.44	1.35	0.169	2.17	(Zhang and Miao, 1985)
26	Albic soil	Spodosols	Clay	52.76	77.60	1.16	0.230	1.66	(Yu et al., 1994)
27	Fluvo-aquic soil	Inceptisols	Clay	56.05	89.82	1.25	0.283	2.76	(Zhang and Miao, 1985)
28	Red earth	Ultisols	Clay	58.88	79.26	1.22	0.195	1.03	(Chen and Wang, 1979)
29	Humid-thermo ferralitic	Latosols	Clay	72.57	85.60	1.15	0.225	1.05	(Chen and Wang, 1979)
30	Fluvo-aquic soil	Inceptisols	Clay	68.81	98.02	1.08	0.303	2.04	(Zhang and Miao, 1985)

Table 2.2 Statistical comparison of soil water contents estimated by the fractional bulk density (FBD) model and fitted by the Campbell model (1974). *t* is the value of Student's *t* distribution, and the critical values of $t_{0.05}$ for 04, 08, 09, 10, 15, 18 and 30 degrees of freedom are 2.776, 2.306, 2.262, 2.228, 2.131, 2.101 and 2.042, respectively; R^2 is determination coefficient; *RMSE* is root mean square errors (cm^3/cm^3); *n* is the number of measured pairs of water content and pressure head.

Soil No.	*t*		R^2		*RMSE*		*n*
	FBD model	Campbell model	FBD model	Campbell model	FBD model	Campbell model	
01	1.600	-0.508	0.662	0.507	0.097	0.117	16
02	-1.316	-0.288	0.939	0.888	0.039	0.040	9
03	-1.924	-0.213	0.982	0.958	0.011	0.014	5
04	-0.123	-0.308	0.968	0.932	0.012	0.015	5
05	-0.191	0.115	0.962	0.900	0.059	0.060	10
06	-1.374	-0.331	0.951	0.922	0.068	0.039	5
07	-1.948	-0.123	0.908	0.922	0.027	0.018	5
08	-2.411	0.125	0.985	0.942	0.020	0.031	9
09	0.532	-0.270	0.954	0.923	0.017	0.024	5
10	1.345	0.179	0.980	0.998	0.042	0.003	9
11	0.144	0.164	0.977	0.995	0.028	0.007	9
12	0.266	0.070	0.995	0.964	0.020	0.020	9
13	10.840	-0.819	0.938	0.899	0.029	0.010	6
14	3.572	3.885	0.951	0.956	0.023	0.024	28
15	-0.883	-0.128	0.932	0.980	0.028	0.013	10
16	-0.209	-0.163	0.876	0.877	0.062	0.057	16
17	-0.794	-0.056	0.908	0.958	0.027	0.014	5
18	-0.441	-0.227	0.957	0.967	0.019	0.014	10
19	-0.256	-0.065	0.891	0.936	0.027	0.017	5
20	1.153	-0.253	0.892	0.920	0.032	0.023	10
21	1.932	-0.156	0.908	0.928	0.030	0.020	10
22	-5.494	-0.218	0.945	0.881	0.035	0.024	20
23	-3.341	-0.067	0.922	0.966	0.056	0.015	5
24	-1.421	-0.061	0.939	0.971	0.023	0.012	5
25	-1.558	-0.077	0.938	0.970	0.023	0.013	5
26	1.707	-0.075	0.953	0.969	0.022	0.010	10
27	-0.108	-0.052	0.916	0.963	0.020	0.013	5
28	-0.346	-0.113	0.958	0.956	0.014	0.014	9
29	-0.026	0.016	0.968	0.969	0.014	0.012	9
30	-1.823	-0.032	0.952	0.965	0.021	0.013	5
Mean	0.375	-0.009	0.934	0.931	0.032	0.024	

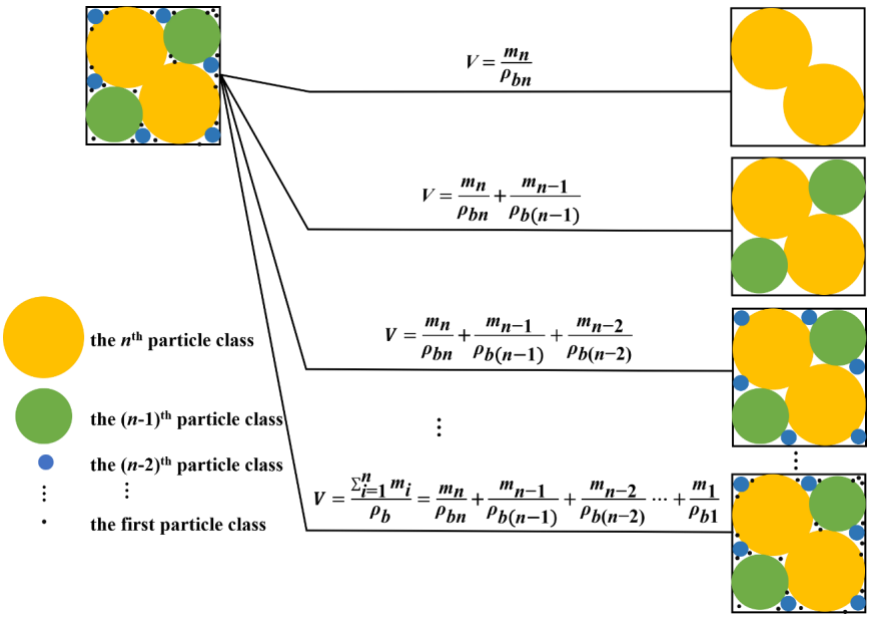

Figure 2.1 Diagrammatic representation of the fractional bulk density (FBD) model. V refers to the volume of bulk soil, and $m_{i,}$ and ρ_{bi} refer to the solid mass, and equivalent bulk density of the i^{th} particle-size fractions, respectively. ρ_b is the bulk density of whole soil.

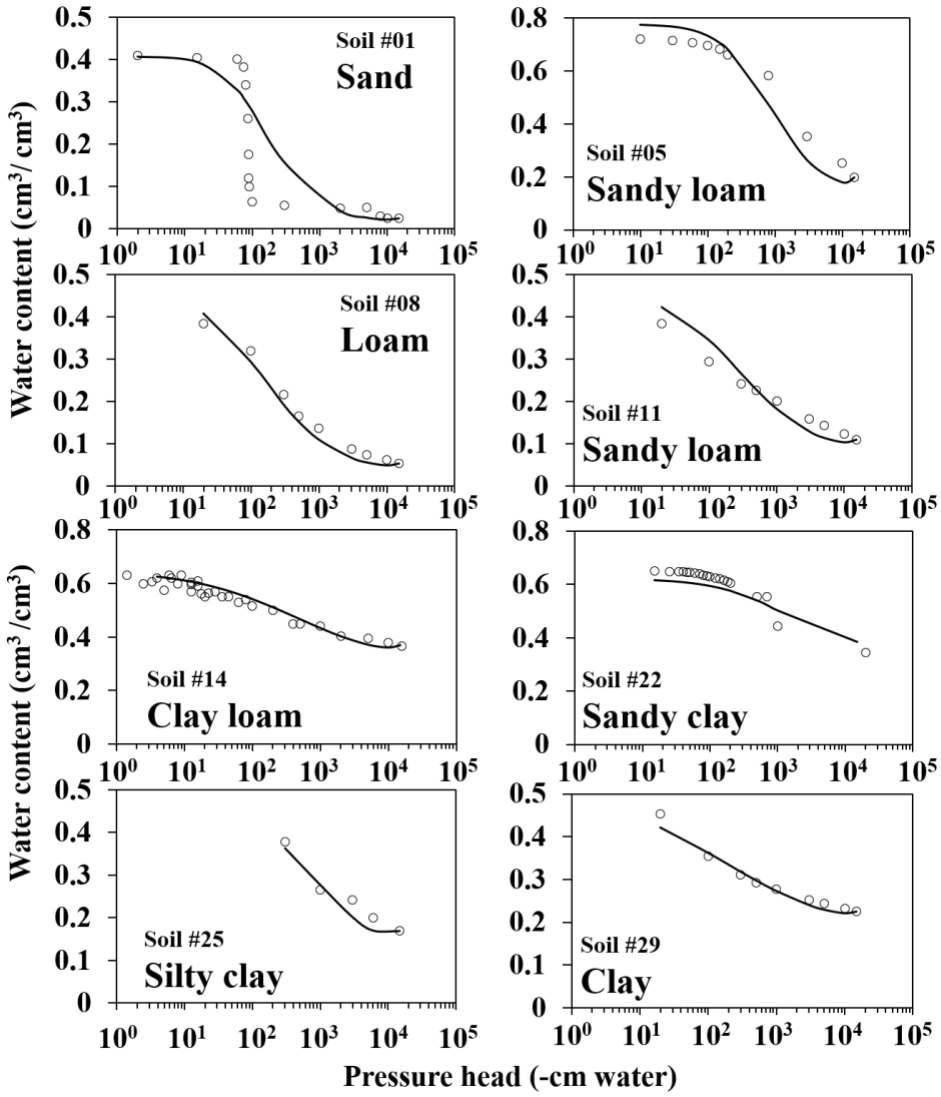

Figure 2.2 Water retention characteristics measured (circle) and estimated (line) using the fractional bulk density (FBD) model for eight different soil textures.

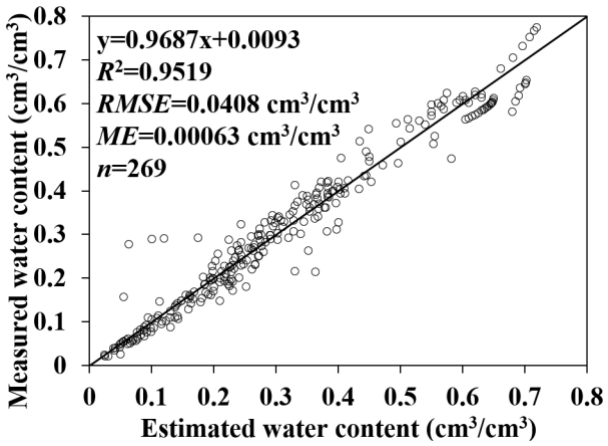

Figure 2.3 Comparison of volumetric water contents measured and estimated using the fractional bulk density (FBD) model for 30 soils with ranges of soil texture from clay to sand and bulk density from 0.33 to 1.65 g/cm^3. The circle represents measured values, and line denotes a 1:1 line.

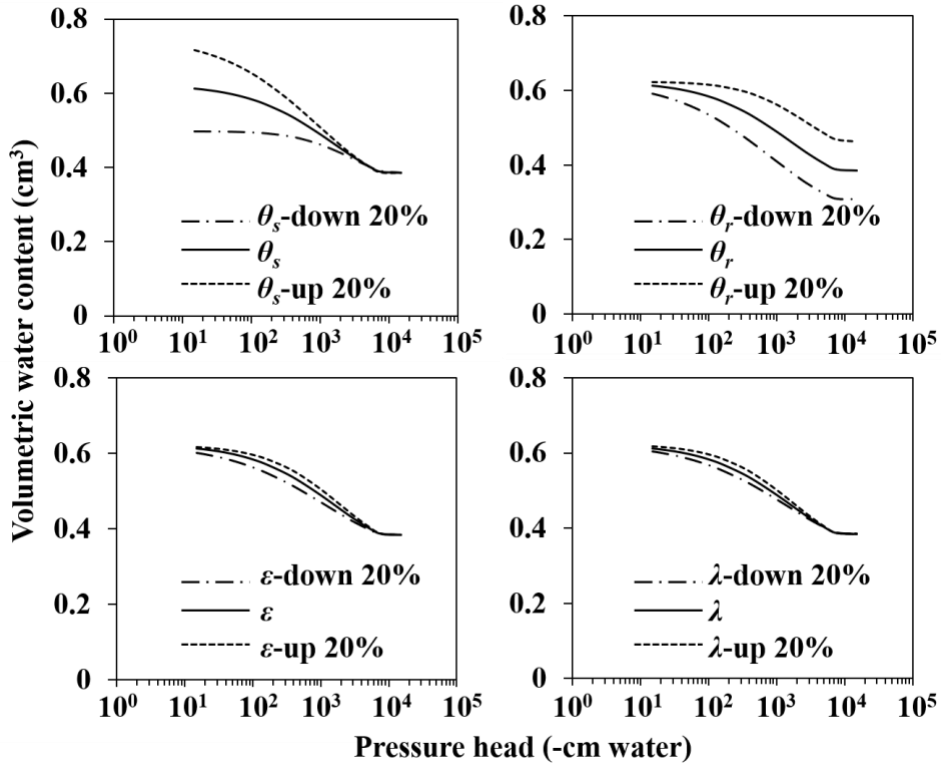

Figure 2.4 A sensitivity analysis on the parameters of the fractional bulk density (FBD) model as Eq. (17). θ_s, θ_r, ε, and λ refer to volumetric saturated water content, volumetric residual water content at a pressure head of 15,000 cm water, particle size distribution index, and rate coefficient in Eq. (12) for particle size distribution, respectively.

Chapter 3. Adhesion on Soil Surfaces Inhibits Bacterial Cell-to-Cell Interaction

Publication Note

The following chapter is in the review for potential publication.

My contribution to this work was experimental design, sample processing, enumeration of bacteria, statistical analysis, and drafting the manuscript.

3.1 Abstract

Bacterial cell-to-cell interactions sustain key processes of soil ecology and health. As habitats of bacteria, the complex pore network and surface properties of soil control spatial distribution, adhesion, and motility of bacteria, influencing bacterial cell-to-cell interactions, such as physical contact-based conjugation. However, our understanding of the controlling environmental factors on the interactions is still limited. In this research, we evaluated the effects of soil surface properties and pore size distribution on bacterial interactions. The conjugation-based bacterial interaction was measured by plasmid transfer between donor and recipient cells within populations of the soil bacterium *Pseudomonas putida*. Using porous sand media that have different surface properties (i.e., surface charge, roughness) and textures from coarse to fine, we observed that the presence of sand increased conjugation frequency compared to sand-free controls, and the frequencies were positively correlated to the pore sizes of sand media. The frequencies were also a function of bacterial adhesion on sand surfaces. The adhesion reduced bacterial conjugation frequency. Collision of bacteria in pore spaces promoted their interactions, while limited motility of bacteria trapped in smaller pores or adhered to sand surfaces reduced the interactions. The study identifies key physical factors that control the interaction and distribution of bacteria in soil pores and provides insight into the role of soil pore systems in biologically mediated processes (e.g., horizontal gene transfer) and soil health.

3.2 Introduction

Soil bacteria share their habitat with a vast diversity of bacterial neighbors, resulting in bacterial interactions. The interactions include horizontal gene transfer mediated by conjugative pili (Soucy et al., 2015), competition and cooperation mediated by diffusible metabolites and chemical signals (Little et al., 2008; Velicer and Vos, 2009), and predatory interactions (Tecon and Or, 2017). Bacterial interactions are vital for evolutionary and ecological processes in soil (Tecon et al., 2018; Zhang et al., 2020). Most interactions occur at the scale of individual bacterial level through close physical contact (Jansson and Hofmockel, 2018; Zhang et al., 2020). The spatial domain of the interactions is limited to the environment surrounding bacteria (Nadell et al., 2016). The individual-based interactions in every domain accumulate and consequently affect community structure in a given habitat, thereby influencing many soil ecological processes such as microbial evolution (Jansson and Hofmockel, 2018; Tecon et al., 2018).

Soils can be viewed as three-dimensional structure consisting of pore spaces and solid grains (Bailey et al., 2013; Wilpiszeski et al., 2019). As bacterial habitats, the highly heterogeneous pore spaces and grains surfaces control bacterial adhesion, distribution, dispersion, and motility (Bailey et al., 2013; Watt et al., 2006). Spatial isolation resulting from the complexity of the soil pore network confines two bacterial microcolonies to unconnected pores or pores with pore throats smaller than 0.2 μm that bacteria cannot pass (Chenu and Stotzky, 2001; Foster, 1988). Evidence shows that about 15%-50% of the soil porosity is inaccessible to bacterial cells (Chenu and Stotzky, 2001). The entrapped bacterial microcolonies may have limited dispersion with short distance and long encounter duration that are favorable to their interaction with neighbors (Tecon and Or, 2017). Additionally, soil remains unsaturated for

most of the time, and the aqueous phase of soil is fragmented by different sizes of pores (Dechesne et al., 2010; Wang and Or, 2013). Tecon et al. (2018) demonstrated that drier conditions where the aqueous phase fragments promoted bacterial cell-to-cell interaction. Motile bacteria are slowed down under drier conditions, which increase the average duration of cell-to-cell contacts, thereby increasing the rate of interactions (i.e., conjugation) (Berthold et al., 2016; Tecon et al., 2018). To sum up, bacterial dispersion and mobility regulate bacterial cell-to-cell interactions in soil. However, related studies of cell-to-cell interactions still limited.

When bacteria move through soil, they adhere to soil surfaces. The adhesion restricts bacterial motility and hence may affect cell-to-cell interactions (Massoudieh et al., 2007). The process of bacterial adhesion is governed by various surface properties, such as surface charge density, wettability, roughness, topography, and stiffness (Carniello et al., 2018; Song et al., 2015; Zheng et al., 2021). Many studies have proposed that van der Waals force and electrostatic interactions are major forces that determine bacterial adhesion onto soil surfaces (Renner and Weibel, 2011). The wall surfaces of bacterial cells typically contain carboxyl, amino, and phosphate groups, which can gain or lose a proton giving the cell surface a net electrical charge under different pH conditions (Rijnaarts et al., 1999). Bacteria generally possess a net negative charge at ambient pH values (Rijnaarts et al., 1999). Consequently, bacterial adhesion occurs more on positively charged surfaces and less on negatively charged surfaces (Gottenbos et al., 1999; Guo et al., 2018; Oh et al., 2018). Currently, it is unclear how bacterial adhesion influences the cell-to-cell interactions and further soil microbial evolution and community diversity.

Conjugation is one of the bacterial cell-to-cell interaction processes. In this process, the conjugative plasmids are transferred from donor to recipient cells through direct cell-to-cell

contact (Couturier et al., 2023; Massoudieh et al., 2007; Von Wintersdorff et al., 2016). In this study, we employed a model system of conjugation between the bacterial donor and recipient cells to explore how soil surface charges and solution ionic strength affect bacterial conjugation. The process was monitored by observing the expression of fluorescent marker genes, which caused the donor, recipient, and transconjugants cells to fluoresce in different colors. Quartz sand with uniform grain size was used to represent the soil particles, and fluorescence imaging and cell counting were used to enumerate various cells and calculate the frequency of conjugation.

3.3 Materials and Methods

3.3.1 Chemicals

Tryptone, yeast extract, agar powder, sodium chloride (NaCl), tetracycline, and iron chloride ($FeCl_3$) were obtained from Fisher Scientific (Waltham, MA, USA). Potassium chloride (KCl), di-sodium hydrogen phosphate (Na_2HPO_4), and potassium phosphate (KH_2PO_4) were obtained from Sigma-Aldrich (St. Louis, MO, USA). All chemicals used were of reagent grade or higher purity.

3.3.2 Porous media preparation

The porous media selected for the study were raw, uniform, Ottawa 20/30 quartz sand (particle size D_{50} = 0.72 mm) and hematite-coated sand. The raw sand was thoroughly rinsed with deionized water to remove any suspended impurities and was then oven-dried at 60 ^{o}C to obtain clean sand (Zhuang et al., 2009). The hematite-coated sand were prepared according to a previously described procedure (Benjamin et al., 1996). Briefly, 80 mL of 2.5 M $FeCl_3$ solution was mixed with 345 g sand and co-heated to 110℃ under stirring hourly for 3 hours until the

sand appeared to be dry. The temperature was raised to 550℃ for additional 3 hours, and then the sand was cooled to room temperature (21±1ºC). Then, the sand was rinsed for five times with Milli-Q water to wash away the dark loose fractions with a dark red coating remained on the sand surface. Since the coating was hygroscopic when the sand was cooled, the coated sand was subjected to seven more drying cycles, each consisting of 3 hours of drying at 110℃ followed by 21 hours at the room temperature. The coating became progressively less hygroscopic during this procedure, and the coating became stable after the final cycle.

3.3.3 Bacterial strains and preparation

The soil bacterium, *Pseudomonas putida* strain KT2440, and its genetically modified strain were used as a model system to examine the effects of cell adhesion and pore confinement on cell-cell contact in terms of conjugation. The wild-type, plasmid-less strain served as the recipient strain. *P. putida* KT2440::*lacI*^{q}*-pLpp-mCherry-Km*^{R} served as the donor strains with the engineered cryptic broad-host range plasmid pKJK5::P*lac*::*gfp* (Klümper et al., 2015). The plasmid-containing donor constitutively expresses the mCherry fluorescent protein as well as the *lacI*^{q} repressor of the P*lac* promoter, which prevents expression of green fluorescent protein (GFP) from the pKJK5::P*lac*::*gfp* plasmid in the donor cell (Tecon et al., 2018). Upon receipt of the plasmid, the recipient cell then becomes a transconjugant when the donor cell makes physical cell-cell contact. GFP can then be expressed in the transconjugant cells because the recipient strain lacks the *lacI*^{q} repressor (Normander et al., 1998; Tecon et al., 2018). In addition, the plasmid encodes resistant genes conferring resistance to tetracycline so that donor and transconjugant cells with the plasmid are resistant and can be selected on tetracycline-containing media.

To prepare bacteria for experiments, both donor and recipient strains were cultivated overnight in the Luria-Bertani (LB) medium containing tryptone at 10 g L^{-1}, yeast extract at 5 g L^{-1}, and NaCl at 10 g L^{-1}at pH 7.2 in the presence or absence of tetracycline (15 μg mL^{-1}). Tetracycline (15 μg mL^{-1}) was added to the donor culture to ensure plasmid maintenance (Tecon et al., 2018). Twenty-five μL of an overnight recipient preculture was transferred into a 50 mL bottle containing 20 mL of fresh LB broth. Because the donor strains grew more slowly under the conditions, 100 μL of an overnight donor preculture was added into a 50 mL bottle containing 20 mL of fresh LB broth with tetracycline. Both strains were cultivated at 30 ℃ with shaking at 280 rpm for approximately 6 h to get cultures in the early stationary phase. The cells of the donor and recipient were then harvested by centrifugation at 6,043 g at 4° C for 10 min. The cell pellets were washed three times using sterile phosphate buffered saline (PBS) after carefully removing the supernatant using a pipette and finally resuspended in 5 mL of PBS. The PBS consisted of NaCl (98 g L^{-1}), 0.2 g of KCl (0.2 g L^{-1}), Na_2HPO_4 (1.15 g L^{-1}), and 0.2 g of KH_2PO_4 (0.2 g L^{-1}). Cell suspensions were diluted in PBS to obtain an optical density of 1 at 600 nm (OD_{600}).

3.3.4 Bacteria adhesion experiments

Bacterial cell adhesion isotherms on clean sand and hematite-coated sand were obtained using a batch equilibration method (Limousin et al., 2007). Briefly, 3.5 g of sterile the clean sand or hematite-coated sand was suspended in 4 mL of bacterial suspension in 0.1× LB broth with a nominal ionic strength of 17 mM at pH 7.2. The mixture was equilibrated at 25 ℃ for 5 min. The un-adhered bacteria were then pipetted from the aqueous phase after the particles sank to the bottom of the tubes. Serial dilutions were plated on LB agar plates to enumerate viable bacteria

as colony forming units (CFU). The number of bacteria absorbed on the clean sand or hematite-coated sand (CFU per g of dry sand) was determined by subtracting the bacteria suspended in the aqueous phase from the total number of bacteria added at the initiation of the equilibration experiments. The adhered bacteria was determined by measuring the extracted amount with different initial bacterial titers of 5.5×10^4, 5.5×10^5, 5.5×10^6, 5.5×10^7, and 5.5×10^8 CFU mL^{-1} *P. putida* KT2440::*lacI*^{q}-*pLpp-mCherry-Km*^{R}). All experiments were performed in triplicate. The bacterial adhesion data was fitted with the following Freundlich isotherm model (Zhao et al., 2014).

$$C_S = K_f \cdot C^{1/n}$$

where C_s is the number of bacteria adhered on sand (CFU g^{-1}), K_f is the coefficient related to adhesion capacity (mL g^{-1}), C is the bacterial cell density in the equilibrium solution (CFU mL^{-1}), and $1/n$ is the linearity exponent.

3.3.5 Conjugation experiments in microcosms

To determine if conditions supporting bacterial growth were required for cell-to-cell conjugation, we incubated the bacteria with recipient-to-donor ratio of 10:1 at different initial total cell densities in PBS without nutrients for growth (no growth) or 0.1× LB media (growth sufficient conditions). The initial cell densities were set as 5.5×10^4, 5.5×10^5, 5.5×10^6, 5.5×10^7, and 5.5×10^8 CFU mL^{-1}. After 24 h incubation, recipient, donor, and transconjugant cells were extracted and enumerated by an adapted drop plate assay (Chen et al., 2003). The frequency of transconjugant cells was obtained by normalizing the number of transconjugants to the sum of transconjugant and recipient cells.

The effect of hematite coating on the bacterial conjugation frequency was investigated. Specifically, 3.5 g of the clean sand or hematite-coated sand was added into 15-mL centrifuge tubes. The total volume of the sand was 2 mL with a pore volume of 700 μL as calculated from the bulk density and sand particle density (2.7 g cm^{-3}). Fifteen μL of a suspension of the recipient and donor cells with a 10:1 ratio was inoculated to 700 μL of sterile 0.1× LB broth, where the microcosms were under saturated conditions (i.e., all pores were liquid-filled without free-standing solution). The bacteria suspension and sand were then mixed evenly in microcosms and incubated at 30 ℃ for 24 h. The experimental conditions of the control microcosms (i.e., free liquid without sand) were set the same as the sand microcosms. After the incubation, 6.3 mL of PBS was added to each tube. The tubes were then placed in a water-bath sonicator (FS20 Ultrasonic Cleaner, Fisher Scientific) to disperse cells for 2 minutes. Recipient, donor, and transconjugant cells were enumerated by an adapted drop plate assay (Chen et al., 2003). In the second set of experiments, background 0.1× LB solution with different ionic strengths adjusted with NaCl concentration (i.e., 0 mM, 17 mM, and 50 mM) was used for bacterial incubation in free liquid and sand microcosms to examine the effect of solution ionic strength on bacterial cell-to-cell conjugation. In the third set of experiments, different intensities of sonication (0-, 2-, and 10-minute sonication) were applied to the incubated samples to detach the bacteria from the sand surfaces. All experiments were performed in triplicate vessels.

3.3.6 Enumeration of cells with fluorescence imaging

Enumeration of donor, recipient, and transconjugant cells were conducted according to an adapted drop plate assay. Briefly, 50 μL-droplets per dilution were pipetted onto agar plates, and the plates were incubated at 30 ℃ overnight. The dilutions resulted in 10-300 CFU per plate for

counting. The total population size, including recipient, donor, and transconjugant cells, was estimated by counting CFU on LB agar plates without tetracycline. Counts on plates with tetracycline were used to get the population size of resistant donor and transconjugant cells. The difference between total and resistant population sizes gave the number of recipient cells. To discriminate donor and transconjugant cells on agar plates with tetracycline, the plates were placed in the fridge for three days to increase the mCherry signal for donors and the GFP signal for transconjugants. IVIS Lumina K w/XGI-8 Anesthesia System (PerkinElmer, Waltham, MA, USA) equipped with the spectral filters for mCherry fluorescence and GFP was used to analyze red and green colonies, respectively.

3.3.7 Statistical analyses

Data were compared with a One-way Analysis of Variance (ANOVA). Duncan tests were applied to assess the statistical differences between mean values. SPSS 28.0 (IBM SPSS Statistics) software was used to perform spearman correlation analyses with different letters (e.g., a, b, c) annotated on graphs to indicate significant statistical differences among treatments at $p<0.05$.

3.4 Results

3.4.1 Effect of initial concentration and bacterial growth on conjugation

Bacterial cells in non-growth media did not occur conjugation events as no transconjugant cells were observed at different initial concentrations (Figure 3.1A). The pre-requirement of cell-to-cell conjugation in this study was bacterial growth (Figure 3.1B), which is consisted with the vast majority of conjugation studies (Barr et al., 1986; Jutkina et al., 2018;

Møller et al., 2017; Schuurmans et al., 2014). The absolute population of transconjugant cells increased to 8.60×10^6, 9.75×10^6, 6.15×10^7, 3.60×10^8, and 1.07×10^9 CFU mL^{-1} following the initial inoculum of 5.50×10^4, 5.50×10^5, 5.50×10^6, 5.50×10^7, and 5.50×10^8 CFU mL^{-1}, respectively (Figure 3.1B). The results indicate that high initial recipient and donor cell concentration boosted the cell-to-cell physical contact increasing the absolute transconjugant population in the limited liquid volume. However, it is worth noting that conjugation frequency was similar at each initial bacterial inoculum except for the highest (5.50×10^8 CFU mL^{-1}). The conjugation frequency was approximately 0.12 at the four lower concentrations, which was 6-fold lower than that at the highest initial cell concentration (Figure 3.1C). Recipient cells with an initial concentration of 5.50×10^8 CFU mL^{-1} grew faster and had stronger competitiveness than the donor cells in the solution, leading to a relatively low conjugation frequency. Accordingly, in this study, all conjugation experiments were conducted in 0.1× LB media for growing bacteria rather than in non-growth media.

3.4.2 Bacterial adhesion isotherms

The clean sand and hematite-coated sand adsorbed the donor cells in different amounts (Figure 3.2). The adsorption followed the Freundlich adsorption isotherm with R^2 values higher than 0.98. The number of adsorbed cells increased with the initial bacterial concentration. The K_f values of donor cells adhesion to the clean sand (0.73 mL g^{-1}) was 2-fold higher than that of hematite-coated sand (0.34 mL g^{-1}). The number of adsorbed cells to hematite-coated sand was higher than those to clean sand, suggesting that iron oxide promotes bacteria adhesion due to the positively charged sites on the hematite.

3.4.3 Effects of hematite on growth and conjugation

The average number of cell doublings for all three types of cells was greater in the presence of either the clean sand or the hematite-coated sand compared to sand-free liquid media (Figure 3.3A). No significant difference in the growth was observed between the clean sand and the hematite-coated sand. Bacterial population increased ~40 folds in the liquid media (corresponding to five to six cell doublings during 24 h incubation time), in comparison with the ~128-fold increase in either the clean sand or hematite-coated sand (Figure 3.3A).

The absolute number of transconjugant cells and conjugation frequency were proposed to evaluate conjugation events in different microcosms. The frequency of conjugation was the number of transconjugants to the sum of transconjugant and recipient cells, which represents the probability of the occurrence of conjugation. The total number of transconjugants enumerated after 24 h of incubation followed the order of sand-free liquid media < hematite-coated sand < clean sand (Figure 3.3B). The absolute numbers of transconjugants were the highest in clean sand microcosms (1.23×10^{7} CFU mL^{-1}) but were the lowest in the sand-free liquid media (4.00×10^{5} CFU per mL^{-1}), suggesting high rate of plasmid transfer in sand microcosms but low rate in sand-free liquid. The conjugation frequency was as low as ~0.005 in the sand-free liquid media. Conjugation frequencies in clean sand and hematite-coated sand microcosms were about 30-fold and 10-fold higher than that in the sand-free liquid media (Figure 3.3C). These results indicate that pores in sand microcosms facilitated cell to cell plasmid transfer, whereas sand surface modification by hematite reduced the frequency of bacterial cell-to-cell conjugation relative to the clean sand.

3.4.4 Effects of ionic strengths on conjugation

Background 0.1× LB broth solutions with different ionic strengths (0, 17, 50, and 100 mM) adjusting with NaCl concentration had no significant influence on bacterial growth in sand-free liquid media or sand-containing microcosms. Likewise, there was no significant difference in the absolute number of transconjugant cells with various IS except at the highest value of 100 mM in sand-free liquid media (Figure 3.4A). At 100 mM, transconjugants approached the highest abundance of approximately 2.10×10^{6} CFU mL^{-1} (Figure 3.4A). The absolute number of transconjugant cells was higher in sand microcosms than in sand-free liquid media., A decreasing trend in the transconjugant cells with increasing ionic strength was observed in the clean sand microcosm (Figure 3.4B). The maximum value (3.55×10^{7} CFU mL^{-1}) was observed at 0 mM, which was 3-fold the minimum value at 100 mM. The decreasing trend was not significant in the hematite-coated sand microcosm (Figure 3.4C). Transconjugants in this microcosm decreased from 2.00×10^{7} to 1.20×10^{7} CFU mL^{-1} with increasing IS from 0 mM to 17 mM but remained constant when the ionic strength is higher than 17 mM.

The frequency of conjugation was not affected by ionic strength in sand-free liquid media, except at the highest ionic strength value of 100 mM where the frequency of conjugation increased significantly (Figure 3.4D). In the presence of clean sand, the frequency of conjugation decreased with increasing ionic strength (Figures 3.4EF). The frequency was about 20-fold larger than that in sand-free liquid media, which the highest value reached to ~0.20 at an ionic strength of 0 mM (Figure 3.4E). However, the frequency of conjugation was not significantly affected by ionic strength in the hematite-coated sand and the value was stable at ~0.1 (Figure 3.4F).

3.4.5 Relationship between transconjugant cells and bacterial adhesion

Sonication was used to detach cells from the sand surfaces. To assess the impact of sonication on the viability of cells each strain was exposed to sonication in liquid media without sand or oxide-coated sand. No statistically significant difference in cell number was observed among the recipient, donor, and transconjugant cells with and without sonication in sand-free liquid media ($P > 0.05$, Figure 3.5A). In the presence of solid phases, the total population of all three bacterial strains in sand microcosms over the 24-h incubation increased by 2.5-4.7 and 3.0-4.6 times after the sonic detachment treatments for 2 and 10 min, respectively (Figures 3.5BC). The results indicated that sonication could detach bacteria from the solid surfaces but had no effect on bacterial survival or reproduction. However, there was no significant difference in transconjugants under different sonic time lengths in clean sand and hematite-coated microcosms (Figures 3.5BC). The results suggested that transconjugants attached to solid surfaces had a minimal contribution to the total abundance of transconjugants.

3.5 Discussion

3.5.1 Conjugation

The study aimed to evaluate the effect of solid surfaces on the frequency of cell-cell interactions. Conjugation was used as a proxy measurement to quantitatively assess cell-to-cell contact with a model bacterial system with fluorescent bioreporters. The presence of sand particles in the aqueous phase promoted conjugation compared with that in the free liquid media (Figure 3.3). The greater conjugation frequency observed in the sand-containing microcosms compared to the sand-free controls may be due to the compartment of aqueous (Figure 3.6). Bacteria have evolved a large array of motility mechanisms to promote colonization in the

environment (Jarrell and McBride, 2008; Miyata et al., 2020; Raina et al., 2019). In aqueous environments, bacterial swimming motility using a single or multiple flagella is the most well characterized mechanism (Berg and Anderson, 1973; Nakamura and Minamino, 2019; Silverman and Simon, 1974). Cells swim freely by rotating their flagellar filament (Nakamura and Minamino, 2019). When all the flagella in a cell spin counterclockwise, the filaments form a bundle behind the cell that pushes it forward in roughly a straight line (Turner et al., 2000; Wadhwa and Berg, 2022). Once cells encounter obstacles or sense a change in the concentration gradient of a chemical attractant/repellant, flagella switch their direction of rotation and then straight swimming of the cell continues in a new direction (Berg and Brown, 1972; Larsen et al., 1974). *P. putida,* used in this study, is a multi-flagellated species that has five to seven flagella at one pole (Harwood et al., 1989). The motility of these cells generally follows a straight line in the aqueous environment, but cells reorient their direction when encountering the sand particles (Turner et al., 2000; Wadhwa and Berg, 2022). The aqueous phase within the porous structure of sand matrices was typically disconnected, forming isolated water filled compartments (Figure 3.6). Each 'compartment' had a smaller volume and a shorter cell-to-cell distance than that in the solid-free aqueous cell suspensions. *P. putida* required direct contact (<1 μm of donor-recipient distance) with rigid pilus to transfer plasmids (Seoane et al., 2011). As a result, conjugation events should be more frequent in the aqueous phase with solid particles of porous matrix either via confinement of cells in smaller pore spaces serving to increase the cell density and probability of cell-to-cell contact or through attachment to surfaces co-localizing cells in close physical proximity (Figure 3.6).

3.5.2 Adhesion affects cell-to-cell conjugation

The confinement of cells in small spaces (microcosms) promotes cell-to-cell contact as we discussed before but bacterial cell adhesion on solid surface might hinder the contact process as shown in our results (Figure 3.3) with higher frequency in hematite-coated sand microcosm. The isoelectric point of *P. putida* KT2440::*lacI*^{q}*-pLpp-mCherry-Km*^{R} is ~pH 6.52 and the point of zero charge for hematite was found to be ~pH 8.8 (Hanna, 2007). Therefore, at pH 7.2 (i.e., the experimental conditions), the net surface charge of the bacterial donor strain was negative while the surface charge of hematite-coated sand was positive. The ionic attraction of cells to the surface allowed cell attachment through electrical attraction forces. More positive charges on sand surfaces result in stronger attraction interactions. The surface charge of hematite-coated sand was more positive than clean sand, which produced larger attraction forces between the bacterial donor strain and the hematite-coated sand surface.

A plausible explanation for the adhesion inhibiting conjugation is that the cellular alignment on the solid surface likely limited bacterial mobility. Bacterial cells, such as *Pseudomonas* strains (Wadhwa and Berg, 2022), aligned themselves in ways that would maximize contact area between the cell and the solid surface (Díaz et al., 2007; Hochbaum and Aizenberg, 2010; Hsu et al., 2013). During this process, motile bacteria firstly differentiate into an aligned chain of cells, and then growing chains further develop fibers and bundles on the solid surface (Honda et al., 2015; Mamou et al., 2016; Mendelson, 1999). These well-aligned structures promote sliding of a colony on a solid surface where the swimming behavior of bacteria is not efficient, which might achieve a stronger and more stable attachment (Van Gestel et al., 2015; Yaman et al., 2019). Typically, conjugation occurred by transferring the plasmid from the donor through the pilus to the side of the recipient cell opposing the location of pilus

attachment (Honda et al., 2015; Mamou et al., 2016; Mendelson, 1999). However, adhesion of bacteria to the surface of sand particles fixed the cells, contributing to the loss of motility and limiting bacteria to contact with other bacteria swimming in liquid phase of inter-sand particles (Honda et al., 2015; Mamou et al., 2016; Mendelson, 1999; Van Gestel et al., 2015; Yaman et al., 2019), and thereby adversely impacting conjugation frequency.

The bacterial plasmid transfer competence on sand surface does not occur in all cells of a population. In the current study, bacterial adhesion was well described using the Freundlich isotherm indicative of multiple layer adsorption (Halsey, 1948; Kalam et al., 2021). Prior studies have demonstrated that conjugation preferentially proceeded at the top surface of the biofilm but not in the deeper layers (Madsen et al., 2012; Molin and Tolker-Nielsen, 2003; Reisner et al., 2012; Stalder and Top, 2016). In addition, discontinuous patches of plasmid transfer between donor and recipient cells appears at the edge of bacterial colonies on solid surfaces (Koraimann and Wagner, 2014; Reisner et al., 2012). These discontinuous patches demonstrate infrequent events of plasmid transfer from some cells of the donor cells to recipient cells but not from all (Koraimann and Wagner, 2014). Based on the available information, donor and recipient cell adhesion hindered the bacterial conjugation likely by affecting bacterial mobility and the number of bacteria available for occurring conjugation.

3.5.3 Impact of ionic strength on cell-to-cell conjugation

The conjugation frequency varied in the presence of the clean sand and hematite-coated sand under different ionic strength conditions. It should be noted elucidating the ionic strength effects were difficult to determine by the inclusion of 0.1× in the experimental solutions because conjugation failed or was below detection in minimal salt solutions that would not support the

growth of the experimental strains. Thus, the true ionic strength of the experimental system was difficult to calculate because 0.1× LB broth was included in the experimental solutions. The normalized ionic strength reported here refers only to the addition of varying amounts of NaCl added to the 0.1× LB broth base media. The interaction between the surface (i.e., particle with relatively large size, sand) and a smaller particle such as a cell, combines the effects of van der Waals attraction and the electrostatic repulsion due to the electric double layer of counterions based on the DLVO theory (Hiemenz and Rajagopalan, 2016; Marshall et al., 1971). Increasing ionic strength in aqueous solutions shields surface electronic charges of both bacteria and the sorbing sand surface yielding the decrease of attraction and electrostatic repulsion (Barrow, 1987; Zhuang and Jin, 2003). Thus, the electrostatic repulsion between the surface and the tiny particle decreases with increasing ionic strength when the surface and the tiny particle have the same sign of charges. As *P. putida* and clean sand surfaces are negatively charged at the experimental pH 7.2, the decrease of conjugation frequency with increasing ionic strength could be caused by the increased bacterial adhesion (Figures 3.4BE), which is the result of reduced electrostatic repulsion between bacterial cells and clean sand. In contrast, increasing ionic strength decreases attraction between the sand particle surface and the cell due to the same shielding effect when the surface and the cell are oppositely charged (Barrow, 1987; Jones and O'Melia, 2000; Zhuang and Jin, 2003). However, as hematite-coated sand surface was positively charged at the experimental pH 7.2, in this study, organic molecules in the LB medium may have adsorbed to the surfaces creating less polar organic films and creating a new surface on which the bacteria may adhere (Bos et al., 1999; Hori and Matsumoto, 2010; Schneider and Marshall, 1994). Some of the sites on the hematite-coated sand that would otherwise be available for bacterial adhesion were probably occupied by organic materials. Increasing ionic strength likely

reduced organic matter adsorption on the surface, which liberated some sites for bacterial adhesion. Indeed, bacteria attached more to the hematite-coated sand surface at high rather than low ionic strength. The enhanced cellular adsorption may have been the cause of the decrease conjugation frequency when the ionic strength was increased in the hematite-coated sand microcosms (Figures 3.4CF).

3.6 Environmental implications

Bacterial cell-to-cell interactions control community diversity, dynamics, and functioning and are of critical importance to evolutionary and ecological processes in environments (Tecon et al., 2018; Zhang et al., 2020). To interact, bacteria have to remain close physical contact, and thus the complex soil pores and rough surface that greatly influence bacterial dispersion, motility, separation, and isolation are crucial for shaping bacterial interactions (Wilpiszeski et al., 2019). Our findings advance the understanding that physicochemical dynamics govern soil microbial spatial distribution and interaction. By extension, these findings have implications for possibly managing microbial activity through environment-friendly physical approaches. Many agricultural operations affect physical conditions in soil, such as the disruption of soil structure due to crop cultivation and tillage (Six et al., 2000). The sustainability of agricultural management necessitates to pay special attention on the relation between key physical factors and microbial life. Our findings also inform quantitative models that predict ecological processes relevant to microbial life in the soil. Integrating basic principles of microbial ecology to predictive models accurately offers evidence-based soil management strategies.

Acknowledgments

We thank Steven Ripp and Larry Millet at the University of Tennessee for providing IVIS Lumina K w/XGI-8 Anesthesia System. We also thank Arnaud Dechesne at Technical University of Denmark for providing the *P. putida* KT2440 and *P. putida* KT2440::*lacl*^{q}*-pLpp-mCherry-Km*^{R}.

References

Bailey VL, McCue LA, Fansler SJ, Boyanov MI, DeCarlo F, Kemner KM, et al. Micrometer-scale physical structure and microbial composition of soil macroaggregates. Soil Biology and Biochemistry 2013; 65: 60-68.

Barr V, Barr K, Millar M, Lacey R. β-Lactam antibiotics increase the frequency of plasmid transfer in Staphylococcus aureus. Journal of Antimicrobial Chemotherapy 1986; 17: 409-413.

Barrow N. Reactions With Variable Charge Soils.‖ Martinus Nijhoff/Dr W. Junk Publishers, Dordrecht, The Netherlands, 1987.

Benjamin MM, Sletten RS, Bailey RP, Bennett T. Sorption and filtration of metals using iron-oxide-coated sand. Water research 1996; 30: 2609-2620.

Berg HC, Anderson RA. Bacteria swim by rotating their flagellar filaments. Nature 1973; 245: 380-382.

Berg HC, Brown DA. Chemotaxis in Escherichia coli analysed by three-dimensional tracking. nature 1972; 239: 500-504.

Berthold T, Centler F, Hübschmann T, Remer R, Thullner M, Harms H, et al. Mycelia as a focal point for horizontal gene transfer among soil bacteria. Scientific Reports 2016; 6: 1-8.

Bos R, Van der Mei HC, Busscher HJ. Physico-chemistry of initial microbial adhesive interactions–its mechanisms and methods for study. FEMS microbiology reviews 1999; 23: 179-230.

Carniello V, Peterson BW, van der Mei HC, Busscher HJ. Physico-chemistry from initial bacterial adhesion to surface-programmed biofilm growth. Advances in colloid and interface science 2018; 261: 1-14.

Chen C-Y, Nace GW, Irwin PL. A 6× 6 drop plate method for simultaneous colony counting and

MPN enumeration of Campylobacter jejuni, Listeria monocytogenes, and Escherichia coli. Journal of microbiological methods 2003; 55: 475-479.

Chenu C, Stotzky G. Interactions between microorganisms and soil particles: an overview. Interactions between soil particles and microorganisms: Impact on the terrestrial ecosystem 2001: 3-40.

Couturier A, Virolle C, Goldlust K, Berne-Dedieu A, Reuter A, Nolivos S, et al. Real-time visualisation of the intracellular dynamics of conjugative plasmid transfer. Nature Communications 2023; 14: 294.

Dechesne A, Wang G, Gülez G, Or D, Smets BF. Hydration-controlled bacterial motility and dispersal on surfaces. Proceedings of the National Academy of Sciences 2010; 107: 14369-14372.

Díaz C, Cortizo MC, Schilardi PL, Saravia SGGd, Mele MAFLd. Influence of the nano-micro structure of the surface on bacterial adhesion. Materials Research 2007; 10: 11-14.

Foster R. Microenvironments of soil microorganisms. Biology and fertility of soils 1988; 6: 189-203.

Gottenbos B, Van Der Mei H, Busscher H, Grijpma D, Feijen J. Initial adhesion and surface growth of Pseudomonas aeruginosa on negatively and positively charged poly (methacrylates). Journal of Materials Science: Materials in Medicine 1999; 10: 853-855.

Guo S, Kwek MY, Toh ZQ, Pranantyo D, Kang E-T, Loh XJ, et al. Tailoring polyelectrolyte architecture to promote cell growth and inhibit bacterial adhesion. ACS applied materials & interfaces 2018; 10: 7882-7891.

Halsey G. Physical adsorption on non-uniform surfaces. The Journal of chemical physics 1948; 16: 931-937.

Hanna K. Adsorption of aromatic carboxylate compounds on the surface of synthesized iron oxide-coated sands. Applied Geochemistry 2007; 22: 2045-2053.

Harwood CS, Fosnaugh K, Dispensa M. Flagellation of Pseudomonas putida and analysis of its motile behavior. Journal of bacteriology 1989; 171: 4063-4066.

Hiemenz PC, Rajagopalan R. Principles of Colloid and Surface Chemistry, revised and expanded: CRC press, 2016.

Hochbaum AI, Aizenberg J. Bacteria pattern spontaneously on periodic nanostructure arrays. Nano letters 2010; 10: 3717-3721.

Honda R, Wakita J-i, Katori M. Self-elongation with sequential folding of a filament of bacterial cells. Journal of the Physical Society of Japan 2015; 84: 114002.

Hori K, Matsumoto S. Bacterial adhesion: from mechanism to control. Biochemical Engineering Journal 2010; 48: 424-434.

Hsu LC, Fang J, Borca-Tasciuc DA, Worobo RW, Moraru CI. Effect of micro-and nanoscale topography on the adhesion of bacterial cells to solid surfaces. Applied and environmental microbiology 2013; 79: 2703-2712.

Jansson JK, Hofmockel KS. The soil microbiome—from metagenomics to metaphenomics. Current opinion in microbiology 2018; 43: 162-168.

Jarrell KF, McBride MJ. The surprisingly diverse ways that prokaryotes move. Nature reviews microbiology 2008; 6: 466-476.

Jones KL, O'Melia CR. Protein and humic acid adsorption onto hydrophilic membrane surfaces: effects of pH and ionic strength. Journal of Membrane Science 2000; 165: 31-46.

Jutkina J, Marathe N, Flach C-F, Larsson D. Antibiotics and common antibacterial biocides stimulate horizontal transfer of resistance at low concentrations. Science of the total

Environment 2018; 616: 172-178.

Kalam S, Abu-Khamsin SA, Kamal MS, Patil S. Surfactant adsorption isotherms: A review. ACS omega 2021; 6: 32342-32348.

Klümper U, Riber L, Dechesne A, Sannazzarro A, Hansen LH, Sørensen SJ, et al. Broad host range plasmids can invade an unexpectedly diverse fraction of a soil bacterial community. The ISME journal 2015; 9: 934-945.

Koraimann G, Wagner MA. Social behavior and decision making in bacterial conjugation. Frontiers in cellular and infection microbiology 2014; 4: 54.

Larsen SH, Reader RW, Kort EN, Tso W-W, Adler J. Change in direction of flagellar rotation is the basis of the chemotactic response in Escherichia coli. Nature 1974; 249: 74-77.

Limousin G, Gaudet J-P, Charlet L, Szenknect S, Barthes V, Krimissa M. Sorption isotherms: A review on physical bases, modeling and measurement. Applied geochemistry 2007; 22: 249-275.

Little AE, Robinson CJ, Peterson SB, Raffa KF, Handelsman J. Rules of engagement: interspecies interactions that regulate microbial communities. Annu. Rev. Microbiol. 2008; 62: 375-401.

Madsen JS, Burmølle M, Hansen LH, Sørensen SJ. The interconnection between biofilm formation and horizontal gene transfer. FEMS Immunology & Medical Microbiology 2012; 65: 183-195.

Mamou G, Mohan GBM, Rouvinski A, Rosenberg A, Ben-Yehuda S. Early developmental program shapes colony morphology in bacteria. Cell reports 2016; 14: 1850-1857.

Marshall K, Stout R, Mitchell R. Mechanism of the initial events in the sorption of marine bacteria to surfaces. Microbiology 1971; 68: 337-348.

Massoudieh A, Mathew A, Lambertini E, Nelson K, Ginn T. Horizontal gene transfer on surfaces in natural porous media: conjugation and kinetics. Vadose Zone Journal 2007; 6: 306-315.

Mendelson NH. Bacillus subtilis macrofibres, colonies and bioconvection patterns use different strategies to achieve multicellular organization. Environmental Microbiology 1999; 1: 471-477.

Miyata M, Robinson RC, Uyeda TQ, Fukumori Y, Fukushima Si, Haruta S, et al. Tree of motility–A proposed history of motility systems in the tree of life. Genes to Cells 2020; 25: 6-21.

Molin S, Tolker-Nielsen T. Gene transfer occurs with enhanced efficiency in biofilms and induces enhanced stabilisation of the biofilm structure. Current opinion in biotechnology 2003; 14: 255-261.

Møller TS, Liu G, Boysen A, Thomsen LE, Lüthje FL, Mortensen S, et al. Treatment with cefotaxime affects expression of conjugation associated proteins and conjugation transfer frequency of an IncI1 plasmid in Escherichia coli. Frontiers in microbiology 2017; 8: 2365.

Nadell CD, Drescher K, Foster KR. Spatial structure, cooperation and competition in biofilms. Nature Reviews Microbiology 2016; 14: 589-600.

Nakamura S, Minamino T. Flagella-driven motility of bacteria. Biomolecules 2019; 9: 279.

Normander B, Christensen BB, Molin S, Kroer N. Effect of bacterial distribution and activity on conjugal gene transfer on the phylloplane of the bush bean (Phaseolus vulgaris). Applied and Environmental Microbiology 1998; 64: 1902-1909.

Oh JK, Yegin Y, Yang F, Zhang M, Li J, Huang S, et al. The influence of surface chemistry on the kinetics and thermodynamics of bacterial adhesion. Scientific reports 2018; 8: 1-13.

Raina J-B, Fernandez V, Lambert B, Stocker R, Seymour JR. The role of microbial motility and chemotaxis in symbiosis. Nature Reviews Microbiology 2019; 17: 284-294.

Reisner A, Wolinski H, Zechner EL. In situ monitoring of IncF plasmid transfer on semi-solid agar surfaces reveals a limited invasion of plasmids in recipient colonies. Plasmid 2012; 67: 155-161.

Renner LD, Weibel DB. Physicochemical regulation of biofilm formation. MRS bulletin 2011; 36: 347-355.

Rijnaarts HH, Norde W, Lyklema J, Zehnder AJ. DLVO and steric contributions to bacterial deposition in media of different ionic strengths. Colloids and Surfaces B: Biointerfaces 1999; 14: 179-195.

Schneider RP, Marshall KC. Retention of the Gramnegative marine bacterium SW8 on surfaces—effects of microbial physiology, substratum nature and conditioning films. Colloids and surfaces B: Biointerfaces 1994; 2: 387-396.

Schuurmans JM, van Hijum SA, Piet JR, Händel N, Smelt J, Brul S, et al. Effect of growth rate and selection pressure on rates of transfer of an antibiotic resistance plasmid between E. coli strains. Plasmid 2014; 72: 1-8.

Seoane J, Yankelevich T, Dechesne A, Merkey B, Sternberg C, Smets BF. An individual-based approach to explain plasmid invasion in bacterial populations. FEMS microbiology ecology 2011; 75: 17-27.

Silverman M, Simon M. Flagellar rotation and the mechanism of bacterial motility. Nature 1974; 249: 73-74.

Six J, Elliott ET, Paustian K. Soil macroaggregate turnover and microaggregate formation: a mechanism for C sequestration under no-tillage agriculture. Soil Biology and Biochemistry 2000; 32: 2099-2103.

Song F, Koo H, Ren D. Effects of material properties on bacterial adhesion and biofilm formation.

Journal of dental research 2015; 94: 1027-1034.

Soucy SM, Huang J, Gogarten JP. Horizontal gene transfer: building the web of life. Nature Reviews Genetics 2015; 16: 472-482.

Stalder T, Top E. Plasmid transfer in biofilms: a perspective on limitations and opportunities. NPJ biofilms and microbiomes 2016; 2: 1-5.

Tecon R, Ebrahimi A, Kleyer H, Erev Levi S, Or D. Cell-to-cell bacterial interactions promoted by drier conditions on soil surfaces. Proceedings of the National Academy of Sciences 2018; 115: 9791-9796.

Tecon R, Or D. Biophysical processes supporting the diversity of microbial life in soil. FEMS microbiology reviews 2017; 41: 599-623.

Turner L, Ryu WS, Berg HC. Real-time imaging of fluorescent flagellar filaments. Journal of bacteriology 2000; 182: 2793-2801.

Van Gestel J, Vlamakis H, Kolter R. From cell differentiation to cell collectives: Bacillus subtilis uses division of labor to migrate. PLoS biology 2015; 13: e1002141.

Velicer GJ, Vos M. Sociobiology of the myxobacteria. Annual review of microbiology 2009; 63: 599-623.

Von Wintersdorff CJ, Penders J, Van Niekerk JM, Mills ND, Majumder S, Van Alphen LB, et al. Dissemination of antimicrobial resistance in microbial ecosystems through horizontal gene transfer. Frontiers in microbiology 2016; 7: 173.

Wadhwa N, Berg HC. Bacterial motility: machinery and mechanisms. Nature Reviews Microbiology 2022; 20: 161-173.

Wang G, Or D. Hydration dynamics promote bacterial coexistence on rough surfaces. The ISME journal 2013; 7: 395-404.

Watt M, Silk WK, Passioura JB. Rates of root and organism growth, soil conditions, and temporal and spatial development of the rhizosphere. Annals of botany 2006; 97: 839-855.

Wilpiszeski RL, Aufrecht JA, Retterer ST, Sullivan MB, Graham DE, Pierce EM, et al. Soil aggregate microbial communities: towards understanding microbiome interactions at biologically relevant scales. Applied and environmental microbiology 2019; 85: e00324-19.

Yaman YI, Demir E, Vetter R, Kocabas A. Emergence of active nematics in chaining bacterial biofilms. Nature communications 2019; 10: 1-9.

Zhang Z, van Kleunen M, Becks L, Thakur MP. Towards a general understanding of bacterial interactions. Trends in microbiology 2020; 28: 783-785.

Zhao W, Walker SL, Huang Q, Cai P. Adhesion of bacterial pathogens to soil colloidal particles: influences of cell type, natural organic matter, and solution chemistry. Water research 2014; 53: 35-46.

Zheng S, Bawazir M, Dhall A, Kim H-E, He L, Heo J, et al. Implication of surface properties, bacterial motility, and hydrodynamic conditions on bacterial surface sensing and their initial adhesion. Frontiers in Bioengineering and Biotechnology 2021; 9: 82.

Zhuang J, Jin Y. Virus retention and transport through Al-oxide coated sand columns: effects of ionic strength and composition. Journal of Contaminant Hydrology 2003; 60: 193-209.

Zhuang J, Tyner JS, Perfect E. Colloid transport and remobilization in porous media during infiltration and drainage. Journal of Hydrology 2009; 377: 112-119.

Appendix

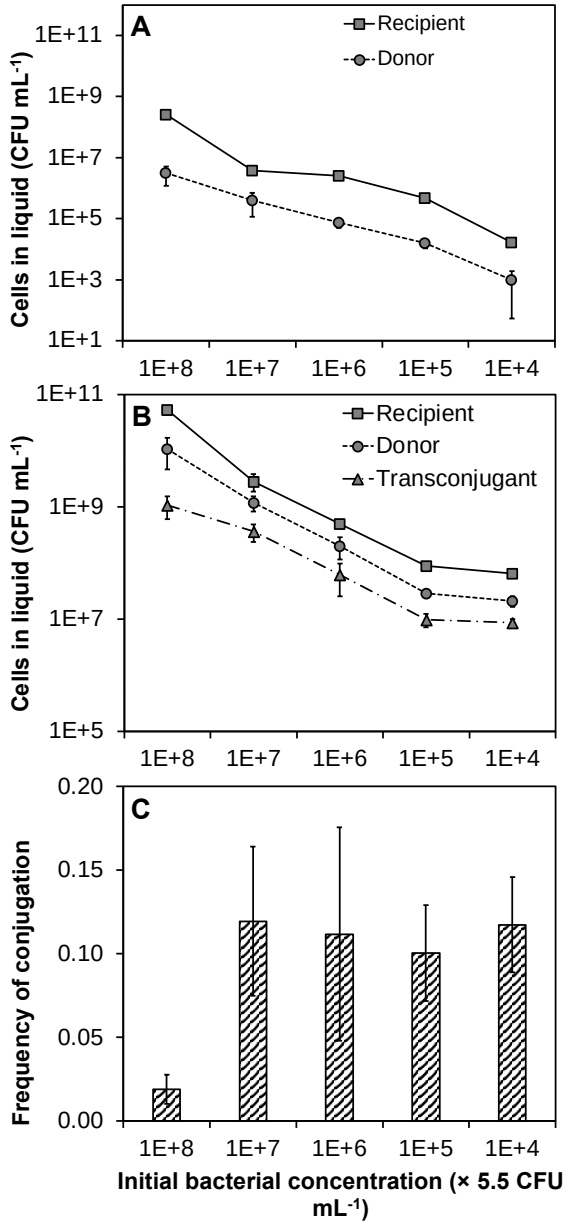

Figure 3.1 Absolute bacterial number and conjugation frequency in non-growth and growth bacterial cultures after 24 h incubation. (A) Absolute number of recipient and donor cells in non-growth culture (PBS). (B) Absolute number of recipient, donor, and transconjugant cells in growth culture (LB medium). (C) Conjugation frequency in LB medium which was calculated by the quotient of transconjugants and the total of transconjugants and recipients. Error bars represent the standard deviations of triplicate vessels.

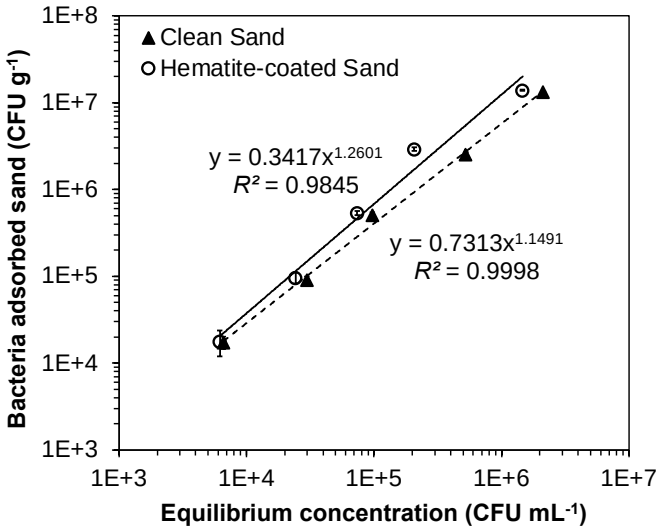

Figure 3.2 Equilibrium adhesion isotherms of donor cells (*P. putida* KT2440::*lacI*^{q}*-pLpp-mCherry-Km*^{R}) to clean sand and hematite coated sand at pH 7.2 in 0.1× LB solution with 17 mM ionic strength adjusting with NaCl concentration. The solid and dashed lines represent fitted curves by the Freundlich equations for clean sand and hematite-coated sand, respectively. Error bars represent the standard deviations of triplicate vessels.

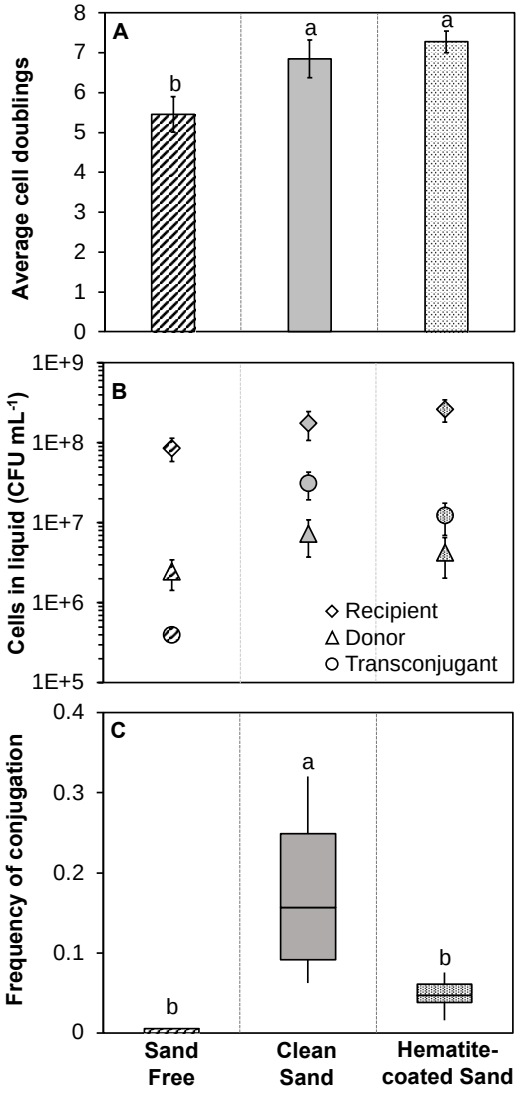

Figure 3.3 Bacterial population after 24 h of incubation at 30°C in liquid and sand microcosms. (A) average cell doublings for total bacterial population. (B) the final number of recipients, donors, and transconjugants after incubation. (C) the frequency of transconjugation calculated as the ratio of transconjugants to the sum of transconjugants and recipients. Error bars represent the standard deviations of triplicate vessels. Different letters (e.g., a, b, c) were annotated on graphs to indicate significant statistical differences among treatments at $p<0.05$.

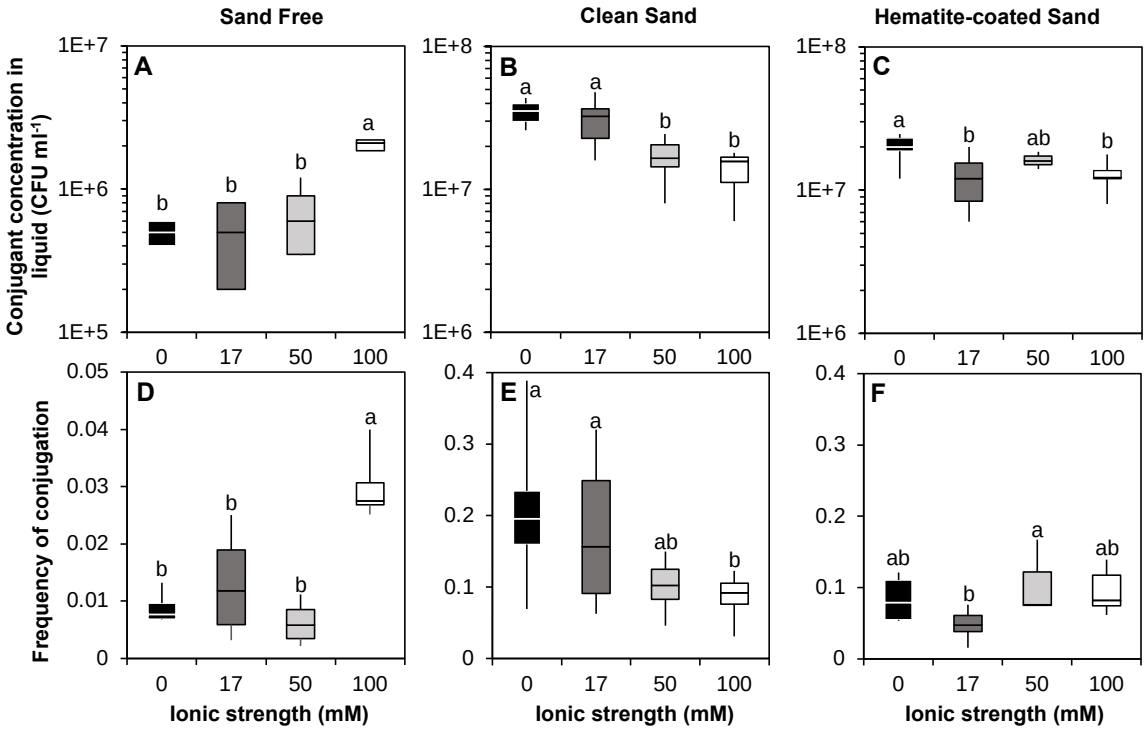

Figure 3.4 Absolute number of transconjugant cells (ABC) and frequency of conjugation events (DEF) after 24 h incubation in sand-free liquid media and in sand microcosms (i.e., clean sand and hematite-coated sand) with different ionic strengths (0, 17, 50, and 100 mM). Error bars represent the standard deviations of triplicate vessels. Different letters (e.g., a, b, c) were annotated on graphs to indicate significant statistical differences among treatments at $p<0.05$.

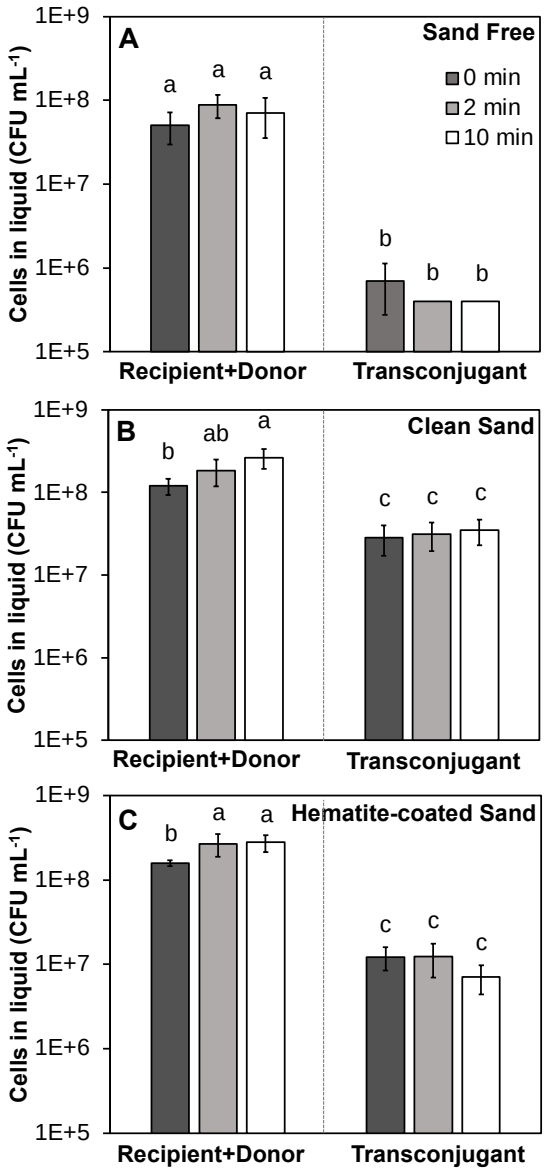

Figure 3.5 Absolute number of recipient, donor, and transconjugant cells after incubation of 24 h in sand-free liquid media (A) and in microcosms (i.e., clean sand (B) and hematite-coated sand (C)) under different exposures to sonication (0 min, 2 min, and 10 min sonic). Error bars represent the standard deviations of triplicate vessels. Different letters (e.g., a, b, c) were annotated on graphs to indicate significant statistical differences among treatments at $p<0.05$.

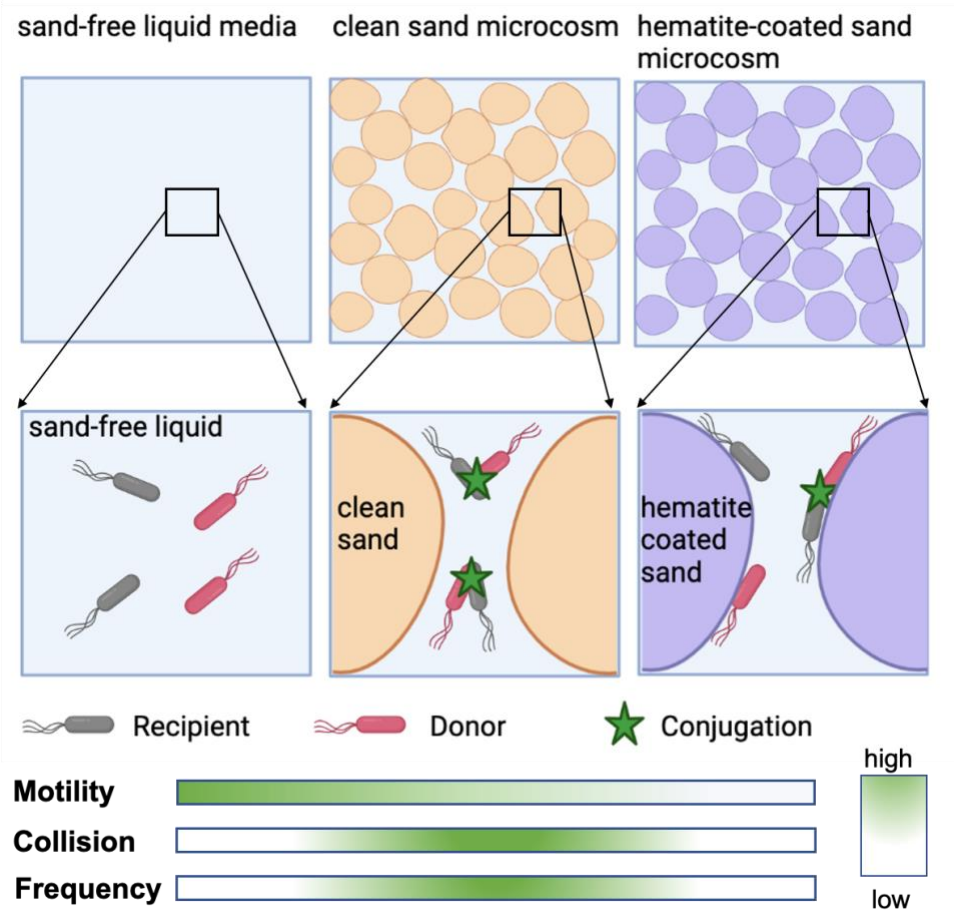

Figure 3.6 Conceptual diagrams of potential impacts sand particles with different surface properties on cell-to-cell contact as measured by conjugation frequency. In sand-free liquid media, donor cells fail to encounter recipient cells due to bacterial swimming with a straight line. The enhanced conjugation frequency observed in the presence of sand particles may have resulted from closer confinement and more collision of interacting cells in smaller pore spaces. However, the hematite-coated surface immobilizes donor and recipient cells, lowering conjugation frequency.

Chapter 4. Pore-scale Distribution of Bacteria and Viruses in Soil Using Small Angle Scattering

Publication Note

The following chapter is in the review for potential publication.

My contribution to this work was experimental design, sample processing, enumeration of bacteria and viruses, SAS data analysis, and drafting the manuscript.

4.1 Abstract

Soil microbe habitats and are active in a complex 3-D soil physical framework. The structure of solid and pore space causes a variety of local conditions at the pore scale in soil, which determines microbial growth, activity, and interaction with one another, thereby affecting soil ecosystem function. However, the quantification of the spatial distribution of microbe at a fine scale remains scarce due to the technique limitation. This study examined relationships between the pore structure of soil macroaggregates and the pore-scale distribution within that structure. Small angle scattering techniques, including ultra-small angle X-ray scattering (USAXS), ultra-small angle neutron scattering (USANS), and SANS, were used to characterize the soil pore structure. The distribution of model bacteria (*Escherichia coli* strain C3000) and viruses (MS2) at different sized pores was evaluated based on the difference in X-ray/neutron contrast among soil, bacteria/viruses, and air. Results imply that the optimal pore size for bacterial colonization was greatly close to bacterial size. In our case, 2 μm-sized *E. coli* distributed in 2.1 to 3.6 μm-sized pores with high abundance. Viruses in soil pores were aggregated together to prevent penetration into nanopores where viruses remain inaccessible until it is eventually dislodged by water flow and removed from the pores, or the stable pores are themselves physically or biologically disrupted. The study provides direct evidence for the microbial distribution at the micro- and nano-pore scale in soil, which is a significant step towards a complete understanding of microbial dynamics in structured soils.

4.2 Introduction

Soils harbor myriads of microbial communities serving as the trophic foundation of the food webs that sustain terrestrial life on Earth (Erktan et al., 2020; Wilpiszeski et al., 2019). Soils and microbes recycle nutrients to support the growth of primary producers and provide the elemental cycling pathways of production and degradation (Jansson and Fredrickson, 2010; Jansson and Hofmockel, 2020; Leff et al., 2018; Tecon and Or, 2017). Due to the large spatial heterogeneity of soils, the microbial distribution is intricately linked with soil structure, such as pore size distribution, pore connectivity, and aggregation (Hartmann and Six, 2023; Vos et al., 2013). The variability of soil structure at different scales of measurement presents difficulty in establishing a reliable predictive comprehension of microbial processes occurring within the soil (Graham et al., 2016). Studying the spatial patterns of soil microbes assists in gaining a deeper understanding of microbial contributions to soil functions.

At the spatial scales that are most pertinent to microbial biogeochemistry, soils consist of microaggreagtes (<250 μm) and macroaggregates (250 to 2,000 μm) (De Gryze et al., 2006; Six et al., 2000). Geometrical characteristics of the pore space of aggregates, including pore volume, shape, connectivity, size, and tortuosity of pathways, can impact microbial distributions and interactions in soil at different length scales (Bailey et al., 2013; Ebrahimi and Or, 2016; Sessitsch et al., 2001). Soil organic matter fills micropores in microaggregates, remaining water to form immobile water film or a hydration shell that restricts microbial movement (Six et al., 2004; Zhuang et al., 2008). Macroaggregates regulate oxygen diffusion through the gaseous phase and water flow, as well as the microbial motility (Carminati et al., 2007; Sexstone et al., 1985). Moreover, the accessibility of pore spaces for various microbes influences microbial interactions, such as the transmission of viruses between bacterial populations. The majority of

microbes live in soil pores ranging from nanometer to millimeter. The sizes of bacteria range from 500 to 10,000 nm, whereas the sizes of viruses range from 20 to 80 nm. Theoretically, viruses could reach into pores down to 30 nm whereas bacteria only access the pores larger than 500 nm (Kuzyakov and Mason-Jones, 2018; Radlinski et al., 2004). The difference in the distribution between bacteria and viruses in soil pores may control their abundance and diversity, interactions in heterogeneous soils (Kuzyakov and Mason-Jones, 2018). Although the significant impact of soil structure on soil microbial activities, it remains an extremely challenging task to non-destructively measure microbial distribution across soil pores of varying sizes, especially at nano- and micro-scale pores.

Small angle scattering (SAS) techniques, including (ultra) small angle X-ray scattering and neutron scattering (i.e., SAXS, SANS, USAXS, and USANS), have been widely applied to study pore structure in a variety of materials, such as petrographic samples (Liu et al., 2019; Vishal et al., 2019), activated or graphitic carbons (Wang et al., 2022), porous alumina (Rasmussen, 2001), and natural soils (Mayer et al., 2004; McCarthy et al., 2008). The SAS refers to the deflection of a beam of radiation (X-rays, neutron) from its original direction by interaction with electrons (for X-ray scattering) or atomic nuclei (for neutron scattering) at pore surfaces within the sample (Glatter et al., 1982). Compared with other techniques, SAS can study a wide range of void sizes (from ~10Å to 15-μm) (McCarthy et al., 2008). Further, because X-rays and neutrons penetrate through the sample, these techniques provide information on the entire void space and its contents, not just those portions accessible from the exterior (Melnichenko, 2016). In addition, the scattering ability of different materials for X-rays or neutrons varies, thereby variations in the material composition within a pore may cause contrasts in scattering intensity (Melnichenko, 2016). Consequently, the SAS techniques can provide

information about porosity, pore size distribution, and the size distribution of water- and microbe-filled pores at μm, even nm, resolution. They could be a powerful approach to examining the microbial distribution within intact soil structures at the fine pore scale.

The goal of this study was to investigate the relationship between the spatial distribution of microbes and macroaggregate structure. We focus on quantifying how the pore system regulates the accessibility of bacteria or viruses to variously sized pores at nano- and micro-scale in soil aggregates. To achieve this goal, we used advanced USAXS, SANS, and USANS techniques to explore internal pore morphology (e.g., pore size distribution, pore volume) of aggregates and the spatial distribution of bacteria and bacteriophage within the aggregate structure.

4.3 Materials and Methods

4.3.1 Chemicals

Tryptone, yeast extract, agar with molecular genetic grade, and sodium chloride (NaCl) were obtained from Fisher Scientific (Waltham, MA, USA). Potassium chloride (KCl), di-sodium hydrogen phosphate (Na_2HPO_4), and potassium phosphate (KH_2PO_4) were obtained from Sigma-Aldrich (St. Louis, MO, USA). Deuterium oxide (D_2O) were purchased from Acros Organics. All chemicals used were of reagent grade or higher purity.

4.3.2 Isolation of soil macroaggregates

Field forest soil was kindly supplied by Andrew Margenot from The University of Illinois Urbana-Champaign, which was collected from Flanagan series in Illinois, United States. The soil is a silty clay loam. Roots, rhizomes, and rocks in the soil were removing by sieving soil

through an 8-mm sieve or manually. The sieved soils were air dried and stored in polyethylene bags at room temperature. Water-stable soil macroaggregates (250-2,000 μm) were from the 8-mm sieved soil by using wet-sieving method (Six et al., 2000). Specifically, air-dried soil samples were transferred to the 2,000-μm sieve and submersed in water for 5 minutes before sieving commenced. Continuous and steady water at a height of 2.5-cm above the 2,000-μm sieve flowed through the sieve while shaking caused the released aggregates to be immediately flushed through the 2,000-μm screen onto the underlying 250-μm sieve. Soils were sieved under water by gently moving the sieve 3 cm vertically 50 times over a period of 10 min through water contained in a shallow pan to ensure that the isolated aggregates are water-stable. Five to eight replicate subsamples of soil were processed to collect sufficient amounts of water-stable macroaggregates for study. The macroaggregates remaining on the sieve was freeze-dried and then stored at room temperature (21±1°C) in capped glass bottles. The mass proportion of macroaggregates in bulk soil was quantified that the isolated macroaggregates comprised about 60% of the bulk soil mass.

4.3.3 Bacteria and bacteriophage preparation

Escherichia coli strain C3000, rod-shaped bacteria with 2 μm of length and 1 μm of diameter, was obtained from ATCC and can be used as a bacteriophage host (Chien et al., 2012). Bacterial cells grew in 300 ml of autoclaved Luria-Bertani (LB) medium containing (per liter) 10 g of tryptone, 5 g of yeast extract, and 10 g of NaCl at pH 7.2 at 37°C with shaking at 280 rpm. After 24 hours of incubation, 100 ml of *E. coli* strain C3000 culture were collected and centrifuged at 8,500 g for 10 minutes at 4°C. The supernatant was discarded carefully using pipette to avoid disturbing the pellet. Then, the cell pellets were washed using sterile phosphate

buffered saline (PBS: (per liter) 8 g of NaCl, 0.2 g of KCl, 1.15 g of Na_2HPO_4, and 0.2 g of KH_2PO_4) three times to wash off LB broth and any other impurities attached on bacterial surface. After that, the washed pellet was resuspended in PBS. The cells suspension was adjusted to 10^8 colony-forming unit (CFU) per mL and stored at 4℃ for further experiments.

MS2 is a male-specific, unenveloped, single-stranded RNA bacteriophage containing 31% of nucleic acid and having a low isoelectric point of 3.9, and its diameter ranges from 24 to 26 nm (Zhuang and Jin, 2003). The bacteriophage was obtained from ATCC. Five hundred μL of MS2 stock mixed with 500 μL of their host, *E. coli* strain C3000, were added into 100 mL of LB medium and incubated 18 hours at 37℃ with shaking at 280 rpm. One hundred mL of the mixture was centrifuged at 5,500 g for 10 minutes, and then the supernatant was passed through a 0.22 μm Millex syringe-driven filter. The filtered solution was ultracentrifuged at 37,000 g for 3 hours and the phage pellet was gotten after discarding the supernatant. After that, the pellet was washed twice using PBS. After that, the pellet was resuspended in PBS and the viral concentration was adjusted to 10^{11} plaque-forming unit (PFU) per mL. The viral suspension was flash-frozen in liquid nitrogen and then stored in -80℃ for further use.

4.3.4 Enumeration of bacteria and viruses

Enumeration of *E. coli* strain C3000 cells was conducted according to an adapted drop plate assay (Chen et al., 2003). Briefly, 50 μL-droplets per dilution were pipetted onto agar plates and the plates were incubated at 37℃ overnight. The dilutions that resulted in 10-300 CFU per plate were counted.

The abundance of MS2 was quantified by the double-agar layer (DAL) method of plaque assay using *E. coli* strain C3000 as the host (Brewster et al., 2012). Briefly, the LB media for the

top and bottom layers contained 0.7% and 1.5% agar (pH 7.5), respectively. The top layer was melted to a liquid state and maintained at 48℃ until plating. *E. coli* strain C3000 was grown in LB media for 5 hours in exponential at the early stationary phase. One hundred μL of MS2 dilution and 100 μL of 5 hours aging MS2 host, *E. coli* strain C3000, were added to 3 mL of 0.7% top layer agar in a water bath or heating block set as 48℃ prior to plating. The inoculated top layer was poured quickly over the surface of a dried and labeled 1.5% LB agar plate. The overlay was allowed to harden for 30 minutes, and then the inoculated plates were incubated at 37℃ for 18-24 hours. After incubation, the phenotype and number of plaques were visualized and used to count MS2 concentration. The infectious phage unit is termed as PFU.

4.3.5 Equilibrium of bacteria and viruses in soil aggregates

Five samples including soil macroaggregates with PBS, *E. coli* strain C3000 with PBS, soil macroaggregates with *E. coli* strain C3000 and PBS, MS2 with PBS, and soil macroaggregates with MS2 and PBS, were collected for SAS measurements. To generate soil macroaggregates with *E. coli* strain C3000 and PBS, 1 mL of *E. coli* strain C3000 suspension with 10^8 CFU/mL in PBS was incubated with 0.6 g (dry weight) of water-stable soil macroaggregates in capped capillary tubes with 5 mm diameter overnight. Preparation of soil macroaggregates in PBS without *E. coli* strain C3000 followed identical procedures. Duplicate samples of each treatment were analyzed with SAS. Preparation of viral samples followed identical procedures and the concentration of viruses was 10^{11} PFU/mL.

4.3.6 SAS data collection and analysis

SAS measures the changes in the scattering intensity of the scattered neutrons or X-rays as a function of the momentum transfer, q, which is related to the three-dimensional solid scattering angle, θ, by

$$q=4\Pi \sin\theta/\lambda \quad (1)$$

where λ is the wavelength of the radiation. Combing Eq. (1) and Bragg's law ($\lambda=2L\sin\theta$) (Melnichenko, 2016) gives the length scale, L, detected at a given q range:

$$L\sim 2\Pi/q \quad (2)$$

The comparative analysis of pore sizes derived from intensity data can provide information about bacterial/viral distribution within the soil macroaggregate pore structure. The pattern of scattering intensity, $I(q)$, is determined by the geometry of the interface between the solid matrix and a pore space containing material, such as air, at different length scales (McCarthy et al., 2008). This pattern can be related to a pore size distribution if the Euclidean shape of the pores is given or reasonably assumed (McCarthy et al., 2008). The intensity of scattered radiation is then related to the scatterers' size distribution. For a two-phase scattering system, the intensity of scattering can be expressed by (Kotzias et al., 1987):

$$I(q)=\left|\Delta\rho^2\right| \int_0^\infty |F(q,r)|^2 V^2(r) NP(r)\mathrm{d}r \quad (3)$$

where $\Delta\rho^2$ represents the scattering contrast which is determined by the difference in the scattering length densities (SLD) between the pores and solid matrix, $F(q, r)$ is the scattering form factor for particulate scatterer shape, $V(r)$ is the volume of sample material within the X-ray or neutron beam, N is the total number of scattering particles, and $P(r)$ is the probability of occurrence of scatterers at size r. The term $V(r)$ is known as the sample thickness since the x- and y-dimensions of the sample are established based on shutter settings on the incoming beam. In

practice, when calculating the sample intensity of scattering ($I(q)$), the known or estimated sample thickness is included as an input parameter. This formula is, for computational purposes, replaced by a summation formula with a limited number of bins in radii:

$$I(q)=\left|\Delta\rho^2\right| \sum_{r_{min}}^{r_{max}} |F(q, r)|^2 \, V^2(r) NP(r) \mathrm{d}r \quad (4)$$

USAXS. USAXS measurements were conducted at the UNICAT beam line of the Advanced Photon Source (APS) at Argonne National Laboratory (Argonne, Illinois, USA). The UNICAT USAXS instrument uses absolute calibration based on first principles (standard-less), providing results directly on an absolute scale. The wavelength of USAXS was 1.109 $Å^{-1}$ with a measurable q-range of 10^{-4} to 10^{-1} $Å^{-1}$. USAXS data were calibrated and analyzed using a software package "Irena".

The maximum entropy method in the Irena software determined the size frequency distribution of voids. The pore volume distribution, which represents the relationship between the volume enclosed in a pore and the size of that pore, is displayed as a function of the larger dimension of the oblate spheroid used as a shape (aspect ratio of 0.1). Using the size distribution as a histogram, f, the scattering equation can be transformed into a linear equation.

$$I=Gf \quad (4)$$

where G is the matrix component which describes the assumed morphology of the scatters underlying the measured data, I.

SANS and USANS. SANS and USANS experiments were conducted using the Bio-SANS and USANS beam lines at the High Flux Isotope Reactor and the Spallation Neutron Source of Oak Ridge National Laboratory (Oak Ridge, Tennessee, USA), respectively. Contrast-variation

SANS measurements involve adjusting the percentage of heavy water in the suspension medium (Mahieu and Gabel, 2018). This approach allows for selective contrast matching of certain regions within the system based on their SLD values, enabling precise tuning of their contributions to the scattering intensity (Semeraro et al., 2021). In this study, soil macroaggregates in water of PBS consisting of various proportions of D_2O (i.e., 0%, 15%, 45%, 65%, and 85%) were analyzed by SANS to determine the contrast match point of soil aggregates.

The data were calibrated and reduced background. The SANS and USANS data were analyzed with a unified model using "Irena" software to approximate the scattering intensity over the range of q in terms of structural levels (Beaucage, 1995):

$$I(q) = \sum_{i=1}^{n} \left(G_i \exp\left(\frac{-q^2 R_{g,i}^2}{3}\right) + B_i \exp\left(\frac{-q^2 R_{g,i+1}^2}{3}\right) q_i^{*P_i} \right) + \text{Bkgd}$$

where $q^* = \frac{q}{\left\{\text{erf}\left(\frac{kqR_{g,i}}{\sqrt{6}}\right)\right\}^3}$ is an error function to provide a smooth transition between the Guinier regime and the Porod regime (Beaucage, 1995). G_i and B_i are pre-factors for the Guinier exponential and power law terms, respectively. R_g can be converted into an equivalent pore radius by assuming some specific shape for the pores, i.e., spherical or cylindrical.

4.4 Results

4.4.1 USAXS results

4.4.1.1 USAXS curves

The scattering intensities (I) as a function of the scattering vector (q) were plotted on log-log scale and on an absolute scale (Figure 4.1). The sequences of scattering data represent the changes in the scatters, soil pores. The intensities are due to X-rays scattered from the electron density difference between the solid phase and the empty pores of soil at various length scales

(Glatter et al., 1982). The intensities in the *q* region larger than 0.3 $Å^{-1}$, between 0.01 and 0.3 $Å^{-1}$, and small than 0.01 $Å^{-1}$) correspond to the features of micropores (pore diameter < 20 Å), mesopores (20 Å ≤ pore diameter ≤ 500 Å), and macropores (pore diameter > 500 Å) respectively. The ordinate is the intensity of X-ray scattering, reflecting the abundance of surface area of pores over a 4 order-of-magnitude range in the size of the scatters, expressed as a function of the momentum transfer, *q*, which is inversely related to the length scale of the scatterer. The negative slope of the scattering curve in Figure 4.1 indicates that the total surface area and/or volume of scatterers (intensity) increases with the length scale of the pores (Liu et al., 2021).

For the original curves in Figure 4.1A, there are some differences in the intensities among soil aggregates, soil with bacteria, and soil with virus, representing the changes in the pore structure, such as pore size and volume. In the low *q* region, the scattering intensities of soil with bacteria were higher than just soil and soil with virus. It means that the specific surface area and volume of macropores increased with the presence of bacteria in soil. As for the intensities at high *q*, the intensities of soil with bacteria or virus were lower than the soil, which indicates the specific surface area and volume of micropores or mesopores decreased with the presence of bacteria or virus in soil. The differences in the intensities between soil without and with bacteria or virus were plotted in Figures 4.1B and 4.1C. These curves were used to further analyze bacteria- or virus-filled pore size and volume distributions. The differences compared with empty soil gave the bacterial and viral distribution in different sized soil pores.

4.4.1.2 Pore volume distribution by USAXS

Representative USAXS fitting curves using the maximum entropy (MaxEnt) method in the "IRENA" software package were presented in Figure 4.2. The size distribution of the pore volume for original soil pores and bacteria/viruses-filled pores can be estimated by fitting curves. The magnitude and size distribution of the pore volume differed substantially among bacterium-filled and virus-filled pores. The pore volume filled by viruses are more than that by bacteria in the pores smaller than 100 Å and larger than 1,000 Å. We assume the results of <10 nm pores are caused by measurement errors. Bacteria distributed in soil pores occupied parts of original pore volume, which caused the decreases of volume fraction of macropores with diameter larger than 1,000 Å. For the pores with diameter ranging from 100 to 1,000 Å, the pore volume with the presence of virus fluctuated. The aggregation of virus in these pores resulted in the decreases of pore volume with specified pore sizes.

4.4.2 SANS and USANS results

4.4.2.1 Determination of the contrast match point for soil macroaggregates

As shown in Figure 4.3, the scatted intensity, *I*, decreased as the D_2O fraction was increased up to 65% v/v; then further increase in D_2O concentration increased *I*. The fitted results of the soil aggregate intensities using a power law fit method were shown in Figure 4.4. The equation, $I(q)=\alpha q^{-\beta}$, was applied to the fitting method. β is the power law exponent and can be determined from the slope of linear parts of log $I(q)$ vs. log q plots. When the exponent varies as $0 \leq \beta \leq 3$, it represents the volume (mass or pore) fractal dimension (D*f*). The fractal information of the pore network is one of the most important parameters to understand the changes of pore morphology. The volume fractal can be used to describe the aggregation of a

network. The red number in Figure 4.4 reflects β value. All β values were close to but less than 3 which indicates the structure of soil pores is a volume fractal. The fractal dimension describes an extremely disordered pore network in three dimensions that is akin to a sponge-like morphology (Liu et al., 2021). The β value decreased from 2.91 to 2.75 as the D_2O/H_2O was increased from 0% to 65% and decreased from 85% to 65%. The minimum value was approached at 65% D_2O/H_2O. Thus, 65% D_2O/H_2O was determined as the contrast matching point for the soil aggregates.

4.4.2.2 Pore accessibility

The fraction of accessible pores as a function of pore size (d) can be estimated based on the scattering intensities under initial and contrast-matched conditions (Melnichenko et al., 2012):

$$Pore\ accessibility\ (d) = 1 - \frac{I_{initial}(d)}{I_{contrast-matched}(d)}$$

where $I_{initial}(d)$ and $I_{contrast\text{-}matched}(d)$ are the background-subtracted scattering intensities under initial and contrast-matched conditions, respectively. The estimated pore accessibilities for soil and soil+bacteria samples are shown in Figure 4.5. The fraction of accessible pores for soil sample (red triangle) sharply increased with increasing of pore size at pore size smaller than 50 Å, and then decreased from 50 to 100 Å of pore size. After that, pore accessibility steady increased up to ~70%. The trend of pore accessibility for soil+bacteria sample (grey cycle) was similar with that for soil sample with a hump shown at the pore size around 50 Å. However, the fraction of accessible pores in the soil+bacteria sample reached to ~43% which was higher than the value in the soil sample with ~37%. There was no significant difference at the pore size larger than 200 Å between these two samples.

4.4.2.3 Changes in pore size due to bacteria within soil aggregates by combined SANS and USANS profiles

To develop an understanding of bacterial pore-scale distribution within pore structure of soil aggregates, combined USANS and SANS analysis was performed, and the data were analyzed with the Unified Fit model. Figure 4.6 shows the combined the USANS and SANS curves in the log-log space. Porous materials often exhibit hierarchical structures, which are reflected in these data by the three Guinier "knees". These knees result from separate distributions of scatterers (pores in this study) with similar sizes, and their locations correlate with the radii of gyration (R_g) of the size limits of those distributions where $R_g \sim 2\pi/Q$ (Krzysko et al., 2020; Weston et al., 2020). R_g was used to represent the pore size because the pores of soil aggregates have irregular and tortuous shapes. Three major populations of pores were present, shown with level 1, level 2, and level 3 for soil sample (Figure 4.6A) and soil + bacteria sample (Figure 4.6B).

The Unified Fit model was developed for modeling hierarchical materials (Beaucage, 1995). In this model, each structural level is defined by an equation with two parts: with a Guinier section defining a maximum intensity (G) and R_g defining the upper size limit of the level, below which the intensity of the Guinier section of the curve drops off rapidly (Guinier et al., 1955). The rapid drop in intensity corresponds to the position of the knees mentioned above. A structurally limited power-law term contains a prefactor B governing its intensity and a power-law slope P related to surface roughness as well as the same R_g used in the Guinier section. This power-law term defines the slope and intensity at Q values above each knee. The prefactor B is often defined in terms of G, R_g, and P and thus is not an independent variable. Based on the observation of three knees in the log-log scattering plots, two samples (i.e., soil shown in Figure

6A, and soil with bacteria shown in Figure 4.6B) appears to consist of three structural levels (i=3) with the size range analyzed by combined USANS and SANS. Level 1, 2, and 3 correspond to the small, medium, and large pores, respectively. The parameters obtained through the model fitting are shown in Table 4.1. The average R_g values for the small, medium, and large pores of soil sample (Figure 4.6A) are 651.15, 7,520, and 27,500 Å, respectively. Upon addition of bacteria, the size of small pores decreased ~70%, while a 32% size increased in the large pores was observed. There were not many changes of pore sizes in the medium pores after adding bacteria.

4.5 Discussion

4.5.1 SAS techniques

Small-angle X-ray and neutron scattering are non-invasive experimental techniques to characterize structural properties of biological membrane (Kučerka et al., 2008). Recent developments have opened the path toward emerging quantitative scattering studies on live cells (Semeraro et al., 2017; Semeraro et al., 2021). The developments of SAS techniques make a possible bridging of molecular to cellular length scales. On the base of such background, in this study, SAS techniques were used to discriminate microbes in the complex soil pore environment. *E. coli* used as a model bacterium is classified as a Gram-negative bacterium and has a cell wall including inner and outer membranes, the peptidoglycan layer, and the periplasmic space, which envelope the cytoplasmic content (Lieb et al., 1955; Silhavy et al., 2010). The cytoplasm of *E. coli* was approximated by a prolate of homogeneous SLD and scattering contributions from macromolecules within the cytoplasm are negligible compared to their surroundings (Semeraro et al., 2021). However, the cell wall architecture contributes different SLD as a “shell” for cell

(Semeraro et al., 2017). Thus, the SLD of the cell wall is used to model the bacterial scattering form factor.

Differences in the elemental composition of different materials result in variations in their SLD. These variations can be exploited to permit experimental control of the contrast between different materials. Contrast in pores filled with different materials has been used to determine details of porosity development (Antxustegi et al., 1998a; Antxustegi et al., 1998b; Calo et al., 2001; Hall et al., 1997). The difference in contrast between hydrogen and deuterium allows for the powerful tool of H/D contrast variation because H_2O and D_2O are at opposite extremes in neutron scattering capacity (Schurtenberger, 2002). A D_2O/H_2O mixture can often be identified with the same SLD as that of the soils. When such SLD-matching liquid fills some size fraction of pores, those pores will not contribute to the total scattering curve. Subtracting the scattering curve for soil wetted with a contrast matching liquid at the desired water content from that of totally air-filled soil can provide information on the size distribution of pores that are accessible to the liquid under that set of water content conditions (Hall et al., 1997; Calo et al., 2001). If the SLD of D_2O/H_2O liquid matches that of soils, but contrasts with that of microbes, the difference in the scattering curves between soil and soil+microbes reveals the microbial distribution in different pores (Figures 4.3 and 4.4).

4.5.2 Effect of soil pore size on microbial distribution

The key goal of this study was to analyze the spatial patterns of microbes at scales associated with nano- and microhabitats using nondestructive techniques, SAS. Our results contribute that the 2 μm-sized model bacterial strain preferred to stay in micropores with a size of 0.1 μm larger than its size (Figure 4.2). The spatial distribution of bacteria was not uniform

and their location in the soil is dependent on factors like pore size distribution and substrate availability (Nunan et al., 2003; Ruamps et al., 2011; Juyal et al., 2019). The cell size of bacteria varies considerably from 0.2 to 750 μm in diameter (Schulz and Jørgensen, 2001). More than 80% of bacteria are preferentially located in the inner part of soil pores compared to adhesion on soil outer surface (Ranjard and Richaume, 2001). Between 50% and 75% of the soil porosity is inaccessible to bacterial cells because bacteria cannot access closed pores and pass pore throats smaller than 0.2 μm (Chenu and Stotzky, 2001; Foster, 1988). Some studies suggest that the mean diameter of the pores most frequently colonized by bacteria was estimated at 2 μm whereas the majority of soil bacteria are less than 0.5 μm in diameter (Bakken and Olsen, 1987; Kilbertus, 1980). In our case, the pore size for optimal bacterial colonization was greatly close to bacterial size. Pores smaller than the size of bacteria are not suited to bacterial colonization, whereas large pores do not provide adequate shelter from predators (Schnee et al., 2016; Vanek et al., 2016). Pores with closer size that bacteria harbored in provide optimal protection for bacteria from predation (Tecon and Or, 2017; Wright et al., 1995). The predation by bacterial consumers (e.g., protozoans) is less in fine-textured soils than in coarse-textured soils (Rutherford and Juma, 1992). The porosity of fine-textured soil is made up largely of small pores (<2-3 μm) as a refuge for bacteria, which are less accessible to bacterial consumers but accessible to bacteria (Erktan et al., 2020; Gupta and Germida, 1989). Since soil is a dark labyrinth, even though there was no predation pressure in our studies, bacteria still actively moved into smaller pores. Additionally, soil organic matter is the endogenous source of carbon substrate and energy for soil microbes (Ranjard and Richaume, 2001). Up to 80% of the soil organic matter is contained in the fine fractions of soil, such as the microaggregated fraction (2-20 μm) (Christensen, 1992). The clay in the aggregates also favors bacterial adhesion by their negative charge (Young and Crawford,

2004). The micropores serve as the major adhesion sites of bacteria due to their similar dimensions to the bacteria, which stabilizes adhesion by allowing multiple contact points between bacteria and pore wall (Karanfil and Kilduff, 1999; Li et al., 2002; Lillo-Ródenas et al., 2005; Urano et al., 1991).

Viral aggregation in soil pores was observed in our study (Figure 4.2). Capsid surfaces of viruses are negatively charged at typical soil pH due to ionizable groups on their protein coats (Kimura et al., 2008; Michen and Graule, 2010). Viruses can therefore be viewed as small colloidal particles permeating the liquid phase of an interaction, porous soil medium (Sim and Chrysikopoulos, 2000). The concepts used in colloids have been applied to describe viral properties, such as aggregation (Jin and Flury, 2002). Viruses may aggregate when they contact each other to protect viruses from inactivation (Grant, 1995). Such behavior of viral aggregation in soil may also reduce the probability that viruses are transferred into nano-pores (<0.1 μm). Due to the small size of viruses, one assumption mentioned that a single virus moves into the nano-pores (<0.1 μm) and this virus will remain inaccessible until it is eventually dislodged by water flow and removed from the pores, or the stable pores are themselves physically or biologically disrupted (Kuzyakov and Mason-Jones, 2018). Increased size due to aggregation makes virus aggregates physically impossible for the virus to penetrate the nano-sized pores.

4.5.3 Effect of pore-scale bacterial distribution on soil pore structure

Bacteria distributed within soil pores modified soil pore sizes, and combined USANS and SANS analysis revealed that this process was coupled with changes to the sizes of small- and large-pores of soil aggregates with and without bacteria (Figure 4.6 and Table 4.1). Since 65% of D_2O in H_2O was used to match the SLD of soils (Figures 4.3 and 4.4), pore sizes calculated by

the combined USANS and SANS profiles of soil sample were the sizes of the pore which was inaccessible for D_2O. The data analysis suggested an increase from 2.75 to 3.62 μm in the size of larger pores following the addition of bacteria (Table 4.1). As mentioned above, bacteria contrasts with soil under USANS and SANS measurement. The measured pore sizes of soil+bacteria sample thus included the pores that bacteria were colonized and the inaccessible pores. This shift of large pore size was presumably due to bacteria entering the accessible pores with ~3.62 μm of size. In addition, the size of small pore decreased and shifted from 0.065 of soil sample to 0.019 μm of soil+bacteria sample (Table 4.1). The addition of bacteria blocked the previous accessible pores making the pores inaccessible. These inaccessible pores contributed the changes of small pores.

4.6 Conclusions

This work sought to investigate the relationship between the pore structure of soil aggregates and the spatial distribution of microbes at a fine scale. Pore volume distribution and pore accessibility were determined for the soil sample with and without bacteria by using small angle scattering techniques. The results suggest that pore size and accessibility influence the distribution of bacteria/viruses in soils at micro- and nanoscales, and vice versa. Bacteria and viruses have their optimal pore as shelters for survival in response to soil harsh environments. The optimal pore size was related to bacterial size or viral aggregate size. Our novel application of small angle scattering provides direct evidence for the quantification of microbial distribution at the pore scale in soils. The observations complement the physical associations between microbes and soil pore system and lead to new frameworks to model the distribution of microbes in a range scale of the 3D soil environment.

Acknowledgments

We thank Shuo Qian at Oak Ridge National Laboratory for USANS and SANS measurement and data reduction, and Jan Ilavsky at Argonne National Laboratory for USAXS measurement and data analysis. We also thank Andrew J. Margenot at University of Illinois Urbana-Champaign for providing soil samples.

References

Antxustegi MM, P.J.Hall, Calo JM. The use of contrast-matching small-angle neutron-scattering techniques to monitor closed porosity in carbons. Journal of Colloid and Interface Science 1998a; 202: 490-498.

Antxustegi MM, P.J.Hall, Calo. JM. Development of porosity in Pittsburgh No. 8 coal char as investigated by contrast-matching small-angle neutron scattering and gas adsorption techniques. Energy & Fuels 1998b; 12: 542-546.

Bailey VL, McCue LA, Fansler SJ, Boyanov MI, DeCarlo F, Kemner KM, et al. Micrometer-scale physical structure and microbial composition of soil macroaggregates. Soil Biology and Biochemistry 2013; 65: 60-68.

Bakken LR, Olsen RA. The relationship between cell size and viability of soil bacteria. Microbial ecology 1987; 13: 103-114.

Beaucage G. Approximations leading to a unified exponential/power-law approach to small-angle scattering. Journal of applied crystallography 1995; 28: 717-728.

Brewster L, Langley M, Twa D. Co-infection of C3000 Escherichia coli with bacteriophages MS2 and, T7 or ΦX-174 results in differential cell lysis patterns. Journal of Experimental Microbiology and Immunology (JEMI) Vol 2012; 16: 139-143.

Calo JM, Hall PJ, Antxustegi M. Carbon porosity characterizationvia small angle scattering. Colloids Surf. A:Physicochem. Engineer Aspects 2001; 187-188: 219-232.

Carminati A, Kaestner A, Ippisch O, Koliji A, Lehmann P, Hassanein R, et al. Water flow between soil aggregates. Transport in Porous Media 2007; 68: 219-236.

Chen C-Y, Nace GW, Irwin PL. A 6× 6 drop plate method for simultaneous colony counting and MPN enumeration of Campylobacter jejuni, Listeria monocytogenes, and Escherichia coli.

Journal of microbiological methods 2003; 55: 475-479.

Chenu C, Stotzky G. Interactions between microorganisms and soil particles: an overview. Interactions between soil particles and microorganisms: Impact on the terrestrial ecosystem 2001: 3-40.

Chien A-C, Hill N, Levin P. Cell size control in bacteria. Current biology 2012; 22: R340-R349.

Christensen BT. Physical fractionation of soil and organic matter in primary particle size and density separates. Advances in Soil Science: Volume 20 1992: 1-90.

De Gryze S, Six J, Merckx R. Quantifying water‐stable soil aggregate turnover and its implication for soil organic matter dynamics in a model study. European Journal of Soil Science 2006; 57: 693-707.

Ebrahimi A, Or D. Microbial community dynamics in soil aggregates shape biogeochemical gas fluxes from soil profiles–upscaling an aggregate biophysical model. Global change biology 2016; 22: 3141-3156.

Erktan A, Or D, Scheu S. The physical structure of soil: determinant and consequence of trophic interactions. Soil Biology and Biochemistry 2020; 148: 107876.

Foster R. Microenvironments of soil microorganisms. Biology and fertility of soils 1988; 6: 189-203.

Glatter O, Kratky O, Kratky H. Small angle X-ray scattering: Academic press, 1982.

Graham EB, Knelman JE, Schindlbacher A, Siciliano S, Breulmann M, Yannarell A, et al. Microbes as engines of ecosystem function: when does community structure enhance predictions of ecosystem processes? Frontiers in microbiology 2016; 7: 214.

Grant SB. Inactivation kinetics of viral aggregates. Journal of Environmental Engineering 1995; 121: 311-319.

Guinier A, Fournet G, Yudowitch KL. Small-angle scattering of X-rays. 1955.

Gupta V, Germida J. Influence of bacterial-amoebal interactions on sulfur transformations in soil. Soil Biology and Biochemistry 1989; 21: 921-930.

Hall PJ, Galan DG, Machado WR, Mondragon F, Barria EB, Sherrington DC, et al. Use of contrast-enhanced small-angle neutron scattering to monitor the effects of solvent swelling on the pore structure of styrene-divinylbenzene resins. Journal of the Chemical Society-Faraday Transactions 1997; 93: 463-466.

Hartmann M, Six J. Soil structure and microbiome functions in agroecosystems. Nature Reviews Earth & Environment 2023; 4: 4-18.

Jansson J, Fredrickson J. Stewards of a changing planet: commentaries from ISME13 Plenary Lecturers. The ISME Journal 2010; 4: 1079-1080.

Jansson JK, Hofmockel KS. Soil microbiomes and climate change. Nature Reviews Microbiology 2020; 18: 35-46.

Jin Y, Flury M. Fate and transport of viruses in porous media. Advances in agronomy 2002; 77: 39-102.

Karanfil T, Kilduff JE. Role of granular activated carbon surface chemistry on the adsorption of organic compounds. 1. Priority pollutants. Environmental science & technology 1999; 33: 3217-3224.

Kilbertus G. Microhabitats in soil aggregates. Their relationship with bacterial biomass and the size of the procaryotes present. Revue d'Ecologie et de Biologie du Sol 1980; 17: 543-557.

Kimura M, Jia Z-J, Nakayama N, Asakawa S. Ecology of viruses in soils: past, present and future perspectives. Soil Science and Plant Nutrition 2008; 54: 1-32.

Kotzias D, Herrmann M, Zsolnay A, Beyerle-Pfnür R, Parlar H, Korte F. Photochemical aging of

humic substances. Chemosphere 1987; 16: 1463-1468.

Krzysko AJ, Nakouzi E, Zhang X, Graham TR, Rosso KM, Schenter GK, et al. Correlating inter-particle forces and particle shape to shear-induced aggregation/fragmentation and rheology for dilute anisotropic particle suspensions: A complementary study via capillary rheometry and in-situ small and ultra-small angle X-ray scattering. Journal of colloid and interface science 2020; 576: 47-58.

Kučerka N, Nagle JF, Sachs JN, Feller SE, Pencer J, Jackson A, et al. Lipid bilayer structure determined by the simultaneous analysis of neutron and X-ray scattering data. Biophysical journal 2008; 95: 2356-2367.

Kuzyakov Y, Mason-Jones K. Viruses in soil: Nano-scale undead drivers of microbial life, biogeochemical turnover and ecosystem functions. Soil Biology and Biochemistry 2018; 127: 305-317.

Leff JW, Bardgett RD, Wilkinson A, Jackson BG, Pritchard WJ, De Long JR, et al. Predicting the structure of soil communities from plant community taxonomy, phylogeny, and traits. The ISME journal 2018; 12: 1794-1805.

Li L, Quinlivan PA, Knappe DR. Effects of activated carbon surface chemistry and pore structure on the adsorption of organic contaminants from aqueous solution. Carbon 2002; 40: 2085-2100.

Lieb M, Weigle J, Kellenberger E. A study of hybrids between two strains of Escherichia coli. Journal of bacteriology 1955; 69: 468-471.

Lillo-Ródenas M, Cazorla-Amorós D, Linares-Solano A. Behaviour of activated carbons with different pore size distributions and surface oxygen groups for benzene and toluene adsorption at low concentrations. Carbon 2005; 43: 1758-1767.

Liu K, Ostadhassan M, Sun L, Zou J, Yuan Y, Gentzis T, et al. A comprehensive pore structure study of the Bakken Shale with SANS, N2 adsorption and mercury intrusion. Fuel 2019; 245: 274-285.

Liu Y, Paskevicius M, Sofianos MV, Parkinson G, Li C-Z. In situ SAXS studies of the pore development in biochar during gasification. Carbon 2021; 172: 454-462.

Mahieu E, Gabel F. Biological small-angle neutron scattering: recent results and development. Acta Crystallographica Section D: Structural Biology 2018; 74: 715-726.

Mayer LM, Schick LL, Hardy KR, Wagai R, McCarthy J. Organic matter in small mesopores in sediments and soils. Geochimica et Cosmochimica Acta 2004; 68: 3863-3872.

McCarthy JF, Ilavsky J, Jastrow JD, Mayer LM, Perfect E, Zhuang J. Protection of organic carbon in soil microaggregates via restructuring of aggregate porosity and filling of pores with accumulating organic matter. Geochimica et Cosmochimica Acta 2008; 72: 4725-4744.

Melnichenko YB. Small-Angle Scattering from Con Ned and Interfacial Fluids: Springer, 2016.

Melnichenko YB, He L, Sakurovs R, Kholodenko AL, Blach T, Mastalerz M, et al. Accessibility of pores in coal to methane and carbon dioxide. Fuel 2012; 91: 200-208.

Michen B, Graule T. Isoelectric points of viruses. Journal of applied microbiology 2010; 109: 388-397.

Radlinski A, Mastalerz M, Hinde A, Hainbuchner M, Rauch H, Baron M, et al. Application of SAXS and SANS in evaluation of porosity, pore size distribution and surface area of coal. International Journal of Coal Geology 2004; 59: 245-271.

Ranjard L, Richaume A. Quantitative and qualitative microscale distribution of bacteria in soil. Research in microbiology 2001; 152: 707-716.

Rasmussen FB. Different approaches to the analysis of small angle scattering experiments on

porous aluminum-hydroxide. Colloids and Surfaces A: Physicochemical and Engineering Aspects 2001; 187: 327-335.

Rutherford P, Juma N. Influence of texture on habitable pore space and bacterial-protozoan populations in soil. Biology and Fertility of Soils 1992; 12: 221-227.

Schnee LS, Knauth S, Hapca S, Otten W, Eickhorst T. Analysis of physical pore space characteristics of two pyrolytic biochars and potential as microhabitat. Plant and Soil 2016; 408: 357-368.

Schulz HN, Jørgensen BB. Big bacteria. Annual Reviews in Microbiology 2001; 55: 105-137.

Schurtenberger P. Contrast and contrast variation in neutron, x-ray and light scattering. 1. North-Holland: Amsterdam, The Netherlands, 2002.

Semeraro EF, Devos JM, Porcar L, Forsyth VT, Narayanan T. In vivo analysis of the Escherichia coli ultrastructure by small-angle scattering. IUCrJ 2017; 4: 751-757.

Semeraro EF, Marx L, Frewein MP, Pabst G. Increasing complexity in small-angle X-ray and neutron scattering experiments: from biological membrane mimics to live cells. Soft Matter 2021; 17: 222-232.

Sessitsch A, Weilharter A, Gerzabek MH, Kirchmann H, Kandeler E. Microbial population structures in soil particle size fractions of a long-term fertilizer field experiment. Applied and environmental microbiology 2001; 67: 4215-4224.

Sexstone AJ, Revsbech NP, Parkin TB, Tiedje JM. Direct measurement of oxygen profiles and denitrification rates in soil aggregates. Soil science society of America journal 1985; 49: 645-651.

Silhavy TJ, Kahne D, Walker S. The bacterial cell envelope. Cold Spring Harbor perspectives in biology 2010; 2: a000414.

Sim Y, Chrysikopoulos CV. Virus transport in unsaturated porous media. Water Resources Research 2000; 36: 173-179.

Six J, Bossuyt H, Degryze S, Denef K. A history of research on the link between (micro) aggregates, soil biota, and soil organic matter dynamics. Soil and tillage research 2004; 79: 7-31.

Six J, Elliott ET, Paustian K. Soil macroaggregate turnover and microaggregate formation: a mechanism for C sequestration under no-tillage agriculture. Soil Biology and Biochemistry 2000; 32: 2099-2103.

Tecon R, Or D. Biophysical processes supporting the diversity of microbial life in soil. FEMS microbiology reviews 2017; 41: 599-623.

Urano K, Yamamoto E, Tonegawa M, Fujie K. Adsorption of chlorinated organic compounds on activated carbon from water. Water Research 1991; 25: 1459-1464.

Vanek SJ, Thies J, Wang B, Hanley K, Lehmann J. Pore-size and water activity effects on survival of Rhizobium tropici in biochar inoculant carriers. J. Microb. Biochem. Technol 2016; 8: 296-306.

Vishal V, Chandra D, Bahadur J, Sen D, Hazra B, Mahanta B, et al. Interpreting pore dimensions in gas shales using a combination of SEM imaging, small-angle neutron scattering, and low-pressure gas adsorption. Energy & Fuels 2019; 33: 4835-4848.

Vos M, Wolf AB, Jennings SJ, Kowalchuk GA. Micro-scale determinants of bacterial diversity in soil. FEMS microbiology reviews 2013; 37: 936-954.

Wang Y, Fan Z, Qian P, Ala-Nissila T, Caro MA. Structure and pore size distribution in nanoporous carbon. Chemistry of Materials 2022; 34: 617-628.

Weston JS, Chun J, Schenter G, Weigandt K, Zong M, Zhang X, et al. Connecting particle interactions to agglomerate morphology and rheology of boehmite nanocrystal suspensions.

Journal of colloid and interface science 2020; 572: 328-339.

Wilpiszeski RL, Aufrecht JA, Retterer ST, Sullivan MB, Graham DE, Pierce EM, et al. Soil aggregate microbial communities: towards understanding microbiome interactions at biologically relevant scales. Applied and environmental microbiology 2019; 85: e00324-19.

Wright D, Killham K, Glover LA, Prosser JI. Role of pore size location in determining bacterial activity during predation by protozoa in soil. Applied and Environmental Microbiology 1995; 61: 3537-3543.

Young IM, Crawford JW. Interactions and self-organization in the soil-microbe complex. Science 2004; 304: 1634-1637.

Zhuang J, Jin Y. Virus retention and transport through Al-oxide coated sand columns: effects of ionic strength and composition. Journal of Contaminant Hydrology 2003; 60: 193-209.

Zhuang J, McCarthy J, Perfect E, Mayer L, Jastrow J. Soil water hysteresis in water‐stable microaggregates as affected by organic matter. Soil Science Society of America Journal 2008; 72: 212-220.

Appendix

Table 4.1 Modeling parameters of USANS and SANS profiles

Parameter	Soil	Soil-Bacteria
G1 (cm-1)	7.12	0.30
Rg,1 (Å)	651.15	189.88
B1 (cm-1)	7.27e-6	3.65e5
P1	2.14	1.75
G2 (cm-1)	1.49e5	1.88e5
Rg,2 (Å)	7.52e3	7.28e3
B2 (cm-1)	2.36e-8	5.29e-8
P2	3.52	3.45
G3 (cm-1)	7.79e5	8.32e5
Rg,3 (Å)	2.75e4	3.62e4
B3 (cm-1)	0.01	0.06
P3	1.00	1.00
Bkgd (cm-1)	0.01	0.01

*Gi and Bi are pre-factors for the Guinier exponential and power law terms. i is the structural level. Rg is the radius gyration, which represents the pore size. Bkgd is the incoherent scattering background.

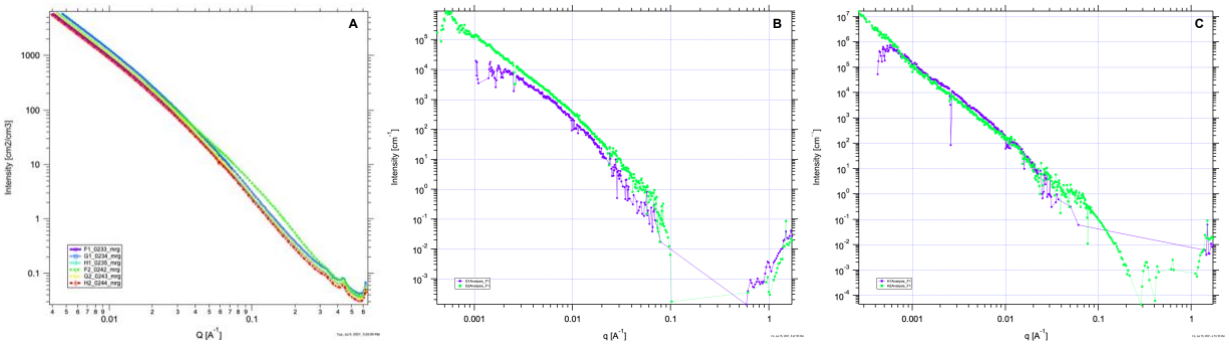

Figure 4.1 USAXS original curves of soil aggregates with and without bacteria (A), USAXS curves of *E. coli* (B) and MS2 (C) on log-log scale. (A) The curves F, G, and H represent samples of soil aggregates + PBS, soil aggregates + PBS + *E. coli*, and soil aggregates + PBS + MS2, respectively. The numbers (i.e., 1 and 2) show replicates. The purple and green curves represent two replicates. (B) The curves were gotten from the difference between soil + PBS + *E. coli* sample and soil + PBS sample. (C) The curves were gotten from the difference between soil + PBS + MS2 sample and soil + PBS sample. The scattering data of soil + PBS + *E. coli* (B) or soil + PBS + MS2 (C) sample have already reduced with PBS + *E. coli* sample. The scattering data of soil + PBS sample have already reduced with PBS solution background.

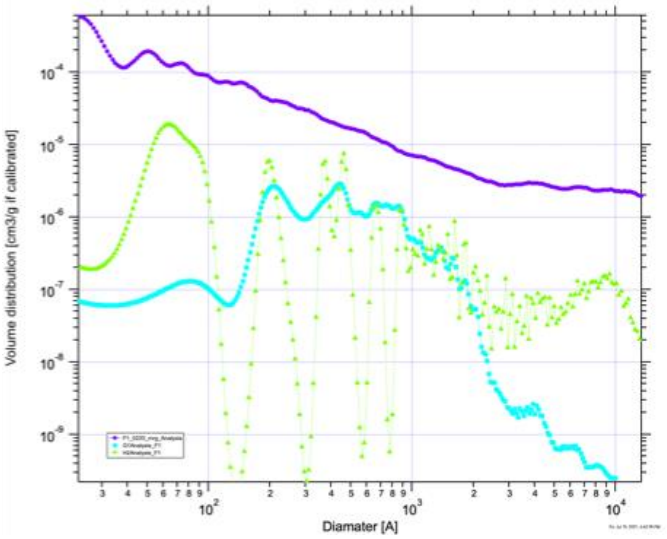

Figure 4.2 Pore size and volume distribution of soil (purple), *E. coli* (blue), and MS2 (green). The results were obtained from the MaxEnt fitting method in IRENA to USAXS data.

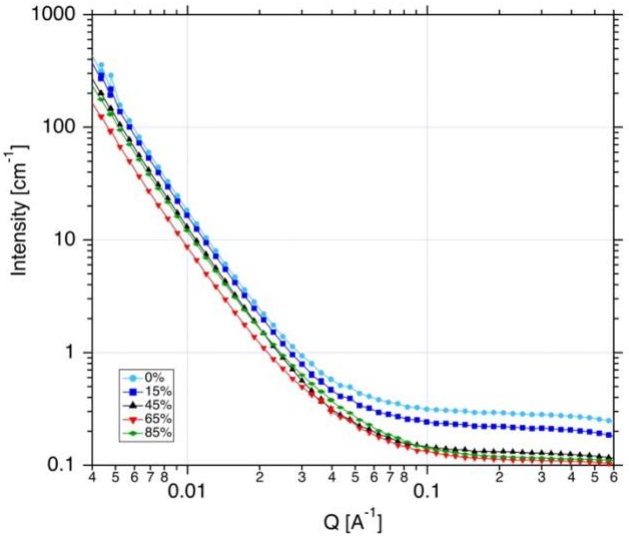

Figure 4.3 SANS log-log curves of soil aggregates in background solution with different ratios of D_2O:H_2O, including 0%, 15%, 45%, 65%, and 85%.

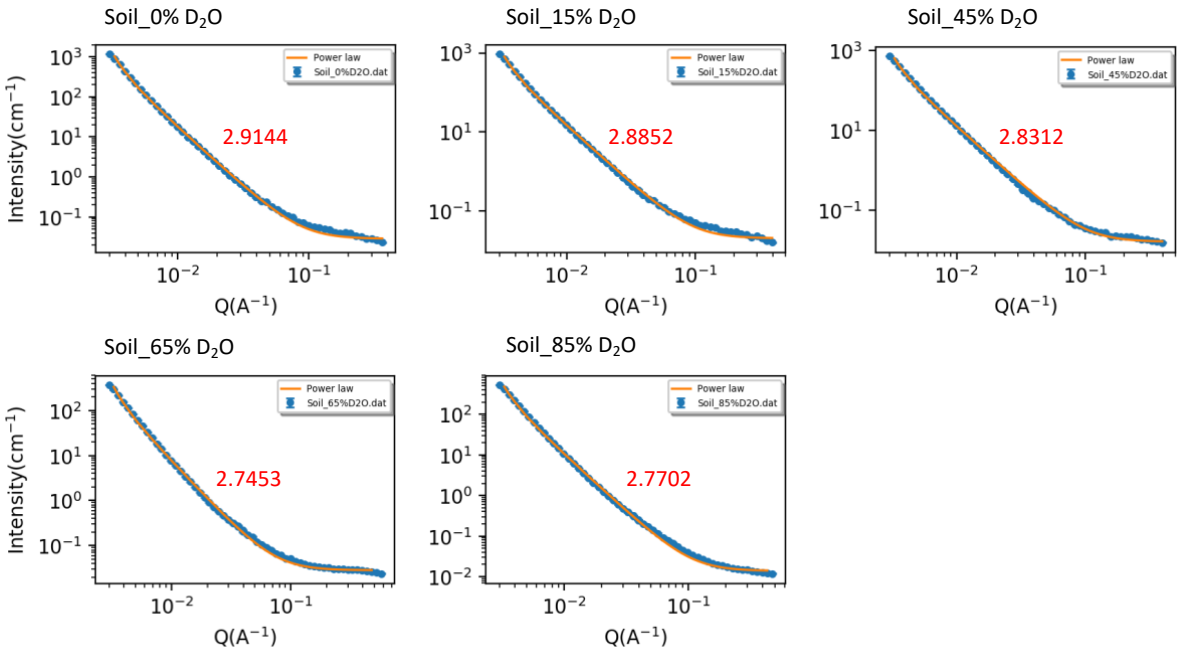

Figure 4.4 Fitted curves of soil + PBS SANS data using Power Law in the SASView software.

The numbers with red color show the fitted power value.

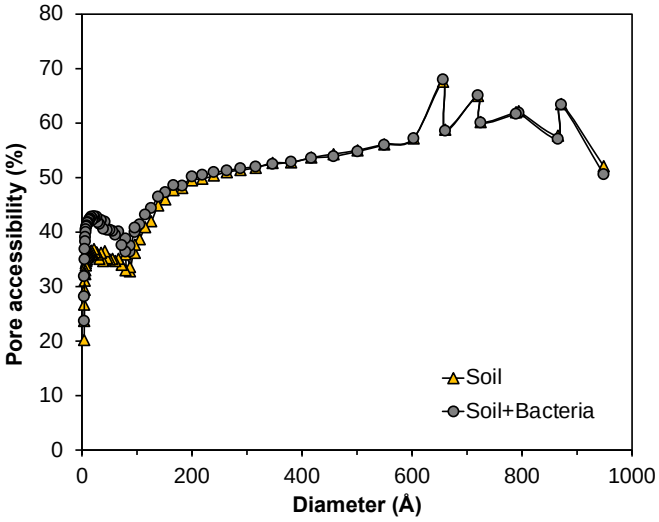

Figure 4.5 Pore accessibility of the soil aggregate and soil+bacteria samples.

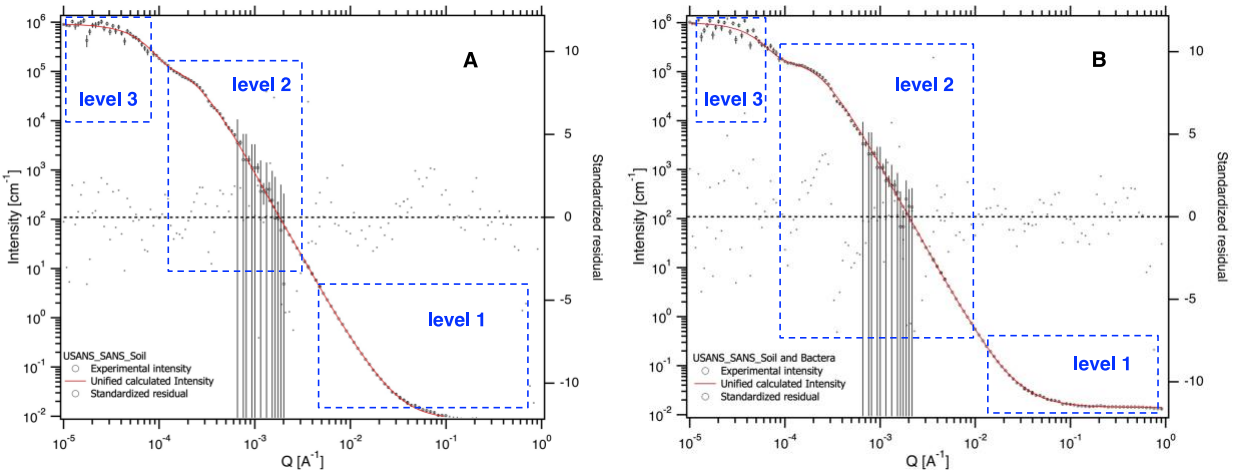

Figure 4.6 USANS and SANS profiles and data modeling. Panel (A) shows the decomposition of total scattering intensity into level structures of soil. Panel (B) shows soil with bacteria. The circles with error bar represent the background-subtracted USANS and SANS profiles for soil (A) and soil with bacteria (B). The solid red lines represent the best fit based on the Unified Fit model. The circles without error bar represent the standardized residual.

Chapter 5. Summary and Conclusions

Soil plays a central role in supporting life and is home to an unimaginable diversity of microbes. While high microbial abundance in soil, microbes occupy no more than a few percent of the pore spaces and only <1% of the available soil surfaces. The spatial context of soil controls essential elements (e.g., water) for microbial activity and limits microbial distribution and interaction. This work comprised three consecutive studies focusing on developing a better understanding of how soil pores as the controlling factors affect water retention characteristics and microbial dynamics.

The first study aimed to develop an approach for estimating soil water retention curves by understanding water characteristics in soil pores. Soil water retention determines microbial activity, plant water availability, and contaminant transport processes. Due to the difficulty of soil water retention characteristics measurement, an analytical model based on a fractional bulk density (FBD) concept was presented in this study. The concept allows the partitioning of soil pore space according to the relative contribution of certain size fractions of particles to the change in total pore space. The input parameters of the model are particle size distribution (PSD), bulk density, and residual water content at a water pressure head of 15,000 cm. Results showed that the FBD model was effective for all soil textures and bulk densities by testing 30 sets of water retention data obtained from various types of soils that cover wide ranges of soil texture from clay to sand and soil bulk density. The proposed model provides a convenient way to evaluate the impacts of soil bulk density on water conservation in soils that are manipulated by mechanical operation.

Secondly, microbial interactions in soil pore water and on surfaces within soil porous systems were investigated. Bacterial cell-to-cell interactions are vital for evolutionary and ecological processes in various environments. Cellular interactions depend on the

physicochemical conditions of their habitats (e.g., particle surfaces, aqueous). To explore how particle surface properties (i.e., surface charge), particle size distribution (i.e., from coarse to fine), and solution chemistry (i.e., ionic strength) affect bacterial cell-to-cell interaction, a model system of conjugation between the bacterial donor and recipient cells and monitored the interaction through the expression of marker genes was employed. The quartz sand with uniform size was used to represent the soil particle and fluorescence imaging and cell counting were used to enumerate various cells and calculate the frequency of conjugation. Based on evidence from experiments in sand microcosms, we demonstrated that close confinement and collision of interacting cells in isolated and small pore spaces in the presence of the solid phase of particles promoted cell-to-cell interaction. However, bacterial adhesion on solid surfaces decreases the probability of cells encountering others due to the limited motility of bacteria.

Thirdly, the distribution of viruses and bacteria in the nano- and micro-pore of soil aggregates was examined. Previous studies demonstrated carbon and nutrients can be moved into and remain stable in nano-pores that viruses can reach but bacteria cannot. Theoretically, Viruses and bacteria could reach into the pores that are close to their size; however, direct information on the pore sizes that viruses and bacteria can enter is still lacking. A methodology to characterize the distribution of viruses and bacteria in pores by using advanced (ultra)-small angle neutron/X-ray scattering techniques were developed. Neutron/X-ray analysis characterizes the pore sizes and corresponding pore volumes in the aggregates. The model virus, MS2 (~25 nm), and model bacterium, *Escherichia coli* strain C3000 (~2 μm), were equilibrated in saturated water-stable soil aggregates for 24 h before measuring by small angel-scattering instruments. The results show that bacteria and viruses have their optimal strategies for survival in soil pores in response

to soil harsh environments. Bacteria preferred to colonize in the pores greatly close to their sizes and viruses aggregated to prevent penetrating into nanopores.

In agroecosystems, agricultural management practices (e.g., cover cropping, mechanical compaction, irrigation) can cause continuous changes in the physical properties of the soil, thus resulting in modifications mainly in its porous system. This project advances the understanding that physical factors affect soil water retention and microbial interactions and provides direct evidence to support viral and bacterial distribution in nano- and micro-scale pores in the soil. It has implications for predicting and possibly managing, microbial activity in agroecosystems.

Vita

Huihui Sun was born in Taian City, Shandong Province, China. She completed her undergraduate study in Environmental Engineering at the University of Jinan, China, in 2014. She got her master's degree in Environmental Science from the Yantai Institute of Coastal Zone Research, Chinese Academy of Sciences, in 2017. After graduating, she spent two years in the State Key Laboratory of Estuarine and Coastal Research, East China Normal University, as a research assistant. She then pursued her doctoral study in Plant, Soil, and Environmental Sciences in the Department of Biosystems Engineering and Soil Science at the University of Tennessee under the guidance of Dr. Jie Zhuang.